Lincoln University
Te Whare Wānaka o Aoraki
CHRISTCHURCH•NEW ZEALAND

Lincoln University Digital Dissertation

Copyright Statement

Assessing seawater intrusion vulnerability associated with sea level rise in Christchurch, New Zealand using GIS-based methods

---

A Dissertation

submitted in partial fulfilment

of the requirements for the Degree of

Bachelor of Agriculture Science

with Honours

at

Lincoln University

by

Irene Setiawan

Lincoln University

2018

Abstract of a Dissertation submitted in partial fulfilment of the requirements for the Degree of Bachelor of Agriculture Science with Honours

Assessing seawater intrusion vulnerability associated with sea level rise in Christchurch, New Zealand using GIS-based methods

by

Irene Setiawan

1116136

Seawater intrusion (SWI) is the landward movement of the seawater-freshwater interface in coastal aquifers. Causes of SWI include groundwater pumping, sea level rise, reduced recharge and land drainage. Christchurch aquifers provide one of the highest quality drinking water sources in the world, which local residents completely rely on for critical needs. In this study, a qualitative GIS-based method called GALDIT (Lobo-Ferreira et al., 2007) was used to assess SWI vulnerability in the shallow confined Riccarton Gravel aquifer in Christchurch, under different sea level rise (SLR) scenarios. To overcome limitations of this method, the analytic solutions of Morgan and Werner (2015) were developed and applied within a GIS framework, for the first time. Both methods were applied based on the following scenarios: current sea level, 1 m SLR with fixed head condition, and 2 m SLR with both fixed head and fixed flux conditions. Both methods showed that the Riccarton Gravel aquifer was most vulnerable to SWI in the locations of Brooklands, Woolston and Ferrymead. The differences

between the two methods and the implications of the results in the local Christchurch context are discussed. The analytic solution was able to quantify SWI vulnerability in greater detail by determining the change in the theoretical seawater wedge toe position along the coast under SLR scenarios. However, neither the analytic solution nor GALDIT account for the possible offshore extension of the Riccarton Gravel aquifer and this is a limitation of both approaches.

Key words: analytic solutions, GALDIT, Riccarton Gravel, inland boundary condition, freshwater-seawater interface, climate change, Christchurch groundwater

Acknowledgements

I would like to hugely thank my supervisor Leanne Morgan for all the knowledge, guidance, feedback, and technical support given to me throughout the project. I thank Henry Chau for all the advice and support for the project. I thank the Waterways Centre of Freshwater Management for providing a work station, and all staff members and students for the many forms of support and encouragement. I thank the Environment Canterbury groundwater team for providing data, guidance, and technical support, without which the project would be impossible to complete. I thank GNS Science for the GIS data on aquifer thickness and depth, as well as for answering my numerous questions. I thank Crile Doscher for the valuable advice and guidance given on the GIS aspects of the project.

Last but not least, I thank my partner, friends, and family for the encouragement and moral support throughout this journey.

Table of contents

List of tables

List of figures

1. Introduction

1.1. The importance of coastal aquifers as a groundwater resource

Coastal aquifers provide freshwater for more than a billion people worldwide (Ferguson & Gleeson, 2012). In New Zealand, most groundwater is extracted from coastal aquifers (PCE, 2015). However, coastal groundwater is at risk from saline groundwater at depth (due to over-extraction) and contaminant sources at land surface (due to pollution) (Michael et al., 2017). Globally, coastal areas often have high population densities with high water demands, which puts pressure on the groundwater supply and drives unsustainable use (Michael et al., 2017).

In Christchurch, New Zealand, aquifers provide one of the highest quality untreated drinking water sources in the world, which local residents completely rely on for critical needs (ECan, 2001). However, as per March 2018, the Christchurch water supply was temporarily chlorinated for up to 12 months, due to a risk of contamination from insecure well heads (CCC, 2018). The main water-bearing aquifer in Christchurch is the shallow confined Riccarton Gravel or Aquifer 1 with a depth of 5 – 40 m below ground (Hertel, 1998), which provides approximately 40% of the Christchurch water supply (ECan, 2001). However, it is also most prone to contamination from the surface and also seawater intrusion (ECan, 2001). According to ECan (2012), Christchurch coastal aquifers have the highest risk for SWI compared to other coastal aquifers along the Canterbury coastline, based on a GIS analysis. Hertel (1998) conducted a modelling study which indicated that the freshwater-seawater interface in the uppermost aquifer (Aquifer 1) was about 3 km offshore, instead of 40 km as previously thought by Talbot et al. (1986). Monitoring groundwater levels and abstraction

near the coast is important to manage the risk of seawater intrusion into coastal aquifers (ECan, 2001).

1.2. Seawater intrusion

Seawater intrusion (SWI) is the landward movement of the seawater-freshwater interface in coastal aquifers (Ferguson & Gleeson, 2012). Causes of SWI include groundwater pumping, sea level rise, reduced recharge and land drainage (Morgan et al., 2013a). The position of the seawater-freshwater interface is commonly characterized by the toe location of the seawater wedge (i.e., the intersection of the interface and the aquifer base) and seawater volume (Werner et al., 2012). SWI may occur by lateral intrusion from the ocean, upward intrusion from deeper and more saline parts of the groundwater system and downward intrusion from coastal waters (Barlow, 2003).

SWI had occurred in the Woolston/Heathcote area in Christchurch (Hertel, 1998), which extended approximately 2 km inland, and was considered to have the greatest extent of SWI inland in confined aquifers in New Zealand (PDP, 2011). The high rates of groundwater abstraction for industrial and public supply caused groundwater levels to decline below high tide levels for prolonged periods in the Woolston/Heathcote area (ECan, 2003). This resulted in a downward hydraulic gradient between the Avon Heathcote Estuary and the wells in the Woolston/Heathcote area, leading to the flow of saline water through the confining layer of the aquifer (Hertel, 1998). The SWI impact (i.e., high groundwater conductivity above the drinking water guideline) persisted for 30-40 years, which emphasises the vulnerability of the Christchurch confined aquifer system to SWI (ECan, 2012).

1.3. Sea level rise

Sea level rise increases saline water heads at the ocean boundary, and thus increases the propensity for SWI (Werner & Simmons, 2009). SWI risk due to sea level rise can be quantitatively assessed using steady-state analytical solutions (Section 2.2), e.g. Werner and Simmons (2009), Werner et al. (2012), and Morgan and Werner (2015).

The Intergovernmental Panel on Climate Change (IPCC) is an international body committed to assessing climate change, by evaluating recent scientific, technical, and socio-economic data produced globally (IPCC, n.d.). They employed four Representative Concentration Pathway (RCP) scenarios in their Fifth Assessment Report, which consist of different greenhouse gas (GHG) trajectories, to generate global mean sea level rise projections (Church et al., 2013). The four RCP scenarios from low to high projected GHG emissions are RCP2.6, RCP4.5, RCP6 and RCP8.5 (Church et al., 2013). Relative to 1986 – 2005, global sea level in 2081 – 2100 is projected to increase by 0.52 – 0.98 m (medium confidence) in the RCP8.5 scenario (Church et al., 2013). Riahi et al. (2011) defined RCP8.5 as a scenario that "combines assumptions about high population and relatively slow income growth with modest rates of technological change and energy intensity improvements, leading in the long term to high energy demand and GHG emissions in absence of climate change policies".

The New Zealand Ministry for the Environment (MfE) adopts the sea level rise projections from the IPCC Fourth Assessment Report as a risk management strategy to guide local governments when planning developments, infrastructure or assets (Ramsay et al., 2009). Around New Zealand, mean sea level has been observed to rise at the same rate as global trends, however it was projected to increase by 10% more than global sea level rise rates (Reisinger et al., 2014). The MfE advises to allow a base sea level rise of 0.5 m and also

consider the consequences of sea level rise of at least 0.8 m in 2090 – 2099, relative to the 1980 – 1999 average (Ramsay et al., 2009).

More recently, Hansen et al. (2016) predicted that the sea level can exponentially rise several meters in 50 – 150 years depending on fossil fuel emissions, as a result of accelerated ice sheet disintegration in Antarctica and Greenland (Figure 1). Hansen et al. (2016) used atmosphere-ocean modelling, information from paleoclimate data and observations from ongoing climate change to predict the sea level rise.

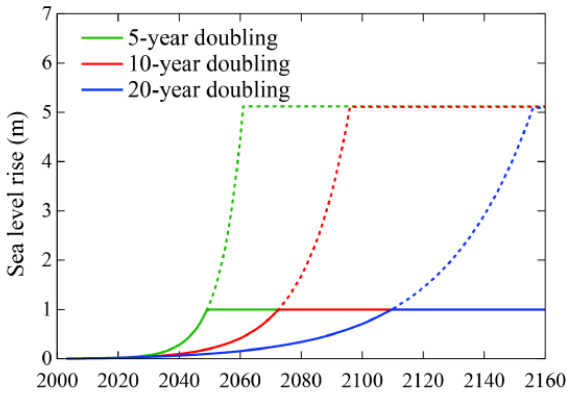

Figure 1. Sea level rise predictions as a result of ice sheet melting exponentially at three different rates (Hansen et al., 2016).

The current study used the RCP8.5 scenario of 0.98 m (rounded up to 1 m) and 2 m to assess seawater intrusion vulnerability in Christchurch.

Sea level rise can induce groundwater table rise, which results in freshwater inundation before seawater inundation occurs, especially in coastal plains (Rotzoll & Fletcher, 2012). Areas that are low-lying and where the water table is close to the surface are most vulnerable to freshwater inundation prior to seawater inundation following sea level rise (Rotzoll & Fletcher, 2012). The rise in water table may cause the creation of new wetlands and the

expansion of existing wetlands, saturation of soil, change in surface drainage, and inundation depending on local topography (Rotzoll & Fletcher, 2012). Seasonal variation such as periods of high rainfall combined with high tide events may exacerbate land inundation (Rotzoll & Fletcher, 2012). However, freshwater inundation is out of the scope of this study, hence it is not is not specifically taken into account in the GIS analysis of this study. Although, elements of land elevation and groundwater level in relation to mean sea level and how they change in sea level rise scenarios are included in this study.

1.4. Study objectives

The objectives of this study are to: (1) Assess SWI vulnerability using GALDIT (Lobo-Ferreira et al., 2007) based on current sea level and sea level rise scenarios, (2) Determine the seawater wedge toe position, and the propensity for the toe to move under sea level rise using the analytical solutions of Morgan and Werner (2015) in a GIS framework, for the first time, (3) Analyse and compare the two outputs, determine which method is best used to assess SWI vulnerability.

1.5. Hypotheses

1. Sea level rise will impact Christchurch coastal aquifers by decreasing the fresh groundwater flux to the sea and moving the seawater-freshwater interface landwards.
2. Analytic solutions, such as those developed by Morgan and Werner (2015), can be incorporated into a GIS framework for quantitatively assessing SWI vulnerability under SLR. This quantitative approach is superior to other qualitative methods such as GALDIT.
3. The Woolston/Heathcote area is most vulnerable to SWI in Christchurch based on past SWI occurrence.

2. Literature review

2.1. Methods for assessing SWI vulnerability associated with sea level rise

2.1.1. Geographic Information Systems (GIS) vulnerability mapping

SWI vulnerability can be qualitatively indexed using GIS-based methods, such as GALDIT (Lobo-Ferreira et al., 2007) and the Ebert et al. (2016) method. These methods are relatively simple to apply in large areas, however they involve some subjectivity and lack theoretical underpinnings when converting hydrogeological factors into SWI vulnerability (Werner et al., 2012). However, they can be useful as preliminary investigation techniques that take into account several hydrogeological factors. Sites that are deemed highly vulnerable to SWI can be prioritized to be further investigated (Werner et al., 2012). To overcome some of the limitations of these methods, the physically-based analytic solutions of Morgan and Werner (2015) were also (and for the first time), applied within a GIS framework as part of the present study.

More recently, a GIS vulnerability mapping method for saltwater up-coning called TAWLBIC was proposed by Motevalli et al. (2018). However, this method is not considered in this study. Saltwater up-coning is not restricted to the coast and may occur further inland, unlike seawater intrusion (Motevalli et al., 2018). TAWLBIC takes into account the type of aquifer, aquifer hydraulic conductivity, well density, bedrock topography, impact of existing status of saltwater up-coning, and cross-resistance. A new vulnerability mapping approach that integrates TAWLBIC and GALDIT called the Comprehensive Salinity Index or CSI was also proposed by Motevalli et al. (2018).

The Coastal Vulnerability Index to Sea Level Rise or CVI(SLR) method developed by Özyurt (2007) is also a GIS indexing method that assesses the vulnerability of the coastline to

the physical effects of sea level rise, but it does not assess SWI vulnerability. Hence this method is not considered in this study. The physical parameters that were taken into account in the CVI(SLR) method include rate of sea level rise, geomorphology, coastal slope, significant wave height, sediment budget, tidal range and others (Özyurt, 2007). Gornitz et al. (1994) also created a similar CVI(SLR) method focusing on the inundation and erosion risks of the coast.

Ebert et al. (2016) used a weighted overlay analysis as their GIS-based method to determine the vulnerability of SWI into wells in Gotland, Sweden. However, this method was not applied in this study. It takes into account several parameters that contribute to the risk of SWI into wells, which were distance to coast, distance to freshwater lakes, soil type, mean annual rainfall, and elevation above sea level.

ECan (2012) assessed SWI vulnerability using GIS along the Canterbury coastline, divided into 47 segments of about 10 km. Their method took into account several parameters with different weightings that affect the likelihood and consequences of SWI. These include groundwater abstraction (represented by the consented maximum volume to abstract), groundwater throughflow (assessed by recharge and aquifer transmissivity), minimum groundwater level, hydraulic connection at the coast (determined by coastal geology), vulnerability to climate change (determined by ground elevation), whether SWI has previously occurred and its level of impact (determined by conductivity levels and the length of time for recovery), current water use (determined by the size of community using the water), and aquifer type. A similar set of data was compiled in the present study, but this specific method was not applied. The Christchurch coastline from Rakaia to Amberley was identified as being most vulnerable to SWI, based on these parameters. However, the SWI

vulnerability of areas within Christchurch was not further identified. It may be important to note that based on this method, lower aquifer transmissivities indicate higher SWI vulnerability, in contrast to the GALDIT hydraulic conductivity parameter elaborated in the subsection below.

2.1.1.1.1. GALDIT method

Lobo-Ferreira et al. (2007) developed a large-scale qualitative indexing method called GALDIT to assess the vulnerability of coastal aquifers to seawater intrusion. The GALDIT approach employs six hydrogeological factors that Lobo-Ferreira et al. (2007) identify as contributing to the risk of SWI, which are:

1) **G**roundwater occurrence (aquifer type)

   This factor relates to the type of aquifer or geological layer where the groundwater occurs; confined, unconfined, leaky confined or bounded by impervious layer(s) parallel to the coast (Chachadi & Lobo-Ferreira, 2005). According to Chachadi and Lobo-Ferreira (2005), confined aquifers are more prone to SWI due to the generation of a larger cone of depression during pumping.

2) **A**quifer hydraulic conductivity

   Hydraulic conductivity refers to the rate of groundwater flow through the porous material of the aquifer (Moghaddam et al., 2017). The slower the flow, the lower the risk of SWI (Chachadi & Lobo-Ferreira, 2005).

3) **L**evel of groundwater above mean sea level (MSL)

   The level of groundwater above MSL indicates the hydraulic head driving groundwater flow to the coast (Chachadi & Lobo-Ferreira, 2005). The higher the level

of groundwater, the less risk there is of SWI (Chachadi & Lobo-Ferreira, 2005).

4) **D**istance perpendicular from the coast

   The risk of SWI decreases as one goes further away from the shore (Chachadi & Lobo-Ferreira, 2005).

5) **I**mpact of existing status of SWI (ratio of Cl^- : [HCO_3^- + CO_3^{2-}])

   Chloride ions (Cl^-) characterise seawater, while bicarbonate and carbonate (HCO_3^- and CO_3^{2-}) ions characterise groundwater (Chachadi & Lobo-Ferreira, 2005). Hence, the current groundwater status indicating SWI is represented as the ratio of Cl^- : [HCO_3^- + CO_3^{2-}] (Chachadi & Lobo-Ferreira, 2005).

6) **T**hickness of aquifer

   This factor refers to the aquifer thickness in a confined aquifer (distance between the bottom and top of aquifer) or saturated thickness in an unconfined aquifer (distance between the bottom and water table of aquifer) (Chachadi & Lobo-Ferreira, 2005). Increased aquifer thickness increases the risk of SWI.

The weightings and risk values for these factors are elaborated in Table 1. The influence of each parameter to SWI is defined by a risk value (R), which is multiplied by the weighting factor (V) to obtain the final weighted risk value (Equation 1). The weighted risk value can range from 37.5 to 150. To compute the final GALDIT index, the weighted risk value is divided by 15 (Equation 2).

Table 2 refers to the final GALDIT index ranges and their interpretations.

$$\text{Weighted risk value} = V_1 \cdot R_1 + V_2 \cdot R_2 + \cdots + V_n \cdot R_n = \sum V_i \cdot R_i \quad (1)$$

$$\text{GALDIT index} = \text{Weighted risk value} \div 15 \quad (2)$$

Table 1. GALDIT factors (Chachadi & Lobo-Ferreira, 2005).

Factor	Value	Class	Risk value	Weight
G groundwater occurrence (aquifer type)	Bounded aquifer	Least vulnerable	2.5	1
	Leaky-confined aquifer	Moderately vulnerable	5	
	Unconfined aquifer	Vulnerable	7.5	
	Confined aquifer	Highly vulnerable	10	
A aquifer hydraulic conductivity (m/day)	< 5	Very low	2.5	3
	5-10	Low	5	
	10-40	Medium	7.5	
	> 40	High	10	
L groundwater level above sea level (m)	> 2	Very low	2.5	4
	1.5-2	Low	5	
	1-1.5	Medium	7.5	
	< 1	High	10	
D distance from the shore (m)	> 1000	Far	2.5	4
	1000-750	Medium	5	
	750-500	Close	7.5	
	< 500	Very close	10	
I impact of existing status of seawater intrusion; $Cl^- : [HCO_3^- + CO_3^{2-}]$	<1	Very low	2.5	1
	1-1.5	Low	5	
	1.5-2	Medium	7.5	
	>2	High	10	
T thickness of aquifer	< 5	Very thin	2.5	2
	5-7.5	Thin	5	
	7.5-10	Medium	7.5	
	>10	Thick	10	

Table 2. GALDIT index ranges and the corresponding vulnerability classes.

GALDIT Index Range	Vulnerability Classes
≥ 7.5	High vulnerability
5 – 7.5	Moderate vulnerability
< 5	Low vulnerability

2.1.2. Analytic modelling

The steady-state analytic approach used in this study is based on the equations of Strack (1976) which estimate the location of the freshwater – seawater interface in idealised coastal aquifers. Conceptual models for unconfined and confined coastal aquifers showing parameters used in the analytic equations are shown in Figure 2 and notation described in Table 5 of Appendix B. This approach is, arguably, more mathematically and physically justifiable compared to the GIS vulnerability mapping methods (Morgan et al., 2013a; Werner et al., 2012). However, it is important to note that the method assumes steady state conditions, a sharp interface, homogeneous aquifer properties and uniform hydrologic stresses (Morgan et al., 2013a). The present study only considers confined aquifers.

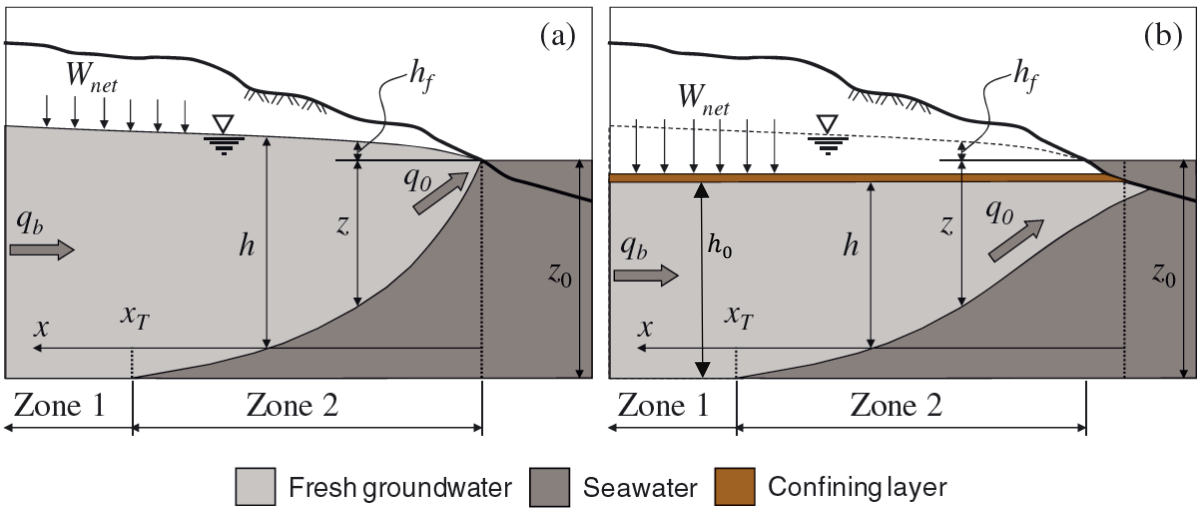

Figure 2. Conceptual diagram of the groundwater-seawater interface based on the steady-state sharp interface approach in an unconfined aquifer (a) and confined aquifer (b), sourced from Werner et al. (2012).

Equation (3) below describes the seawater wedge toe position, x_T [L], in a confined aquifer, where net recharge, W_{net} [L^2/T] is zero (Werner et al., 2012):

$$x_T = \frac{K\delta {h_0}^2}{2q_0} \quad (W_{net} = 0) \tag{3}$$

It is common to assume zero recharge in the case of confined aquifers (Morgan & Werner, 2015). Here, h_0 [L] is the saturated aquifer thickness inland of x_T. δ [-] is the dimensionless density ratio derived from $(\rho_s - \rho_f) / \rho_f$, where ρ_s [M/L^3] is seawater density, and ρ_f [M/L^3] is freshwater density. K [L/T] represents hydraulic conductivity. q_0 [L^2/T] is freshwater discharge to the sea from a confined aquifer at the coast, as described in Equation (4) for the case where the water level relative to MSL (h_b [L]) is measured at a location relative to the coast (x_b [L]), that is equal to or further inland than x_T (Morgan & Werner, 2015):

$$q_o = \frac{K}{2\delta x_b}(2\delta h_b h_0 + (\delta h_0)^2 - 2\delta^2 z_0 h_0) + \frac{W_{net} x_b}{2} \quad (x_b \geq x_T, h_b > \delta(z_0 - h_0)) \tag{4}$$

Here, z_0 [L] represents the distance between MSL and the bottom of the aquifer.
Equation (5) below derives the freshwater discharge to sea in a confined aquifer, where water level is measured at a location on the coastal side of the seawater wedge toe position (Morgan & Werner, 2015):

$$q_0 = \frac{K}{2\delta x_b}(h_b + \delta h_0 - \delta z_0)^2 + \frac{W_{net} x_b}{2} \quad (x_b < x_T, h_b > \delta(z_0 - h_0)) \tag{5}$$

The Ghyben-Herzberg relation $z = h_b / \delta$ was used to determine whether the water level is measured inland or coastward of the toe (Morgan et al., 2013a). It was considered that $h_b = z_0 \delta$ at the toe. Hence if $h_b \geq z_0 \delta$, water level is measured equal to or inland of the toe, while if $h_b < z_0 \delta$, water level is measured coastward of the toe.

The density-corrected freshwater head in confined aquifers that end at the coast is represented in Equation (6) (Morgan et al., 2013b). To have fresh groundwater discharge to the sea ($q_0 > 0$), the head in the aquifer or h_b is required to be greater than h_{coast} (Morgan et al., 2013b), which is described in Equation (6) below. It is important to compare h_b and h_{coast} to: (i) Avoid a false positive q_0 due to the squared values in Equation (5), and (ii) Detect active

SWI which occurs when $h_b < h_{coast}$ due to the downward hydraulic gradient in the inland direction (Morgan et al., 2013b).

$$h_{coast} = \delta(z_0 - h_0) \quad (6)$$

The analytic solutions discussed here assumes that the confined aquifer terminates at the coast and does not extend offshore (Morgan et al., 2013b). The analytic solutions presented by Bakker et al. (2017), Bakker (2006) and Kooi and Groen (2001) account for the extension of confined coastal aquifers offshore. Werner and Robinson (2018) further developed these analytical solutions for the extent of offshore fresh groundwater in confined aquifers, by including the offshore aquitard salinity as an input variable. However, the application of their methods is outside of the scope of this study.

Sea level rise is represented by an increase in z_0, with two different freshwater-seawater boundary conditions: (1) fixed flux boundary and (2) fixed head boundary (Werner et al., 2012). The fixed flux boundary condition assumes that groundwater discharge to the sea remains constant despite sea level rise, and the groundwater level inland changes freely (Werner et al., 2012). The fixed head boundary condition assumes that the groundwater level inland remains the same despite sea level rise, which can be due to increased pumping, increased evapotranspiration or groundwater seepage, and/or head is controlled by a surface water feature (Werner et al., 2012). The fixed head boundary assumes the worst-case scenario due to the decrease in groundwater level relative to MSL, under sea level rise conditions.

Equation (7) below describes the propensity for x_T to move due to sea level rise under head-controlled and no net recharge conditions in confined aquifers, which was derived by differentiating equation (3) (Werner et al., 2012):

$$\frac{\partial x_T}{\partial z_0} = \frac{\delta(1+\delta)K^2{h_0}^3}{2{q_0}^2 x_b} \quad (W_{net} = 0) \tag{7}$$

Werner et al. (2012) showed that SLR does not effect the toe position in flux-controlled settings.

Ferguson and Gleeson (2012) applied a modified version of the Strack (1976) analytical model and used GIS to synthesize coastal aquifers based on hydrogeological parameters (i.e. hydraulic gradient), population densities and recorded SWI cases in the United States. They found that SLR has a minimal effect on SWI risk compared to groundwater extraction, based on a fixed head boundary condition (Ferguson & Gleeson, 2012, 2013). However, Lu et al. (2013) commented that the distribution of inland boundary conditions need to be assessed more thoroughly, and changes in seawater volume should be considered, before arriving at the aforementioned conclusions.

Cook et al. (2013) conducted a vulnerability factor analysis as a first pass, national-scale assessment of SWI vulnerability indicators for Australia. They evaluated groundwater levels (trends, minimum levels and inter-decadal changes in minimum levels), rainfall trends, salinity (maximum salinity and inter-decadal changes in salinity), and groundwater extraction from production wells (locations and rates). The present study has compiled information similar to Cook et al. (2013) on groundwater levels, recharge, salinity (related to conductivity and Cl : HCO_3), and groundwater extraction (represented as consented groundwater take).

2.2. Hydrogeology of the Christchurch coastal aquifers

2.2.1. Geology

Christchurch lies on multi-layered aquifers that comprise four confined aquifers namely the Riccarton, Linwood, Burwood, and Wainoni Gravel (Figure 3) (Begg et al., 2015; ECan, 2001). The main water-bearing aquifer in Christchurch is the Riccarton Gravel or Aquifer 1, which is the uppermost aquifer at 5 – 40 m depth below the surface (Hertel, 1998). In 2001 it was reported that over 40% of the Christchurch water supply was taken from this aquifer (ECan, 2001). However, since then groundwater extraction is increasingly from deeper aquifers, due to concerns around contamination, although data on groundwater extraction from the different aquifers is not publically available. Groundwater extraction in Christchurch is further discussed in Appendix A. The confined aquifers and aquitards lie in the coastal area of Christchurch, stretching from the continental shelf, to approximately 12 km inland (ECan, 2001; Begg et al., 2015). The aquifers and aquitards were formed during the Middle and Late Quartenary on the geologic timescale, as a result of glacial/interglacial cycles and sea level fluctuations (Begg et al., 2015). The west of Christchurch and the rest of Canterbury Plains lie on predominantly unconfined and semi-confined aquifers (Begg et al., 2015; ECan, 2001).

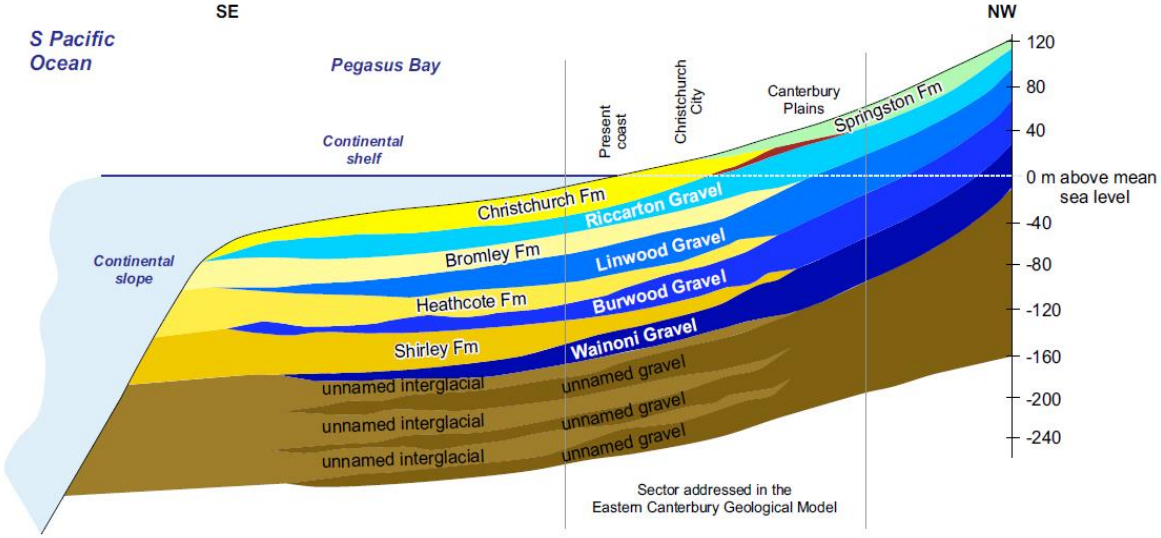

Figure 3. Diagrammatic cross-section of Quarternary deposits that compose the groundwater system underneath Christchurch (Begg et al., 2015). Adapted from Brown & Weeber (1992), Browne & Naish (2003), and Forsyth et al. (2008).

The Christchurch Formation is considered to be an aquitard, which is defined as a layer with low permeability that can store groundwater and transmit it from the aquifer(s) it is connected to (Fetter, 2001). The water level in the Christchurch Formation is often referred to as the water table, and it is actively pumped by numerous wells that contribute to the Christchurch water supply (Canterbury Maps, 2018c). There has also been recorded incidences of saline water leakage from the Avon-Heathcote estuary, through the Christchurch Formation, into the Riccarton Gravel aquifer (Hertel, 1998). It is acknowledged that the Christchurch aquifer system may be categorized as semi-confined, but for the purposes of the analysis, it is considered as a confined aquifer system.

2.2.2. Hydraulic heads

Hydraulic head is the elevation to which groundwater rises relative to a datum, which is usually mean sea level (MSL) (Fetter, 2001). Hydraulic head is a measure of the total energy of fluid in the porous media or aquifer matrix (Fetter, 2001). It is measured using a piezometer, which is a pipe with open ends that is drilled or installed into an aquifer (Fetter, 2001). The change in hydraulic heads over a distance is expressed as hydraulic gradient (Fetter, 2001). In an unconfined aquifer, hydraulic head is equal to the water table (Fetter, 2001). In a confined aquifer, the groundwater is under pressure and the hydraulic head rises above the top of the aquifer (Fetter, 2001). Groundwater flows from high to low hydraulic head (Fetter, 2001).

Figure 4 shows the average hydraulic (or piezometric) head contour map of the confined Riccarton Gravel aquifer in Christchurch, using water level data from wells of three or more readings (Weeber, 2008). Hydraulic heads onshore indicate the groundwater flows to the coast (Lobo-Ferreira et al., 2007).

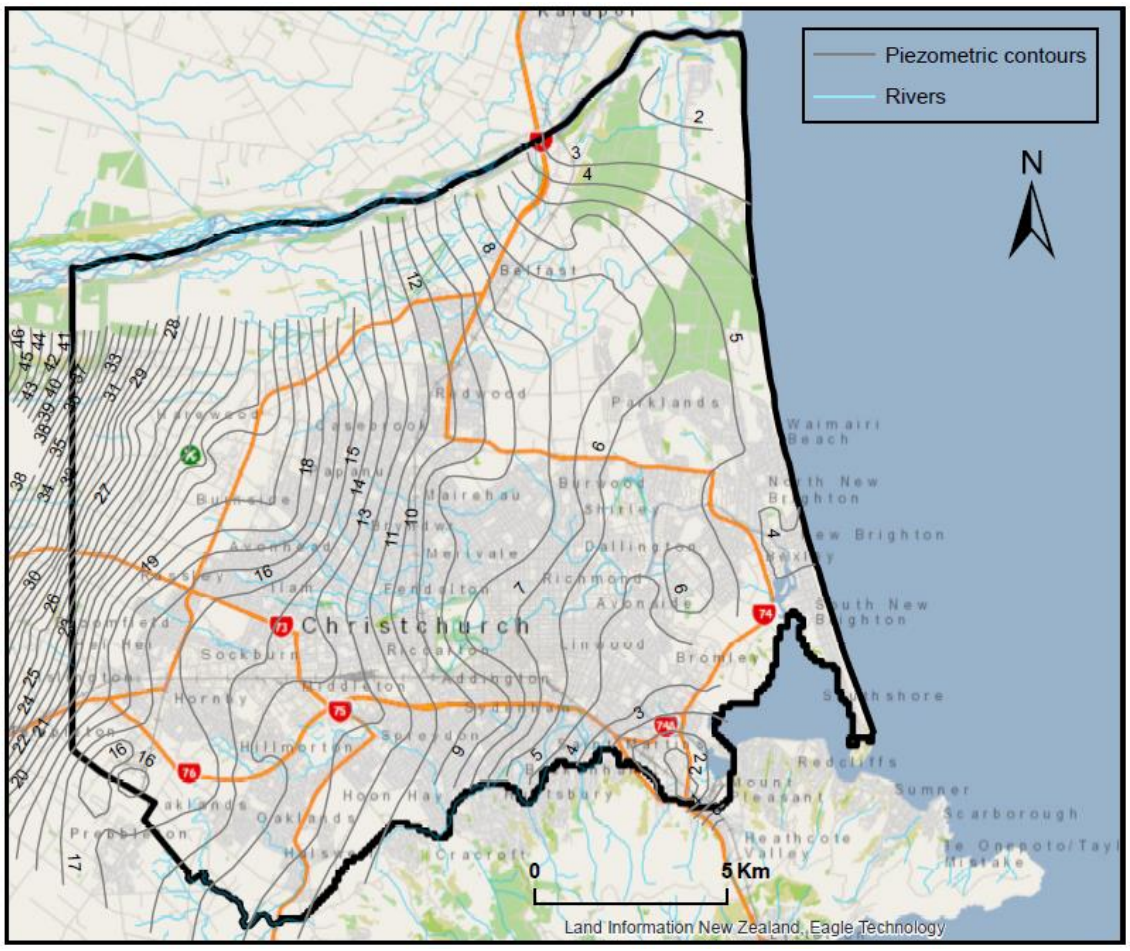

Figure 4. Average piezometric contours of the Riccarton Gravel aquifer, using water level data from wells of three or more readings, by Weeber (2008). Retrieved from Canterbury Maps (2017b).

2.2.3. Recharge

The recharge of the Christchurch confined aquifers is dominantly sourced from the leakage of the Waimakariri River flow (White et al., 2012). Rainfall in the Southern Alps and foothills contribute to the Waimakariri River flow (ECan, 2001). Other sources of groundwater recharge include rainfall infiltration into the unconfined aquifers, and upward movement of older and deeper groundwater to the aquifer above it (ECan, 2001; White et al., 2012). Rainfall constitutes 32% of land-based recharge in Christchurch, where the mean annual rainfall is 682 mm/year (ECan, 2004).

2.2.4. Salinity

Salinity is a measure of the total dissolved salts in the water (CalEPA, 2004). While conductivity is the capability of water to conduct electric current, which is related to the concentration of major ions and total dissolved solids (mostly mineral salts) (Chapman, 1996). Dissolved ions increase the amount of salinity and conductivity, hence the two measures are related (CalEPA, 2004). Figure 5 shows the average of sampled groundwater conductivity in 2012 – 2016, although the different aquifers and depths were not taken into account. As a comparison, the conductivity of drinking water ranges from 5 – 50 mS/m, while the conductivity of seawater is about 5000 mS/m (Lenntech, n.d.).

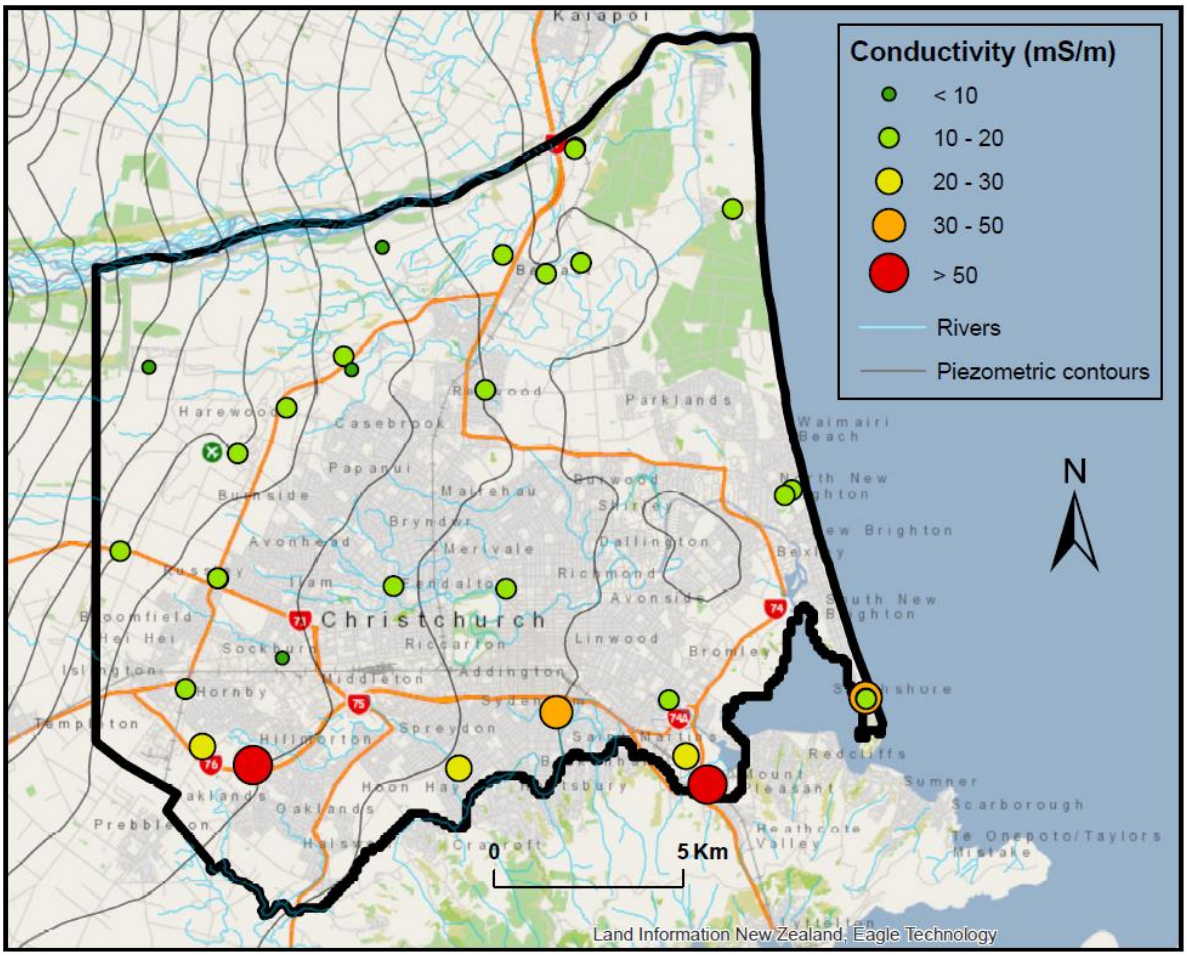

Figure 5. Average groundwater conductivity (mS/m) in 2012 – 2016 in Christchurch (ECan, 2016).

Salinity is also strongly related to Chloride ions (Cl^-) (Vernier, n.d.), which characterise seawater, while bicarbonate and carbonate (HCO_3^- and CO_3^{2-}) ions characterise groundwater (Chachadi & Lobo-Ferreira, 2005). The current groundwater status indicating SWI can be represented as the ratio of Cl^- : [HCO_3^- + CO_3^{2-}] (Chachadi & Lobo-Ferreira, 2005). For simplicity reasons, the average ratio of Cl^- : HCO_3^- was used, following Lobo-Ferreira et al. (2007) and Trabelsi et al. (2016).

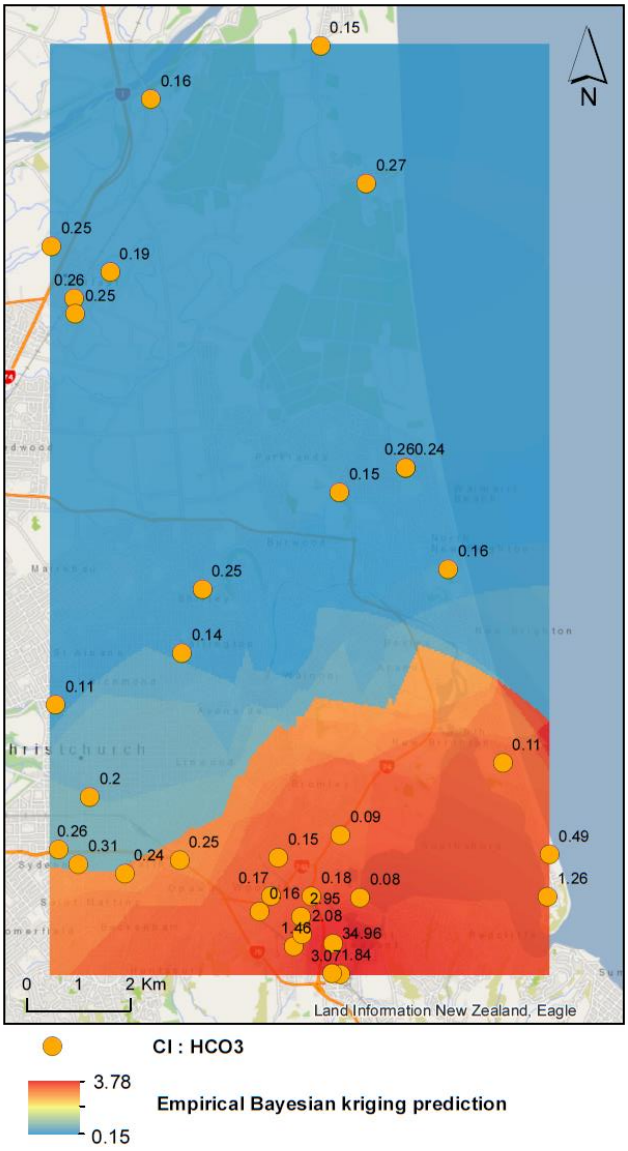

Figure 6. Cl : HCO_3 Empirical Bayesian kriging prediction map.

The majority of sampled wells had Cl : HCO_3 ratios of less than one, which classify them as low risk in terms of existing SWI impact (Chachadi & Lobo-Ferreira, 2005). Cl : HCO_3 ratios of more than two, indicating very high risk in terms of existing SWI impact, were centred around Woolston. Well M36/1159 in Woolston had an average ratio of 34.96 from 1983 to 2010 (n=34), which markedly increased the surrounding spatial average (Figure 6). There has been recorded incidence of localised seawater intrusion in the Woolston/Heathcote area, due to primarily the flow of saline water from the Avon Heathcote Estuary through the confining layer of the aquifer (Hertel, 1998). A downward hydraulic gradient between the estuary and the wells in the Woolston/Heathcote area led to the SWI (Hertel, 1998). The effect of SWI lasted for a

relatively long period of time compared to other recorded SWI sites in New Zealand (Figure 7), potentially due to the shallow bedrock in the area which limits groundwater recharge, and lack of management (Charteris, 1999; ECan, 2016; PDP, 2011). The average conductivity of well M36/1159 from December 1983 to November 2010 was 478 mS/m (n=39). The well was damaged in the earthquake and was not repaired, hence the data stopped in 2010. The peak conductivity was 700 mS/m in January 2001 (Figure 7). This well had the highest average conductivity compared to the other wells within the locality of the estuary (ECan, 2016). As a comparison, the median conductivity of Canterbury groundwater was 17 mS/m according to the 2001 annual groundwater quality survey of 243 wells (ECan, 2003), and 12.8 mS/m according to the 2014 and 2015 annual groundwater quality survey of 28 wells in the Christchurch-West Melton area (ECan, 2015). From this, the Woolston/Heathcote area may be the most vulnerable to SWI in Christchurch.

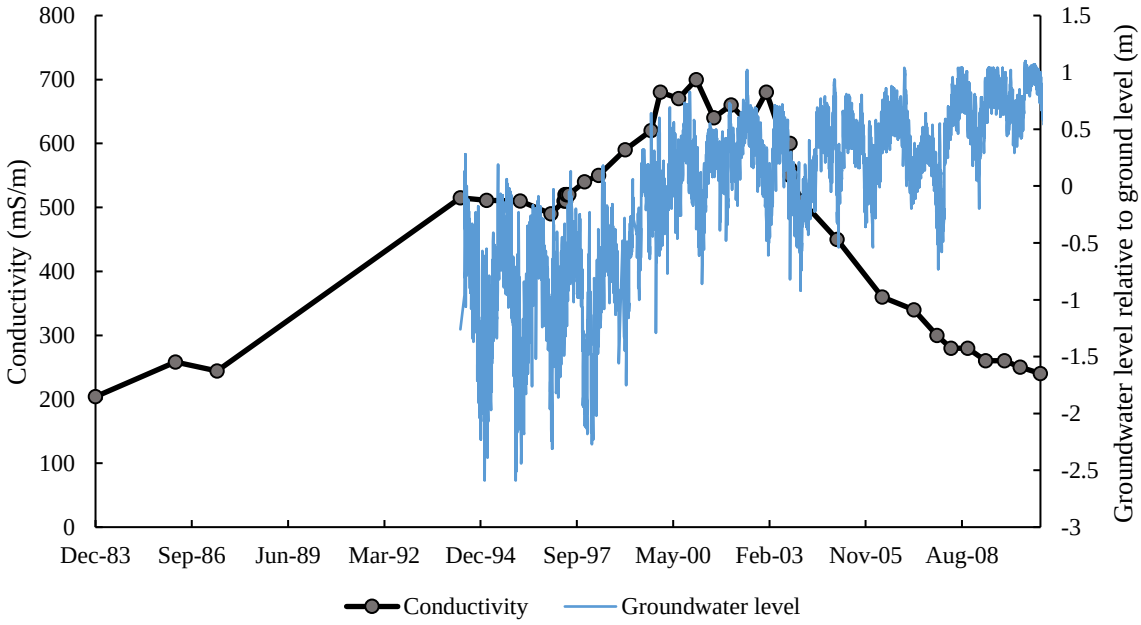

Figure 7. Conductivity and groundwater level of well M36/1159 located on Scruttons Road, Ferrymead (ECan, 2016, 2017).

3. Methodology

3.1. Study area

The study area was located in Christchurch (Figure 8), which is on the east coast of New Zealand's South Island. The study area was 210 km^2, with the coastal area being the main focus of the study. The study area was chosen according to the coverage of available data listed in Table 3.

Figure 8. Study area map.

3.2. Data

The data used, types and sources in the GALDIT analysis are listed in Table 3.

Table 3. Data used, types, and sources.

Data	Type	Source
Christchurch boundary	Vector polygon	Lincoln University network (J:\Data\Administrative_Boundaries)
Groundwater quality (Cl^- : HCO_3^-)	Table	Data requests to ECan
Christchurch 1 m digital elevation model (DEM)	Raster	LINZ (2015)
Canterbury 1m DEM	Raster	LINZ (2014)
Water level	Table	ECan online well database, data requests to ECan
Aquifer type	Vector polygon	Canterbury Maps (2017a)
Thickness of the Riccarton Gravel aquifer	Raster (resolution 100 m)	Begg et al. (2015)
Top and bottom elevation of the Riccarton Gravel aquifer, relative to the Lyttelton 1937 datum	Raster (resolution 100 m)	Begg et al. (2015)
Aquifer test wells (transmissivity values)	Points	Canterbury Maps (2018a)
Hydraulic conductivity values	Table	CRC (1997), Lovell & Weeber (2000), Ettema (1999), Bowden Environmental (2017), and McLean (2018)

3.3. GALDIT method

The GALDIT method (described above in Section 2.1.1.1.1) was applied to assess SWI vulnerability in Christchurch. The details and derivation of each hydrogeological factor that contribute to SWI vulnerability in Christchurch, are in the subsections below and Figure 65 in Appendix B. Essentially, all the obtained polygon and raster layers were reclassified

according to the GALDIT risk values in Table 1. The point layers were interpolated into raster, before they were reclassified according to the GALDIT risk values.

3.3.1. Groundwater occurrence (aquifer type)

The Christchurch aquifer type polygons were derived from Canterbury Maps (2017b) (Table 3), however there were holes found in the confined aquifer polygon (Figure 9). The holes corresponded to areas with less than three metres thickness of fine surface sediments, which may classify them as unconfined aquifers (Weeber, 2008). However, they are within the area of upward pressure gradient, i.e. discharge zone (Weeber, 2008) and were grouped as confined aquifers for simplicity. These particular areas, in any case, are not within 5 km of the coast. One exception was the hole located on the intersection between Lincoln Road and State Highway 76; it was located on the boundary between the upward and downward pressure gradient zones (Weeber, 2008). Hence, it may be more conservative to categorise the hole as unconfined aquifer. The aquifer types were then reclassified according to the respective GALDIT risk values.

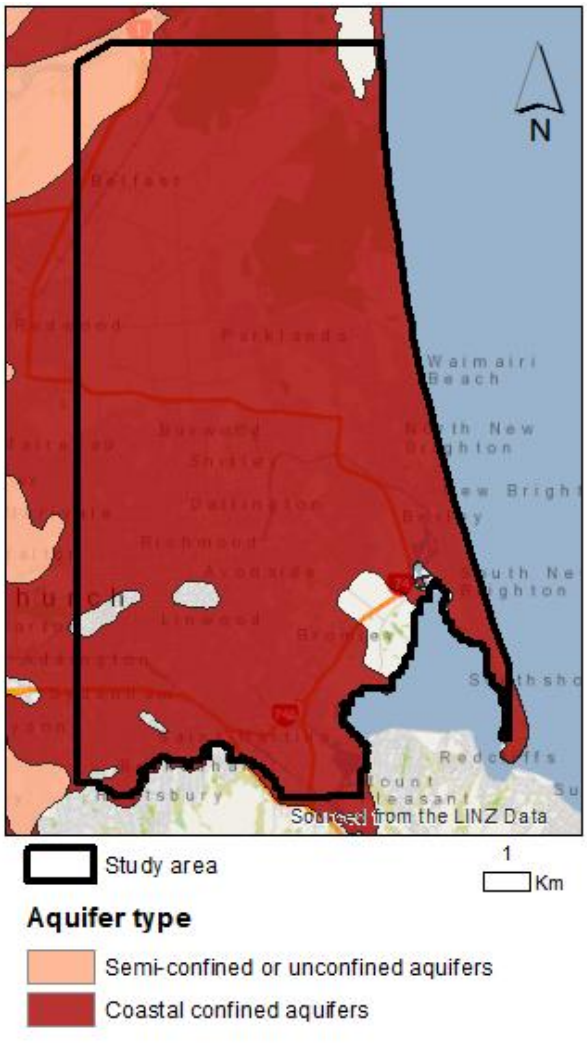

Figure 9. Aquifer types within the study area from Canterbury Maps (2017b).

3.3.2. Aquifer hydraulic conductivity

The hydraulic conductivity values of the Riccarton Gravel aquifer were derived from: (i) the Aquifer Test Wells point layer from Canterbury Maps (2018), and (ii) literature review from CRC (1997), Lovell & Weeber (2000), Ettema, (1999), Bowden Environmental, (2017), and McLean, (2018).

The Aquifer Test Wells point layer (Table 3) are wells that had an aquifer test undertaken, which generated data including transmissivity values. The values derived from literature also included both transmissivity and hydraulic conductivity. Transmissivity is the flow of water under one unit of hydraulic gradient, through one unit of saturated aquifer thickness width (Fetter, 2001). Transmissivity can be related to hydraulic conductivity and saturated aquifer thickness using the equation $T = K\,b$, where T [L^2/T] is transmissivity, K [L/T] is hydraulic conductivity, and b [L] is saturated aquifer thickness (Fetter, 2001). Aquifer thickness was derived from Begg et al. (2015), using the extract multi values to points tool. The hydraulic conductivity values were derived based on the equation using field calculator.

The hydraulic conductivity point values within and around the study area were used for the analysis. The aquifer which the individual wells are tapping into were identified using:

- Ground elevation (1 m resolution) raster layer relative to the NZVD2016 (New Zealand Vertical Datum 2016) from LINZ (2014, 2015),
- Point layer of the offsets between New Zealand Vertical Datum 2016 (NZVD2016) and Lyttelton 1937 (LINZ, 2017a) interpolated into a raster surface using the natural neighbour tool with a resolution of five metres, and

- Top and bottom elevations of the Riccarton Gravel aquifer, relative to the Lyttelton 1937 datum (Begg et al., 2015).

The ground elevation was converted from NZVD2016 to Lyttelton 1937 datum by adding the offset grid values using the raster calculator. Then, the well depth relative to the Lyttelton 1937 datum was derived by subtracting the well depth from ground level to the ground elevation relative to the Lyttelton 1937 datum (Figure 10). Finally, the wells that had depths within the top and bottom Riccarton Gravel aquifer elevations were kept, and the remaining wells were removed. The hydraulic conductivity values were interpolated using the Empirical Bayesian Kriging tool to create a raster layer. The hydraulic conductivity values were then reclassified according to the respective GALDIT risk values.

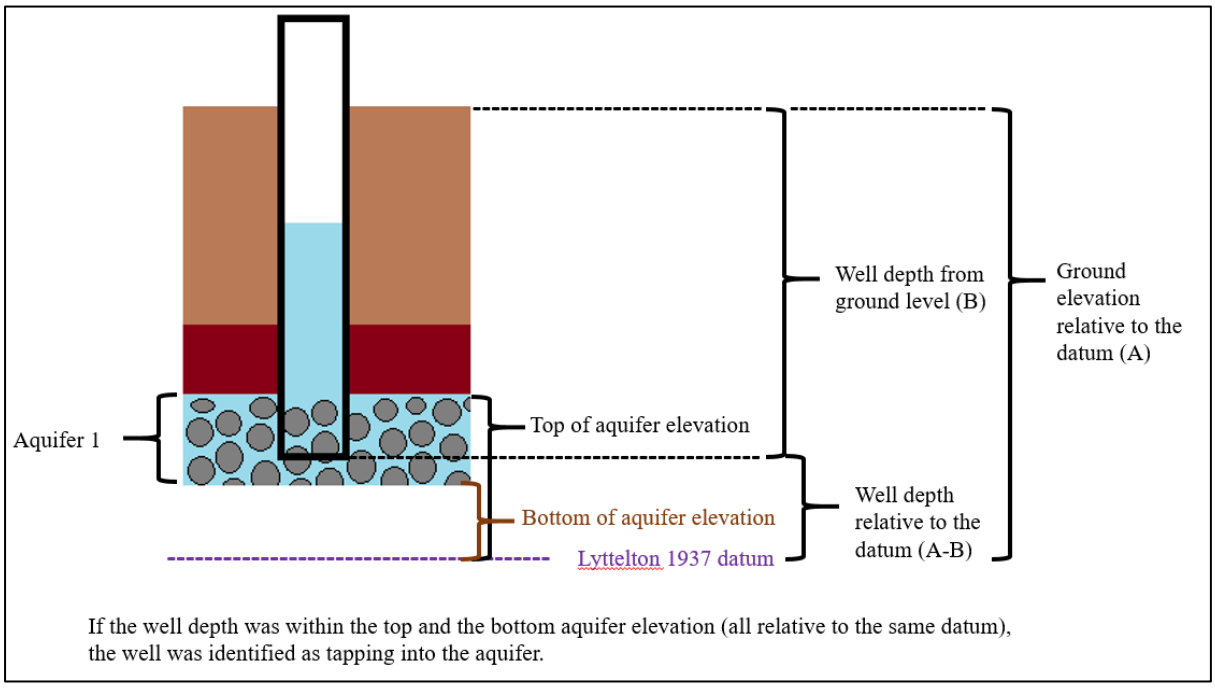

Figure 10. Illustration of how each well was identified as tapping into the Riccarton Gravel aquifer.

3.3.3. Level of groundwater above MSL

The first aspect of deriving this parameter is the groundwater level data. The groundwater levels in the Riccarton Gravel aquifer relative to ground level, were derived from the Environment Canterbury (ECan) online well database and data requests to ECan. Minimum groundwater levels were used in this parameter to consider the highest SWI risk due to maximum inland head stress. A 20-year time frame was used whenever possible to derive minimum groundwater levels. In cases where the 2010 and 2011 Christchurch earthquakes, or other possible disruptions deviated the water level readings (i.e. caused major outliers in the hydrographs), the outliers were manually removed from the dataset, and were not used in deriving averages or minimum levels. Data from previous years were used to achieve the 20-year time frame, in the case of major data removal (i.e. over one year). Wells that have readings for a period of less than 20 years were still used as water level data points. The minimum time frame used was three years. Seasonal water level variations were taken into account by using data that end and start on the same month (e.g. July 1997 to July 2017). A large proportion of time was devoted to assure high quality data.

The raw data or information gathered to derive groundwater level relative to MSL were:

- Minimum water level relative to ground level, which is negative (if it is below ground level) or positive (if it is above ground level)
- Ground elevation (1 m resolution) raster layer relative to the NZVD2016 (New Zealand Vertical Datum 2016) from LINZ (2014, 2015)
- Point layer of the offsets between NZVD2016 and Lyttelton 1937 (LINZ, 2017a) interpolated into a raster surface using the natural neighbour tool with a resolution of five metres

- MSL relative to the Lyttelton 1937 datum is 3.098 m, based on tidal observation data from 1998 – 2016 (LINZ, 2017b) (Figure 11). This was derived from the Lyttelton datum relative to the chart datum (4.508 m), subtracted by MSL relative to the chart datum datum (1.41 m).

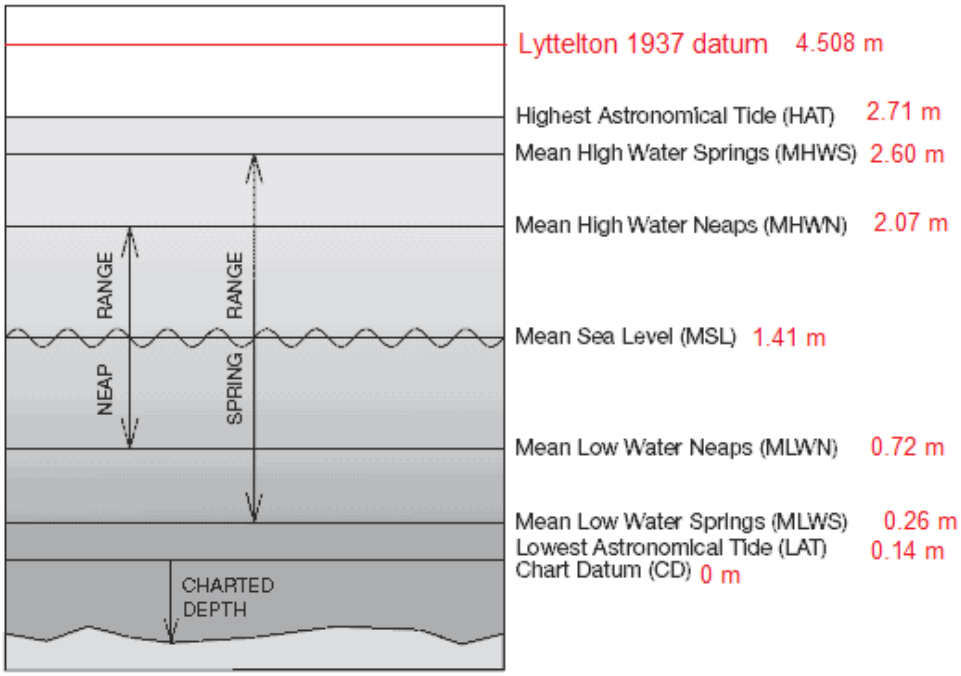

Figure 11. Tidal terms diagram from LINZ (2018), with added information of Lyttelton tidal levels from LINZ (2017b).

First, the extract multi values to points tool was used to extract the raster values of ground elevation relative to NZVD2016 and offset grid values between NZVD2016 and Lyttelton 1937 at each well point. Groundwater level relative to MSL at each well point was derived by adding groundwater level relative to ground level, ground elevation relative to NZVD2016, MSL relative to the Lyttelton 1937 datum (3.098 m), and the NZVD2016 to Lyttelton 1937 offset grid values, using the field calculator (Figure 12). The groundwater level relative to

MSL points were interpolated using the Empirical Bayesian Kriging tool to create a raster layer, then reclassified according to the respective GALDIT risk values.

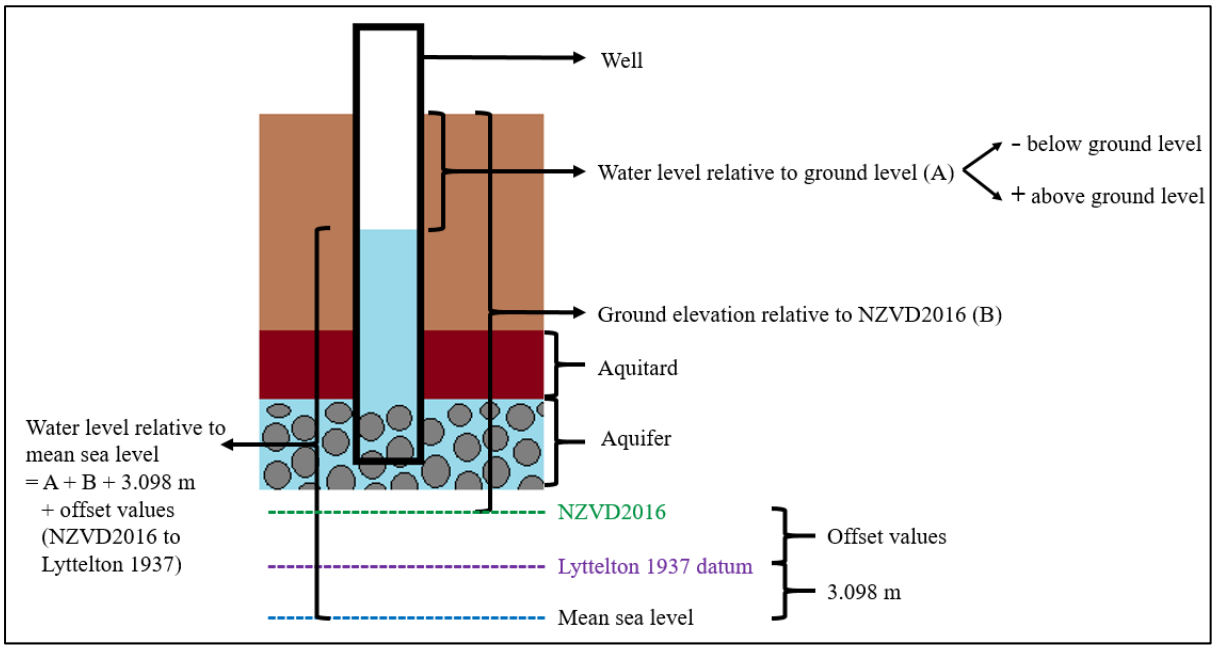

Figure 12. The derivation of groundwater level relative to MSL.

3.3.4. Distance from the coast

First, the coastline including the Avon-Heathcote estuary was traced based on the NZTM basemap while checking the satellite imagery. Then, the Euclidean distance tool was used to create a raster layer of distance from the coast. The resulting layer was clipped to the study area, and reclassified according to the GALDIT risk values.

3.3.5. Impact of existing status of SWI (ratio of Cl^- : $[HCO_3^- + CO_3^{2-}]$)

For simplicity reasons, this study used the average ratio of Cl^- : HCO_3^- to determine this parameter, following Lobo-Ferreira et al. (2005) and Trabelsi et al. (2016). Groundwater quality data were derived by requesting data from ECan. No time frame was chosen to derive

the average ratio of Cl^- : HCO_3^-; all historical water quality data were used to derive the average. This was to indicate the propensity of SWI to occur. The calculation to derive the ratio was (Cl^- (mg/L) ÷ 35.45) ÷ (Alkalinity as HCO_3^- (mg/L) ÷ 61).

The method to identify the wells that tap into the Riccarton Gravel aquifer were filtered out by joining the attribute table with another table from ECan that has information on aquifer name derived from bore log data. They were selected and exported as a new layer. The resulting point layer was geostatistically interpolated using the empirical Bayesian kriging tool to create a continuous raster layer of Cl^- : HCO_3^-. The semivariogram model type used was power, and no data transformation was applied. The search neighbourhood parameter was set to standard circular, with the radius of 6 km, maximum neighbours of 15, and minimum neighbours of 1. This was adjusted according to the density of the sampled wells. The measure tool was used to gauge the maximum distance between wells. The layer was then clipped to fit the study area geometry, then reclassified according to the GALDIT risk values.

3.3.6. Thickness of aquifer

The raster layer of the Riccarton Gravel aquifer thickness was derived from Begg et al. (2015). The geological map was created by interpolating available water bore log data and therefore it was not a completely accurate representation of the aquifer. However, it was the most reliable one available. Three aquifer thickness cells were found with no data located in the Woolston area, around the intersection of Gould Crescent and Ferry Road. The focal statistics tool was used to derive the average of the surrounding cells to fill the hole within the layer. The layer was then clipped to the study area. It was subsequently reclassified according to the GALDIT risk values.

3.3.7. Analysis

The prepared raster layers of the GALDIT factors were combined using raster calculator, while taking their individual weightings into account. The map algebra expression inputted based on the weightings was G*1 + A*3 + L*4 + D*4 + I*1 + T*2. The resulting raster layer resolution was based on the coarsest raster layer, which was thickness of aquifer (resolution of 100 m).

3.3.8. Sea level rise

The GALDIT factors that changed in the sea level rise (SLR) scenario were: (i) Level of groundwater relative to MSL and (ii) Distance from the coast.

3.3.8.1. Level of groundwater relative to MSL

The change in level of groundwater relative to MSL due to SLR depends on the boundary condition. The fixed head boundary condition represents the worst case scenario because the groundwater level inland remains constant despite SLR, resulting in decreased groundwater level relative to MSL in the SLR scenarios. For example, a SLR of 1 m will result in a decrease of 1 m in groundwater level relative to MSL. While the fixed flux boundary condition assumes that the groundwater flux to the sea remains constant despite SLR and the groundwater level inland changes with SLR. For example, a SLR of 1 m will result in a 1 m rise in groundwater level in the aquifer. Consequently, the groundwater level relative to MSL does not change in the SLR scenarios based on the fixed flux boundary condition. The conservative fixed head boundary condition was applied to both 1 m and 2 m SLR scenarios, while the fixed flux boundary condition was applied to only the 2 m SLR scenario. It is also important to note that the Riccarton Gravel aquifer is considered a confined aquifer, thus a

potentiometric head above the ground level is possible in the fixed head scenario. Therefore, the groundwater level hitting the ground surface is not an issue in the analysis.

To derive the groundwater level relative to MSL in the 1 m SLR fixed head scenario, the current groundwater level relative to MSL layer was subtracted by 1 m using the raster calculator. Similarly, to derive the groundwater level relative to MSL in the 2 m SLR fixed head scenario, the current groundwater level relative to MSL layer was subtracted by 2 m. In contrast, the current groundwater level relative to MSL layer was used in the 2 m SLR fixed flux scenario because the SLR did not impact the groundwater level onshore in this scenario. The derived values were then reclassified into GALDIT risk values.

3.3.8.2. Distance from the coast

The mean high water spring (MHWS) was considered to represent a conservative high tide scenario based on 1 m and 2 m SLR. MHWS describes the highest level that spring tides reach around every new and full moon, on average, over a long timescale of usually 18-20 years (MfE, 2017). Generally, only 10 – 15% of all high tides exceed the nautical MHWS in New Zealand, except the central-eastern coasts of the South Island such as Kaikoura, where nearly 43% of high tides exceed the MHWS level (MfE, 2017). The assessment of land inundated by sea water in this study was based on the MHWS level, rather than MSL. It is important to note that MHWS was used to derive the distance to coast layers under the sea level rise scenarios, in contrast to the measure of groundwater level in the aquifer which was relative to MSL.

MSL and MHWS are 1.19 m apart based on the Lyttelton tidal levels (Figure 11), derived from MHWS relative to the chart datum (2.60 m) subtracted by MSL relative to the chart datum (1.41 m). Therefore, land with elevation below 2.19 m relative to MSL was classified as inundated with sea water under 1 m SLR at the MHWS level. This was derived from the 1.19 m difference in MHWS and MSL, added with the 1 m SLR (Figure 13). While in the 2 m SLR scenario, land with elevation below 3.19 m relative to MSL was classified as inundated with sea water at the MHWS level.

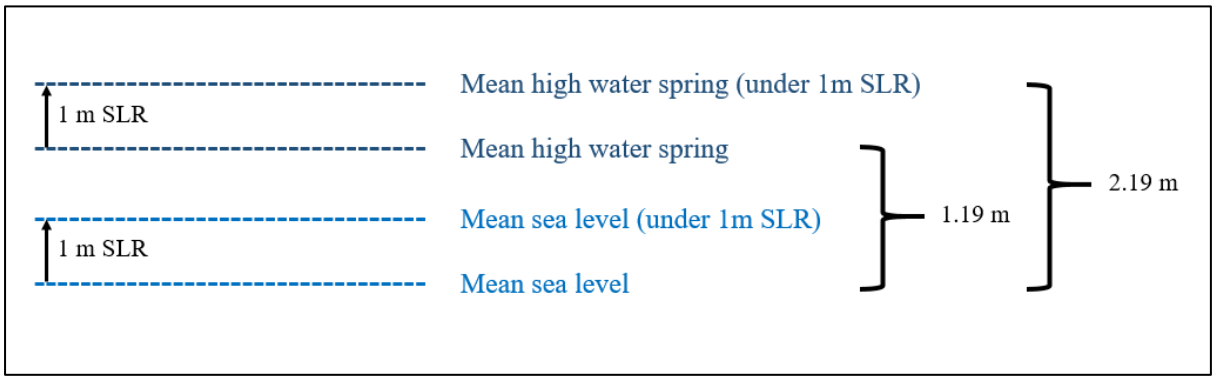

Figure 13. Mean high water spring under 1 m SLR relative to current MSL based on Lyttelton tidal levels (LINZ, 2017b).

The inundated land under SLR conditions was considered the new coastline. Therefore, the distance to coast under SLR conditions was altered. To accomplish this, the inundated land polygon was converted to line, merged with the existing coastline, then the Euclidean distance tool was used to derive distance to the new coast under SLR conditions. Then, the values were reclassified into to the GALDIT risk values according to Table 1 (Figure 65 in Appendix B).

3.4. Analytic solutions in a GIS framework

The analytic solutions of Morgan and Werner (2015) were applied in a GIS framework, for the first time. The parameters used in the analytic equations here are described interchangeably with their notation listed in Table 5 in Appendix B. The derivation of each equation parameter is described below and in Figure 66 in Appendix B. x_T and q_0 values along the coast, at a distance of 500 m perpendicular from the coast, were visualized as a strip of raster cells.

3.4.1. Freshwater discharge, q_0

q_0 was derived by preparing raster layers for each equation parameter; K, h_0, h_b, z_0, and x_b. The equation parameter layers except for z_0 were the same as for the GALDIT method in Section 3.3 before they were reclassified into GALDIT risk values. While the δ used was 0.025, in line with Morgan et al. (2013a).

The equation to derive q_0 depends on whether the water level is measured at a location on the inland (Equation 4) or coastal (Equation 5) side of the seawater wedge toe position. If $h_b \geq z_0 \delta$, water level is measured inland of the toe, while if $h_b < z_0 \delta$, water level is measured coastward of the toe. If $h_b \geq z_0 \delta$ holds true for all of the study area, the method assumes that the toe is anchored at the coast and does not take into account offshore toe locations. The conditional evaluation in the raster calculator was used to determine this. The raster calculator input used was = Con(h_b >= z_0 * 0.025, 1, 2).

3.4.1.1. Groundwater level relative to MSL, h_b

The groundwater level relative to MSL layer under current sea level was derived as per Section 3.3.3. The groundwater level relative to MSL under SLR conditions was derived as per Section 3.3.8.1. The interpolated raster layers derived by empirical Bayesian kriging were used.

3.4.1.2. Hydraulic conductivity, K

The hydraulic conductivity was derived as per Section 3.3.2. The interpolated raster layer derived by empirical Bayesian kriging was used.

3.4.1.3. Saturated aquifer thickness, h_0

The saturated aquifer thickness was derived as per Section 3.3.6.

3.4.1.4. Distance between MSL and bottom of aquifer, z_0

The distance between MSL and bottom of aquifer was derived by adding the bottom of aquifer elevation relative to the Lyttelton datum (negative if below the datum and positive if above the datum) and 3.098 m, which is the distance between the Lyttelton datum and MSL (Figure 14).

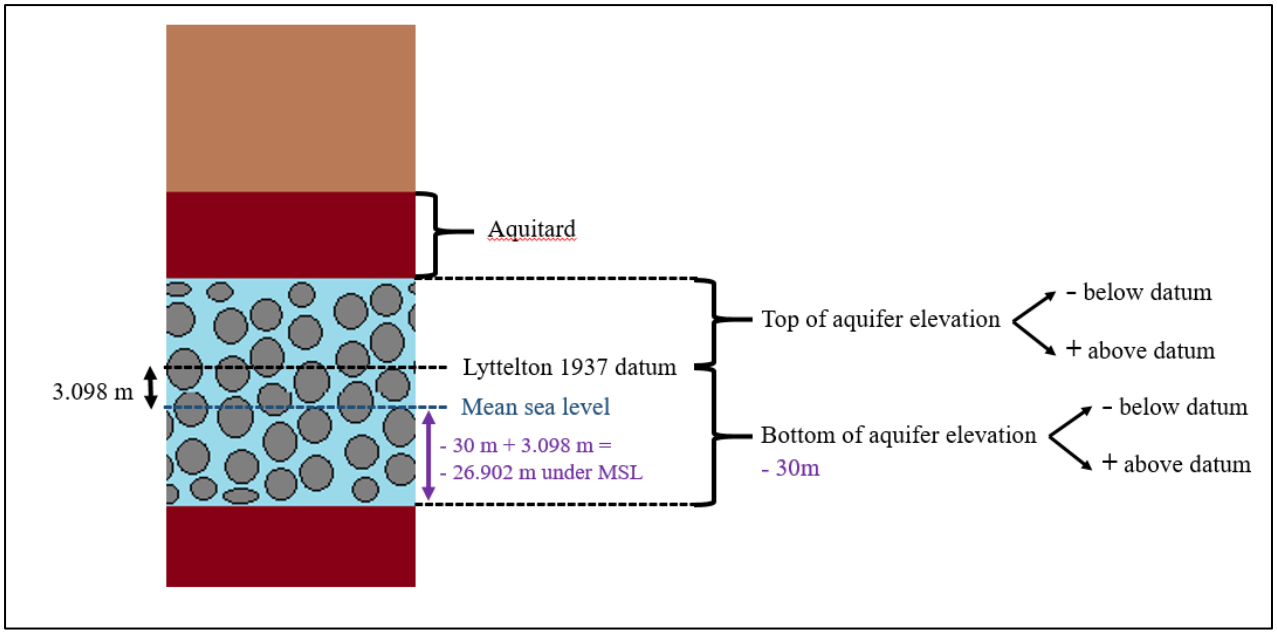

Figure 14. The derivation of distance between MSL and bottom of aquifer elevation. An example of - 30 m bottom aquifer elevation relative to the Lyttelton 1937 datum was given.

3.4.1.5. Distance from the coast, x_b

Distance from the coast under current sea level was derived as per Section 3.3.4. Distance from the coast under SLR conditions was derived as per Section 3.3.8.2.

3.4.1.6. Analysis

The raster calculator was used to process the parameters to derive q_0. If the condition of $h_b \geq z_0\ \delta$ was met, Equation 4 was used. The equation was broken down into four simpler components (A, B, C, D) to derive q_0. The following inputs were made in the raster calculator to derive A, B, C, D, and ultimately q_0:

- A = 0.05 * h_b * h_0
- B = Power(0.025 * h_0, 2)
- C = 0.00125 * z_0 * h_0

- D = 0.05 * x_b
- q_0 = K * ("A" + "B " - "C") / "D"

The method of breaking down the equation into components resulted in a more accurate q_0 output when compared to manual calculations, in comparison to another method of directly inputting the whole equation in the raster calculator at once. The latter method used the following input in the raster calculator: (K * (0.05 * h_b * h_0 + Power(0.025 * h_0, 2) - (0.00125 * z_0 * h_0))) / (0.05 * x_b). The resulting q_0 raster layer using the break down method was then used as one of the equation parameters to derive x_T. Retrospectively, improving the alignment of raster layers used in the equation could have increased the accuracy of the q_0 output layer (more in Section 5.2.1).

If the condition of $h_b < z_0\ \delta$ was met, Equation 5 was used. The equation was broken down into two steps to derive q_0. The following inputs were made in the raster calculator:

- A = Power(h_b + 0.025 * h_0 - 0.025 * z_0, 2)
- q_0 = K * "A" / (0.05 * x_b)

It is important to note that h_b and z_0 were adjusted according to the boundary condition and SLR scenarios.

3.4.2. Seawater wedge toe position relative to the coast, x_T

x_T was derived using Equation 3, which requires the parameters q_0, K, and h_0. The derivation of these parameters were discussed in Section 3.4.1 above. The raster calculator input to derive the x_T layer was: K * 0.025 * Power(h_0, 2) / (2 * q_0). The output was cross-checked with manual calculations, which proved to be accurate.

3.4.3. *Sea level rise*

SLR was represented as the increase in z_0. For example, z_0 increased by 1 m in the 1 m SLR scenario, and z_0 increased by 2 m in the 2 m SLR scenarios regardless of the inland boundary condition. In the SLR scenarios, the same h_b and x_b raster layers were used as per Section 3.3.8.

The density-corrected freshwater head (h_{coast}; Equation 6) was compared against groundwater level relative to MSL (h_b) based on the different boundary condition and SLR scenarios using the conditional evaluation in the raster calculator. The following input were made in the raster calculator to compare h_b and h_{coast}: Con(h_b <= 0.025 * (z_0 - h_0), 0, 1). Areas where h_b < h_{coast} were categorized as areas of active SWI and therefore represented accordingly on the map.

3.4.4. *Propensity for x_T to move under sea level rise, $\partial x_T / \partial z_0$*

$\partial x_T / \partial z_0$ was derived using Equation 7 in the raster calculator. The parameters required were K, h_0, q_0, and x_b. The raster calculator input was: (0.025 * 1.025 * Power(K, 2) * Power(h_0, 3)) / (2 * Power(q_0, 2) * x_b).

3.4.5. *Visualization of q_0 and x_T*

The q_0 and x_T values along the coast at a distance of 500 m perpendicular from the coast were visualized because it was assumed that the interface would not extend inland beyond 500 m. To achieve this, a polygon to clip the raster layers along the coast at a distance of 500 m perpendicular from the coast was created. Both q_0 and x_T raster layers were clipped, and symbolized accordingly. Due to the physical change in the coastline shape in the SLR

scenarios, raster cells which were: (i) Intersecting the projected SLR, (ii) Located less than 500 m from the coast, and (iii) Located in areas of active SWI ($h_b \leq h_{coast}$) were removed because they gave misleading values and were not comparable against values along the coast at a distance of 500 m perpendicular from the coast. For example, cells that intersect the projected SLR had q_0 values that were higher by orders of magnitude compared to the neighbouring cells.

4. Results

4.1. GALDIT method

The GALDIT method was applied to produce SWI vulnerability maps. The end results were GALDIT index maps based on the current sea level, 1 m SLR (fixed head), and 2 m SLR (fixed head and fixed flux) scenarios. Each of the hydrogeological factor layers are shown in the subsections below. The map colour scheme from green to red indicates increasing susceptibility of each factor to SWI.

4.1.1. Groundwater occurrence (aquifer type)

The aquifer type within the study area was primarily categorized as confined (Weeber, 2008), which had the highest risk of SWI according to the GALDIT method (Figure 15). The exception was the area proximal to the Waimakariri River.

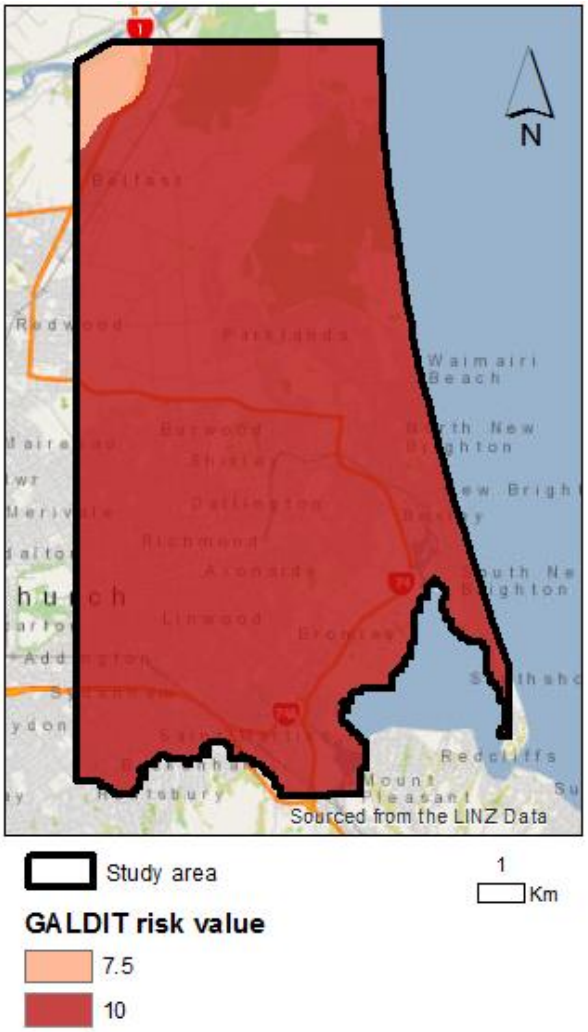

Figure 15. GALDIT risk values based on aquifer type; 7.5 (vulnerable; unconfined aquifer) and 10 (highly vulnerable; confined aquifer).

4.1.2. Aquifer hydraulic conductivity

The Riccarton Gravel aquifer hydraulic conductivity within the study area ranged from 32 – 292 m/day based on the gathered data (Figure 16). The Riccarton Gravel hydraulic conductivity generally increased towards the north of the study area, indicating a greater risk for SWI (Figure 16). However, the GALDIT approach categorized nearly the whole of the study area as only one group (> 40 m/day), as having the highest risk (Figure 17).

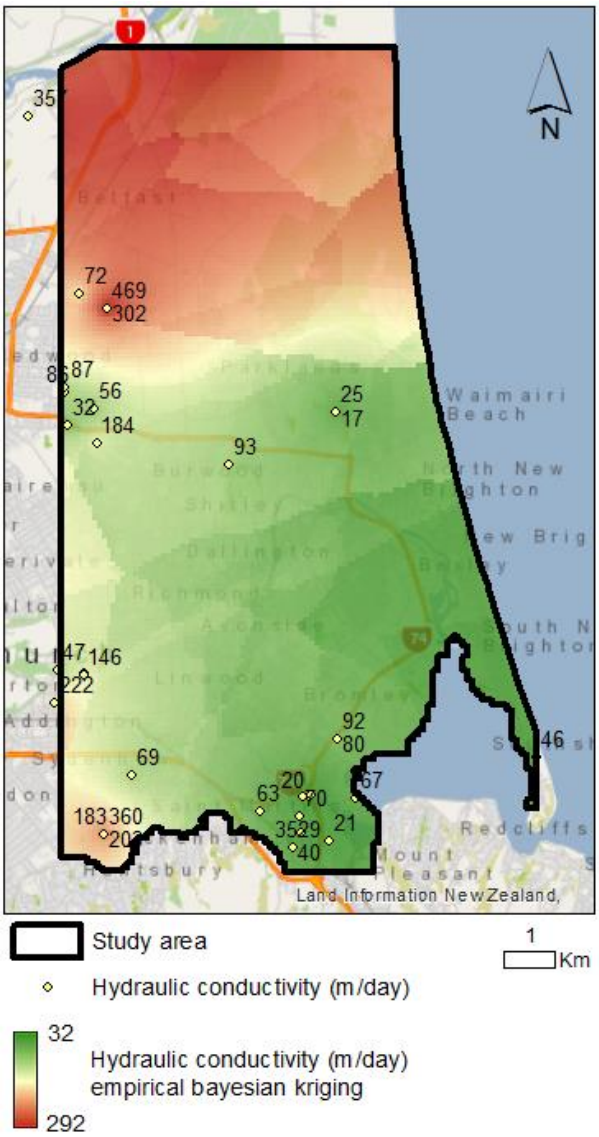

Figure 16. Hydraulic conductivity empirical Bayesian kriging interpolation across the study area.

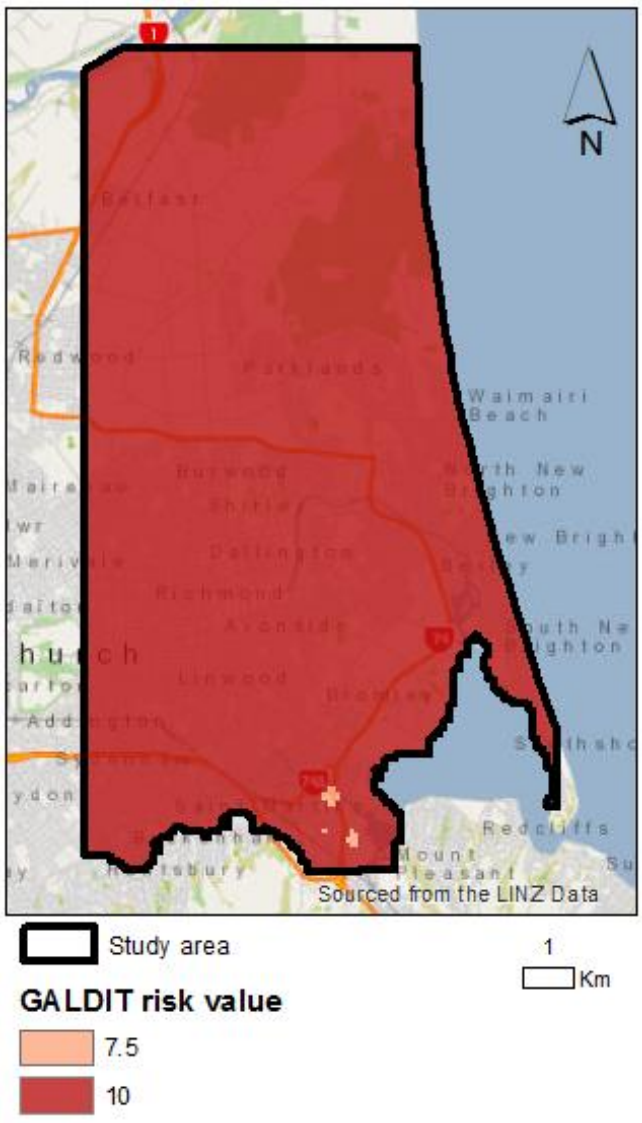

Figure 17. GALDIT risk values based on hydraulic conductivity; 7.5 (medium; 10 – 40 m/day) and 10 (high; > 40 m/day).

4.1.3. Level of groundwater above MSL

The minimum level of groundwater above MSL based on a 3 – 20 year time frame within the study area ranged from 1.6 to 11.7 m above MSL (Figure 18). The vast majority of the study area was categorized as having very low risk (> 2 m above MSL), while the southwest of the estuary and the north side of the coast were categorized as having low risk (1.5 – 2 m above MSL) (Figure 19).

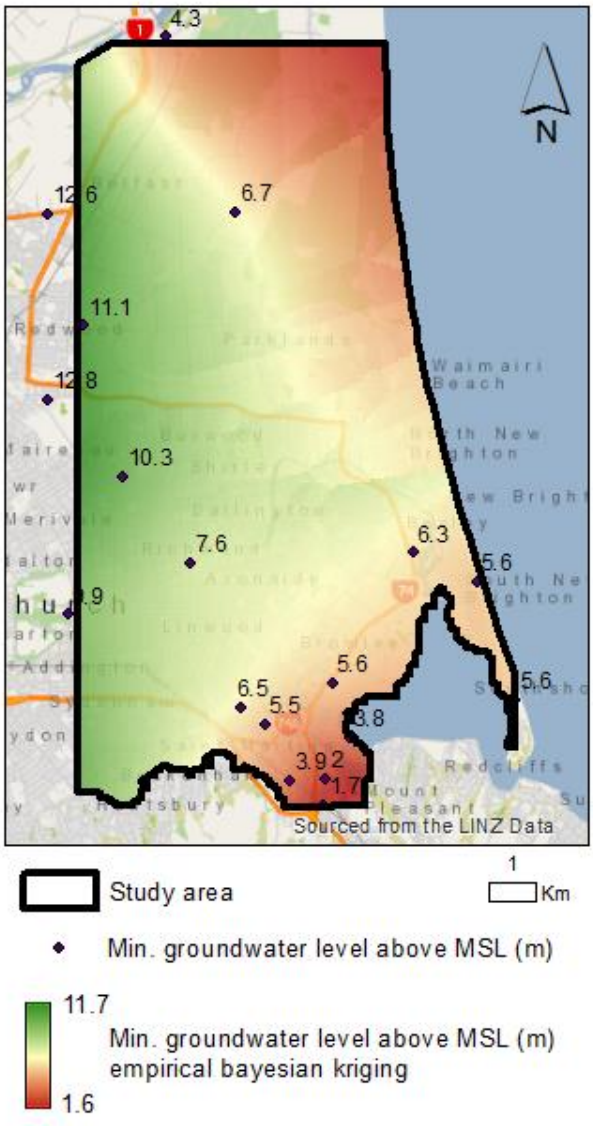

Figure 18. Minimum groundwater level above MSL empirical Bayesian kriging interpolation across the study area.

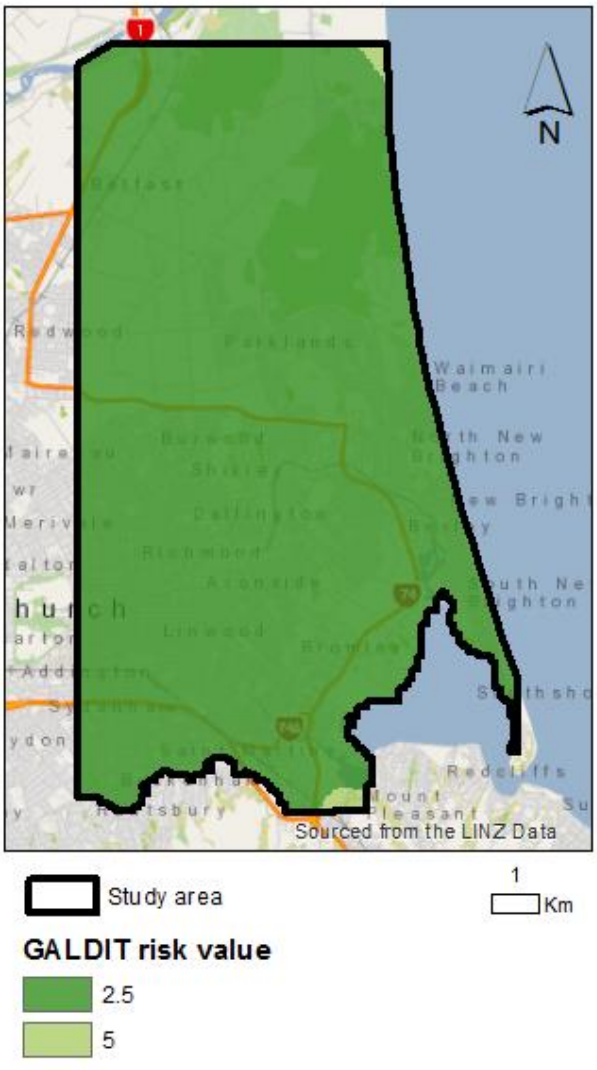

Figure 19. GALDIT risk values based on groundwater level above MSL; 2.5 (very low; > 2 m) and 5 (low; 1.5 – 2 m).

4.1.4. Distance from the coast

The distance perpendicular from the coast (including estuary) based on the current sea level is shown in Figure 20. The distance from the coast based on the current sea level reclassified into GALDIT risk values is shown in Figure 21.

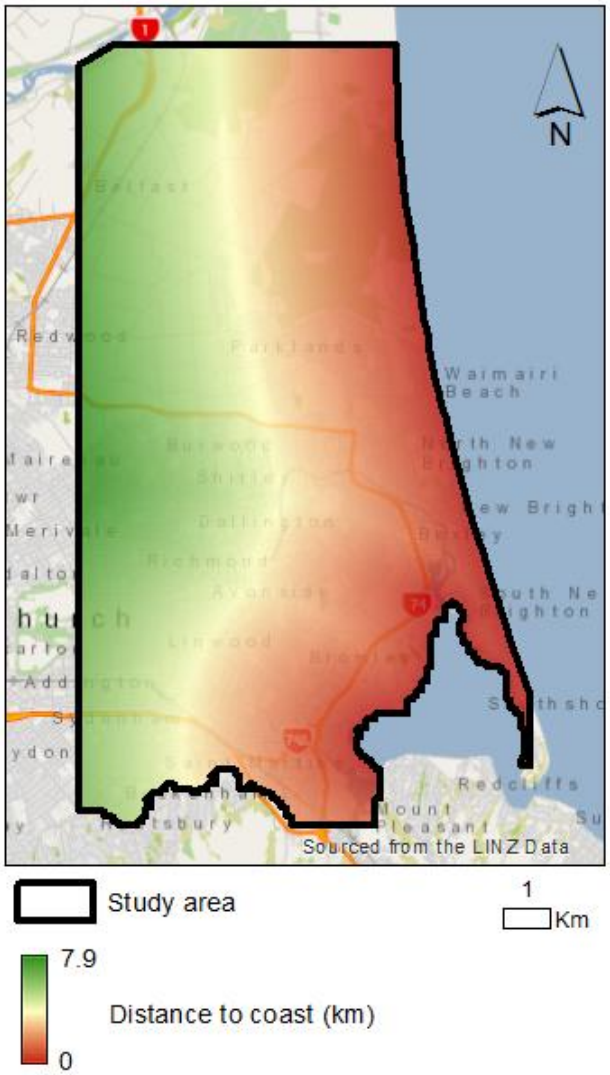

Figure 20. Distance from the coast (km) across the study area.

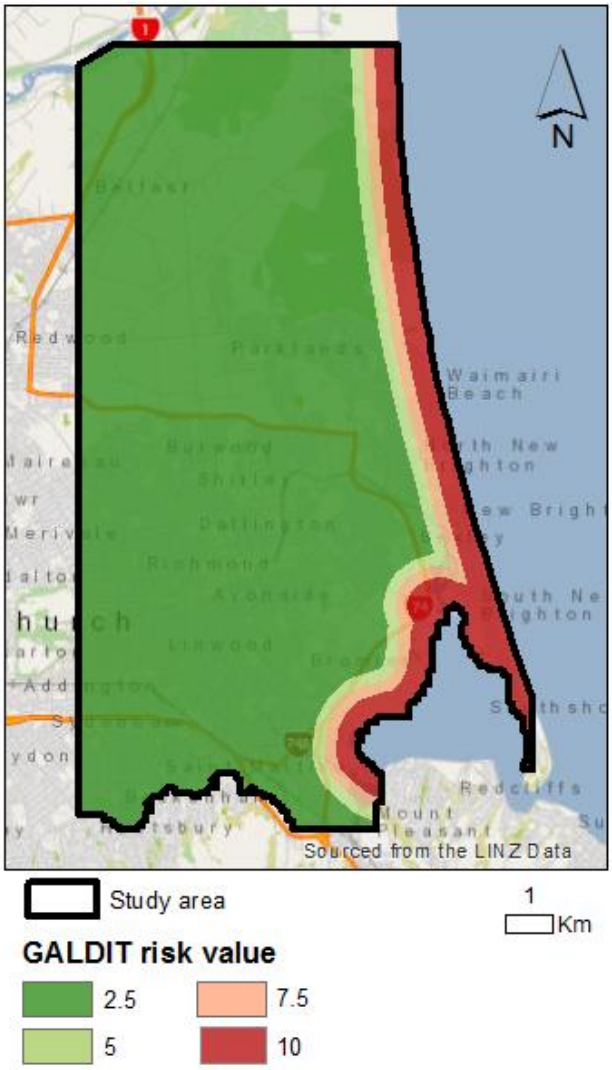

Figure 21. GALDIT risk values based on distance from the coast (km); 2.5 (far; > 1000 m), 5 (medium; 1000 – 750 m), 7.5 (close; 750 – 500 m), and 10 (very close; < 500 m).

4.1.5. Impact of existing status of SWI

The area around the Avon-Heathcote estuary had the highest risk of SWI with regards to current groundwater quality measurements (Cl^- : HCO_3^-) (Figure 22). The Cl^- : HCO_3^- layer reclassified into GALDIT risk values is shown in Figure 23.

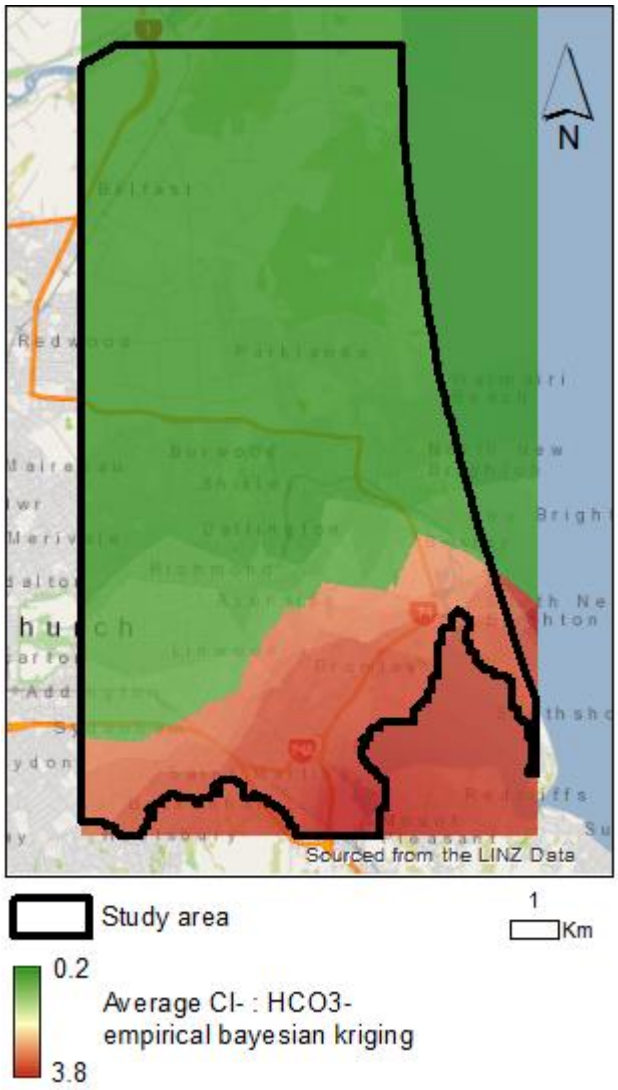

Figure 22. Average Cl^- : HCO_3^- empirical bayesian kriging across the study area.

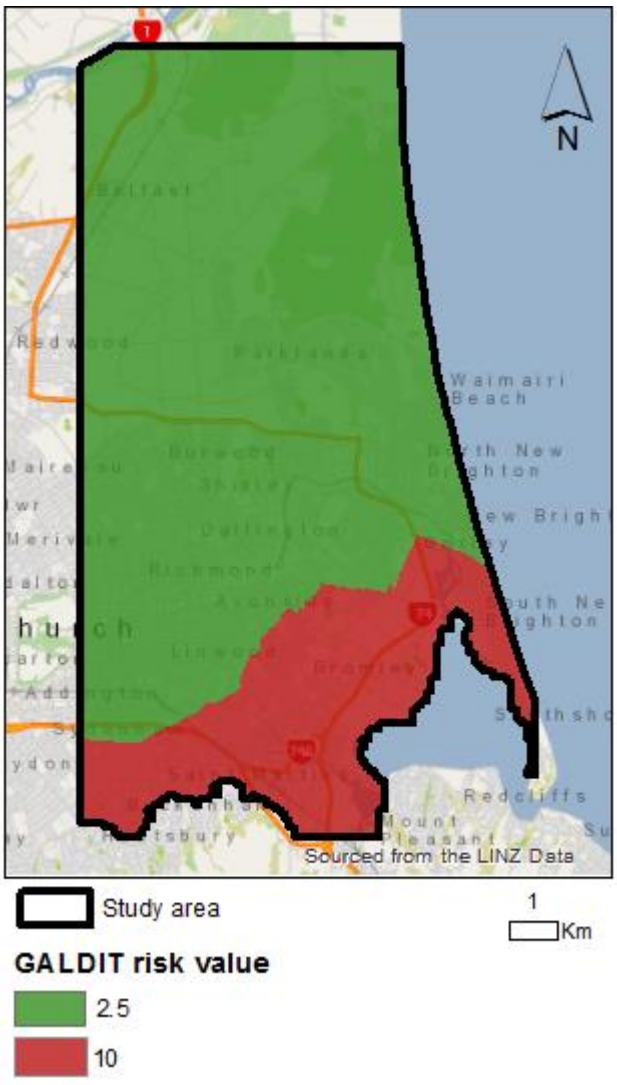

Figure 23. GALDIT risk values based on Cl^- : HCO_3^-; 2.5 (very low; < 1) and 10 (high; > 2).

4.1.6. Thickness of aquifer

The thickness of Riccarton Gravel aquifer layer from Begg et al. (2015) is shown in Figure 24. The aquifer thickened in the inland direction, and thinned towards the Port Hills. The aquifer thickness layer reclassified into GALDIT risk values is shown in Figure 25.

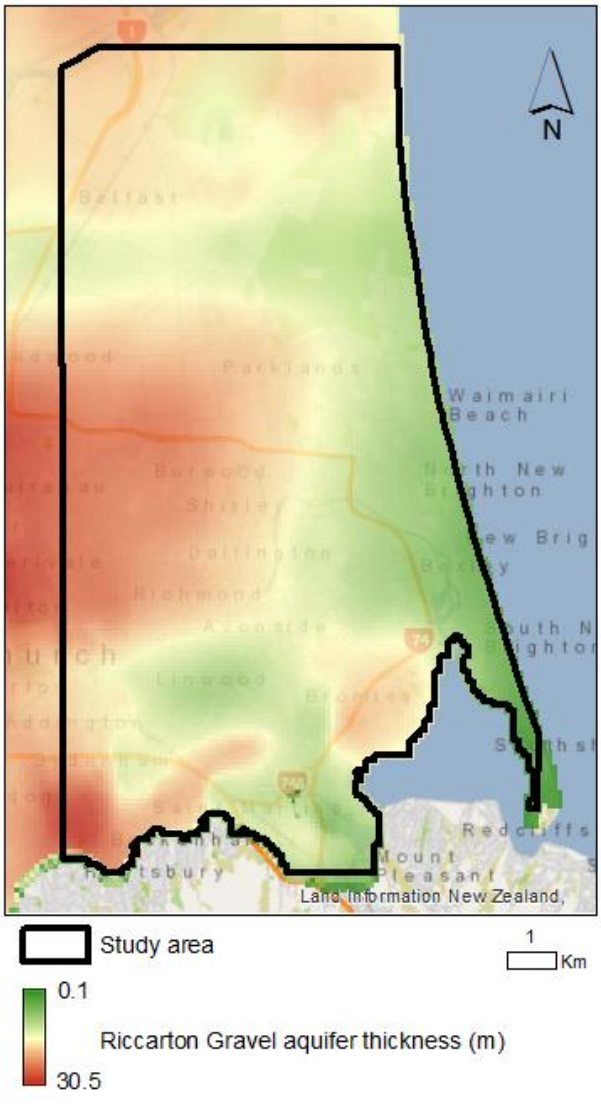

Figure 24. Riccarton Gravel aquifer thickness (m) from Begg et al. (2015).

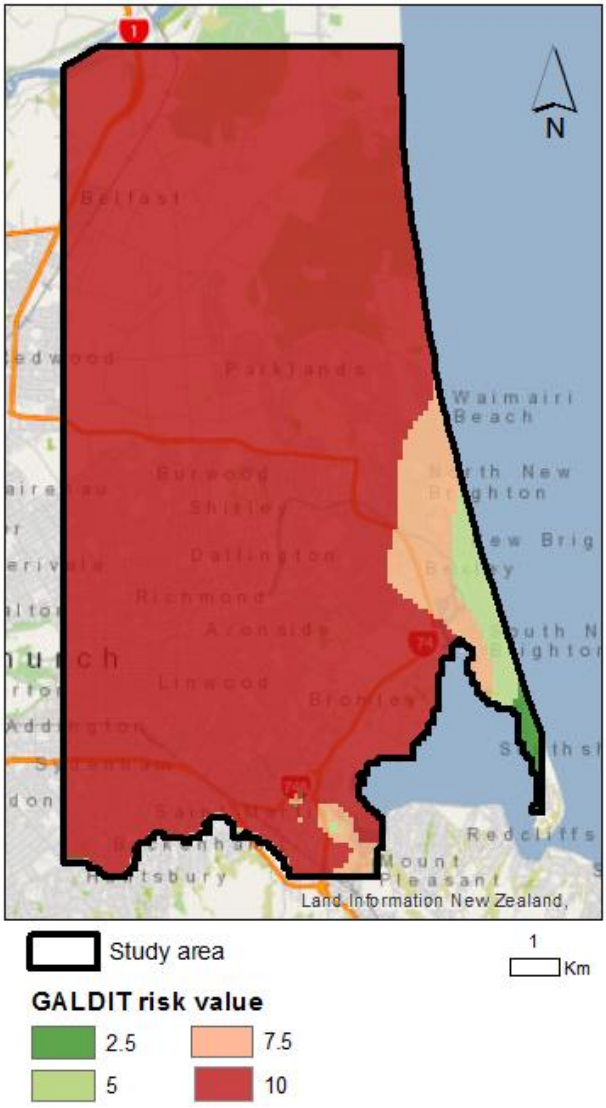

Figure 25. GALDIT risk values based on aquifer thickness; 2.5 (very thin; < 5 m), 5 (thin; 5 - 7.5 m), 7.5 (medium; 7.5 - 10 m), and 10 (thick; > 10 m).

4.1.7. Sea level rise

4.1.7.1. Level of groundwater relative to MSL

The groundwater level above MSL was changed based on the SLR scenario and boundary condition, as per Section 3.3.8.1. The 1 m SLR fixed head scenario resulted in a 1 m reduction in groundwater level above MSL, proportionately reducing the groundwater level range to 0.6 – 10.7 m above MSL. The area of highest risk to SWI remained the same with regards to groundwater level, i.e. the southwest of the estuary and the north side of the coast. The SWI risk was exacerbated in the 2 m SLR fixed head scenario, which resulted in a groundwater level range of -0.4 – 9.7 m relative to MSL. It is important to note that some areas had groundwater level below MSL in the 2 m SLR fixed head scenario. This scenario resulted in a larger area of high risk within the same vicinity. The groundwater level layers reclassified into the GALDIT risk values are shown in Figure 26 based on the 1 m SLR fixed head scenario and Figure 27 based on the 2 m SLR fixed head scenario. While the 2 m SLR fixed flux scenario had no change in groundwater level relative to MSL, hence it used the same groundwater level layer as the current sea level scenario.

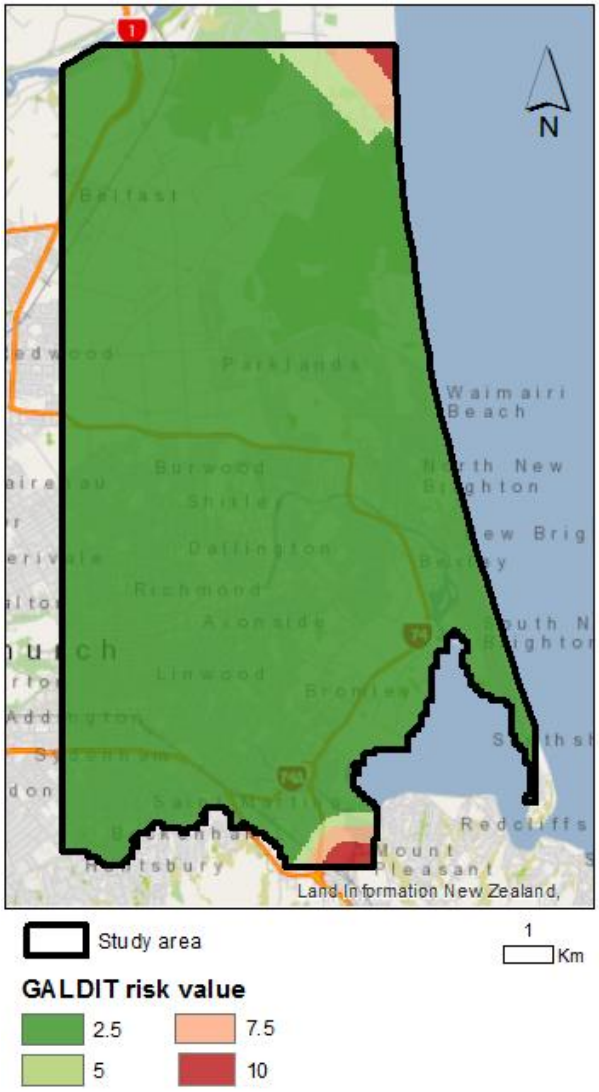

Figure 26. GALDIT risk values based on groundwater level above MSL in a 1 m SLR fixed head scenario; 2.5 (very low; > 2 m), 5 (low; 1.5 – 2 m), 7.5 (medium; 1 – 1.5 m), 10 (high; < 1 m).

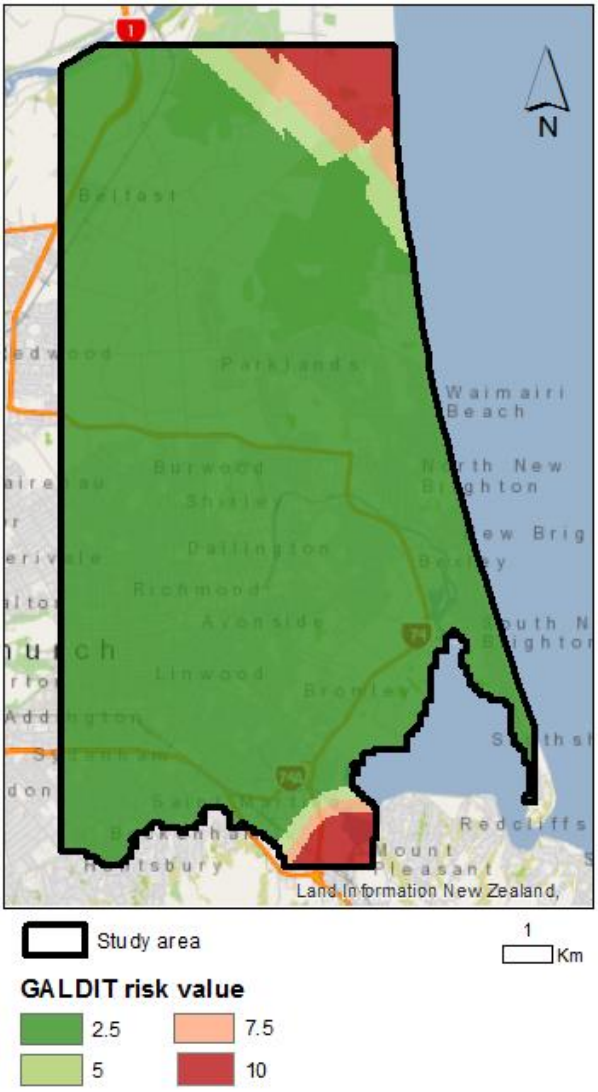

Figure 27. GALDIT risk values based on groundwater level above MSL in a 2 m SLR fixed head scenario; 2.5 (very low; > 2 m), 5 (low; 1.5 – 2 m), 7.5 (medium; 1 – 1.5 m), 10 (high; < 1 m).

4.1.7.2. Distance from the coast

Sea level rise physically changed the shape of the coastline. The new coastline under SLR conditions at high tide (MHWS) as per Section 3.3.8.2 was considered in the distance to coast layers. The distance from coast under 1 m and 2 m SLR scenarios at MHWS are shown in

Figure 28 and Figure 29, respectively. In the 1 m SLR scenario, seawater infiltration only occurred in the Brooklands Lagoon, which is located in the northeast of the study area. Whereas in the 2 m SLR scenario, seawater infiltration additionally occurred in the Styx River which is connected to the Brooklands Lagoon. It also occurred in the Avon-Heathcote Estuary, the Avon River (north of the estuary), and the Heathcote River (west of the estuary). The reclassification of distance from coast layers based on 1 m and 2 m SLR scenarios into GALDIT risk values are shown in Figure 30 and Figure 31, respectively.

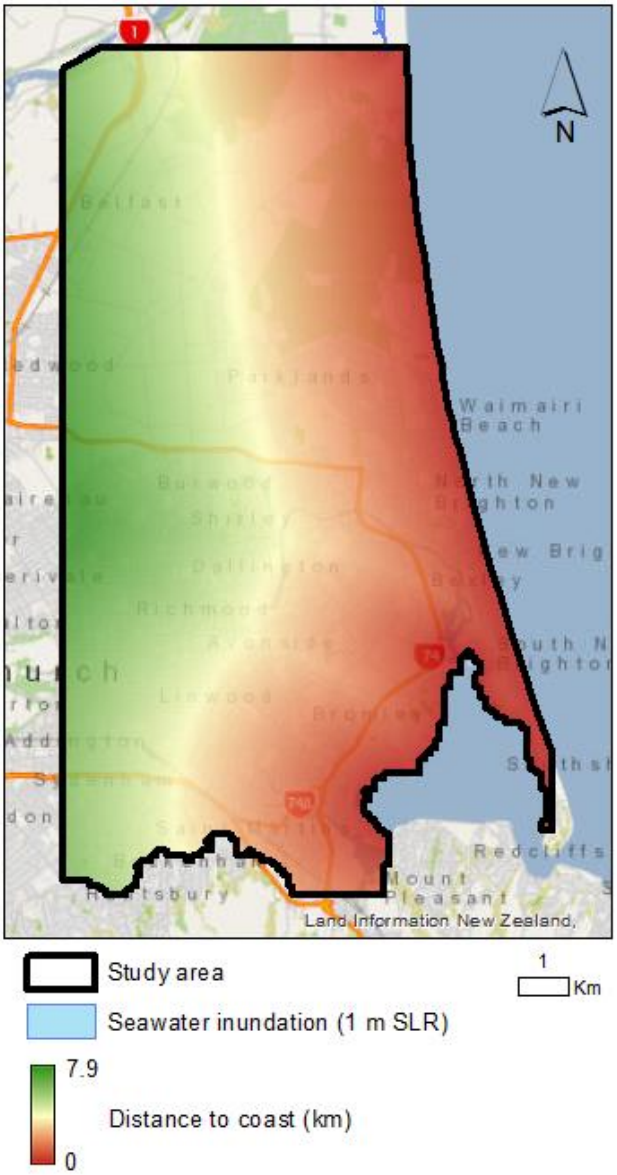

Figure 28. Distance to coast under 1 m SLR scenario based on MHWS.

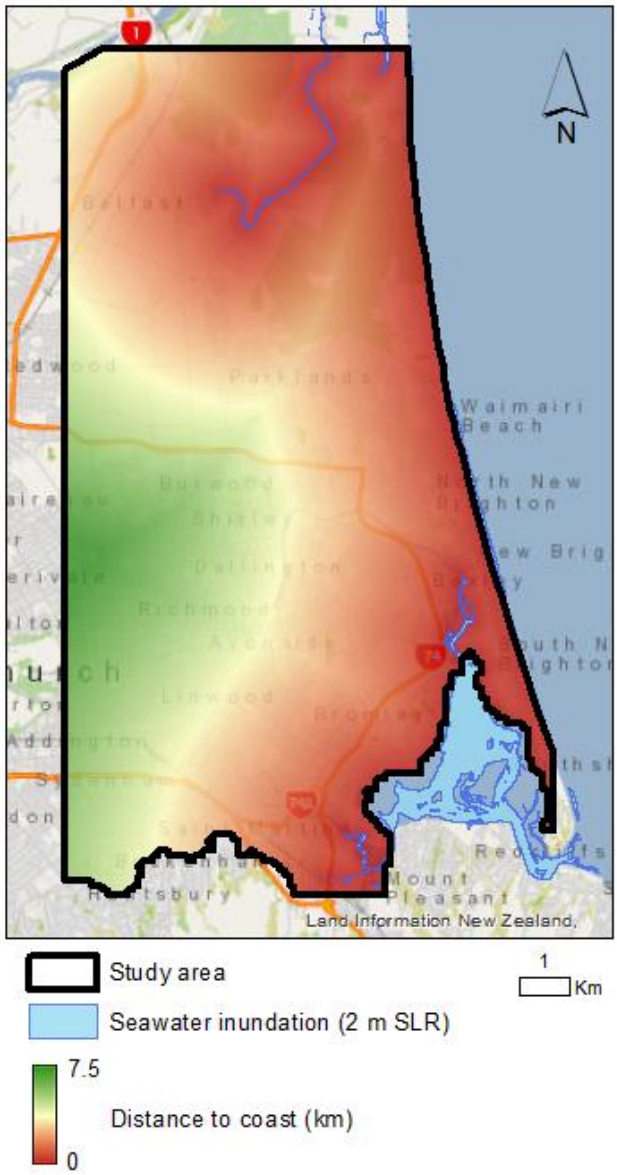

Figure 29. Distance to coast under 2 m SLR scenario based on MHWS.

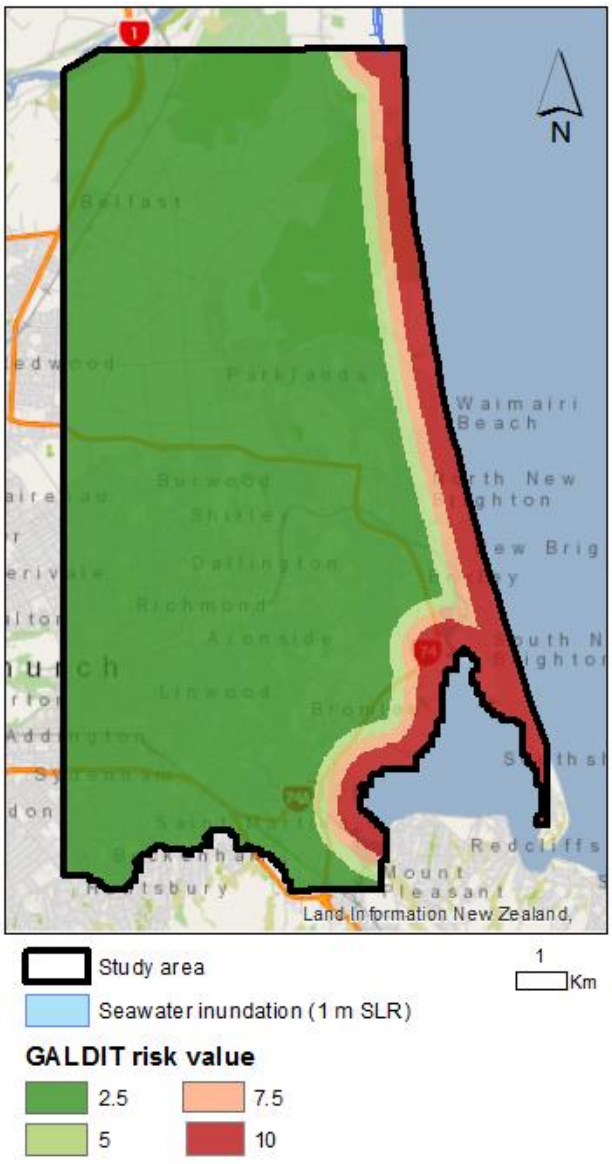

Figure 30. GALDIT risk values based on distance from the coast under 1 m SLR scenario at MHWS; 2.5 (far; > 1000 m), 5 (medium; 750 - 1000 m), 7.5 (close; 500 - 750 m), and 10 (very close; < 500 m).

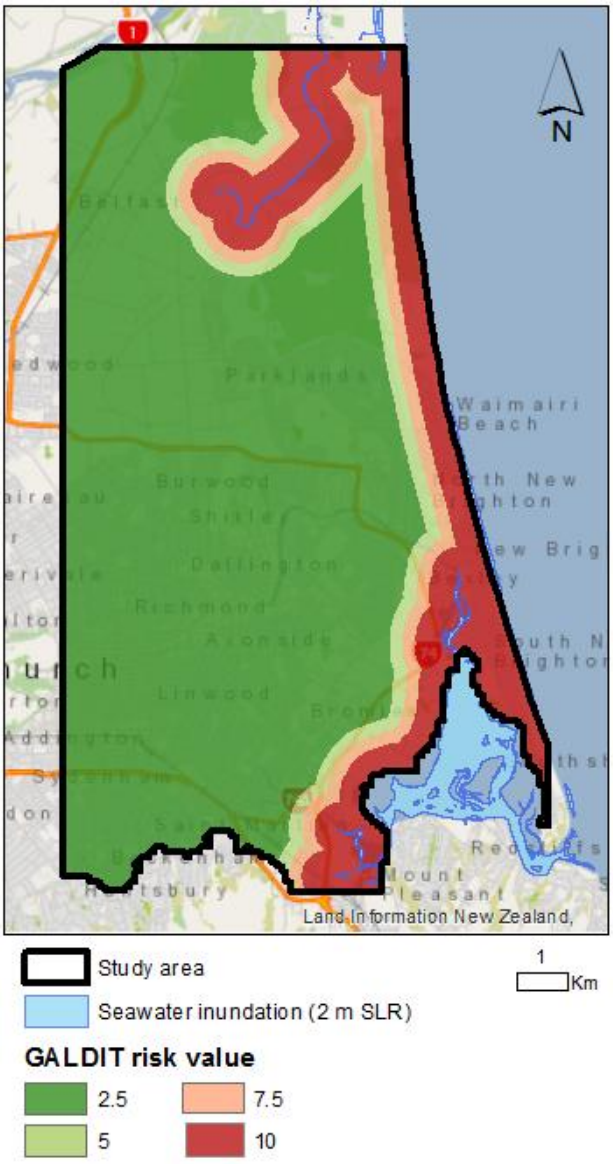

Figure 31. GALDIT risk values based on distance from the coast under 2 m SLR scenario at MHWS; 2.5 (far; > 1000 m), 5 (medium; 750 - 1000 m), 7.5 (close; 500 - 750 m), and 10 (very close; < 500 m).

4.1.8. GALDIT index maps

The GALDIT index map based on the current sea level (Figure 32) indicated the highest SWI vulnerability around the estuary and the northern shore of the study area. While the GALDIT index map based on the 1 m SLR scenario (Figure 33) indicated more vulnerability along the northern shore of the study area (Brooklands), as well as the southwest side of the estuary (Woolston and Ferrymeade). The GALDIT index map based on the 2 m SLR (fixed flux) scenario (Figure 34) indicated heightened vulnerability in the same areas as the 1 m SLR scenario. While the GALDIT index map based on the 2 m SLR (fixed head) scenario (Figure 35) also indicated the same area of highest vulnerability, however with greater risk. In general, the areas of highest vulnerability to SWI were consistent, which were southwest of the estuary and the northern shore of the study area. As the sea level increased, the areas of highest vulnerability expanded and intensified.

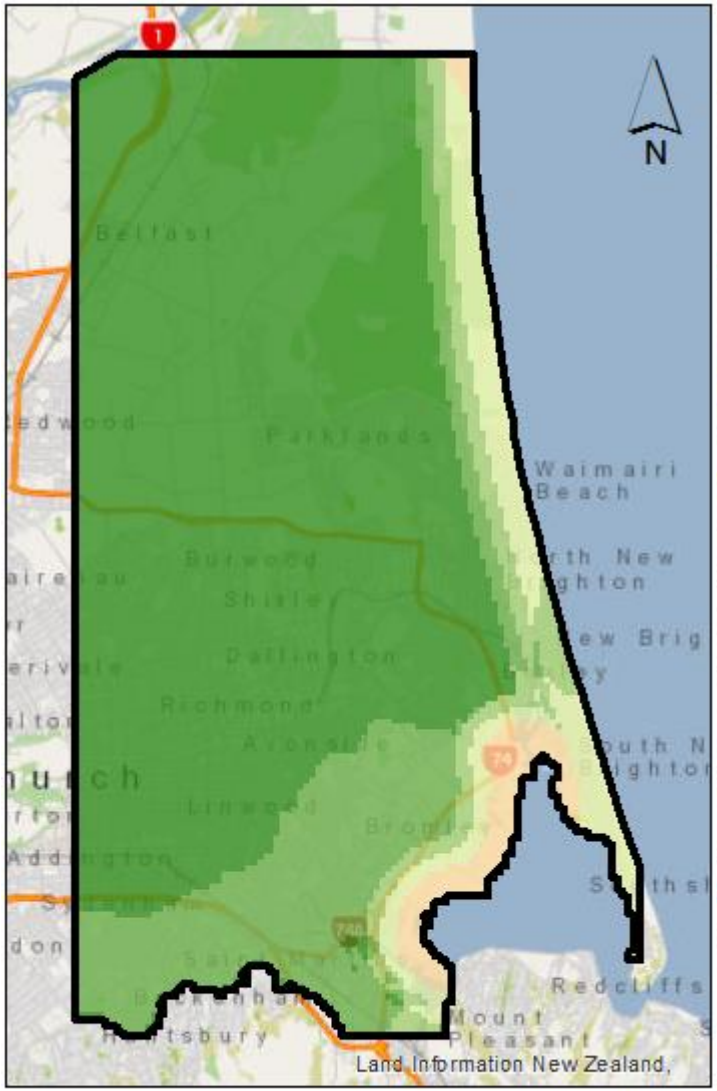

Figure 32. GALDIT index map based on the current sea level.

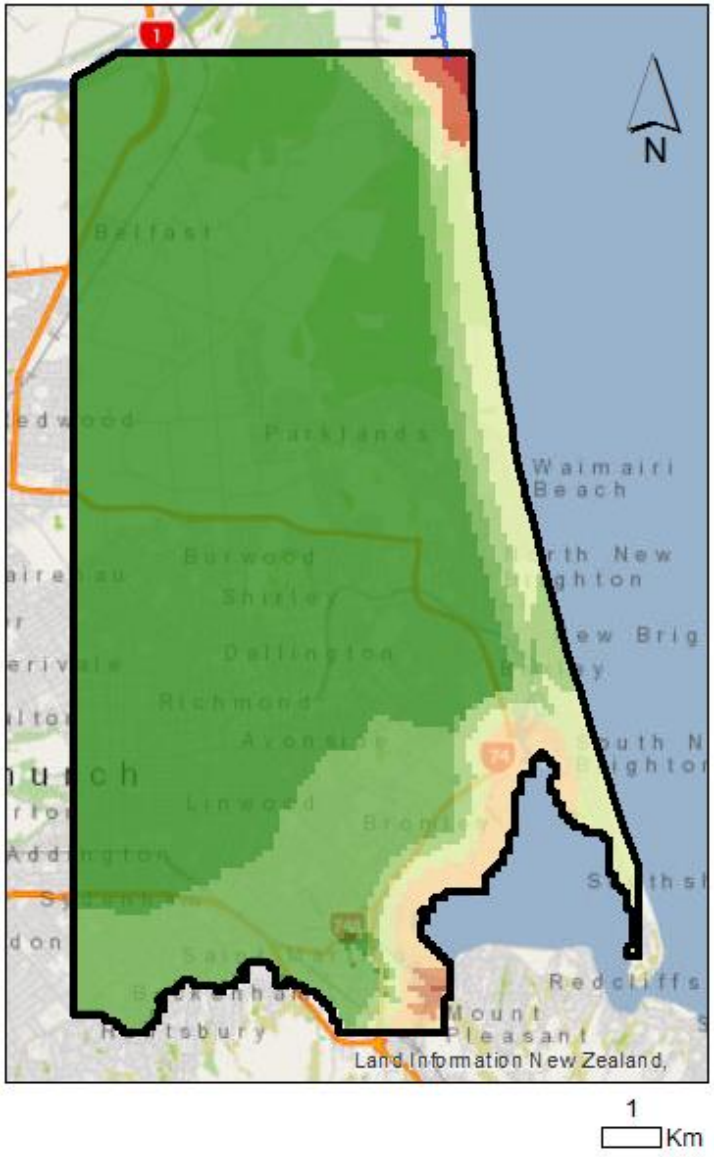

Figure 33. GALDIT index map based on a 1 m sea level rise (fixed head) scenario.

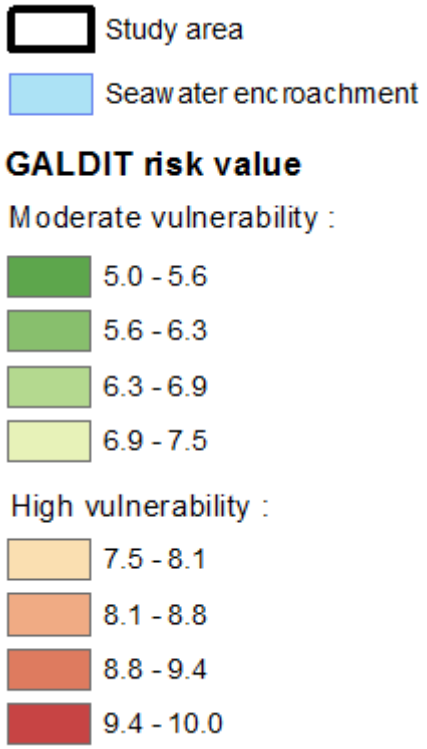

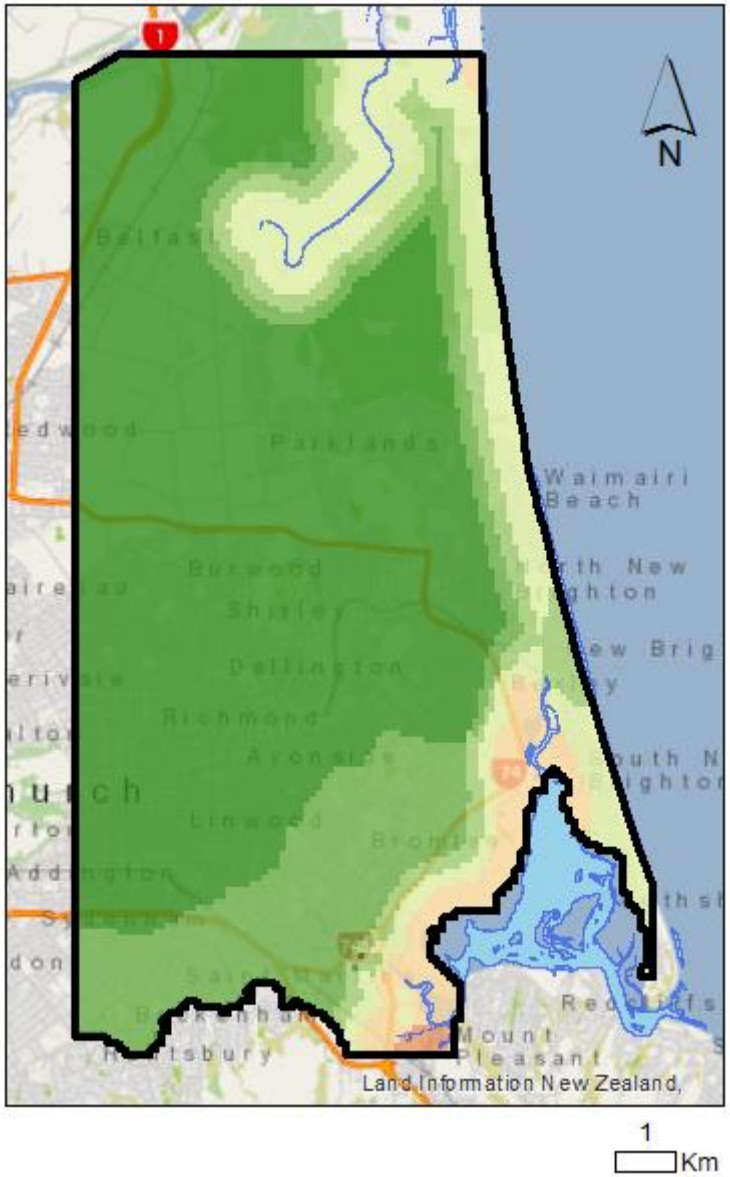

Figure 34. GALDIT index based on a 2 m sea level rise (fixed flux) scenario.

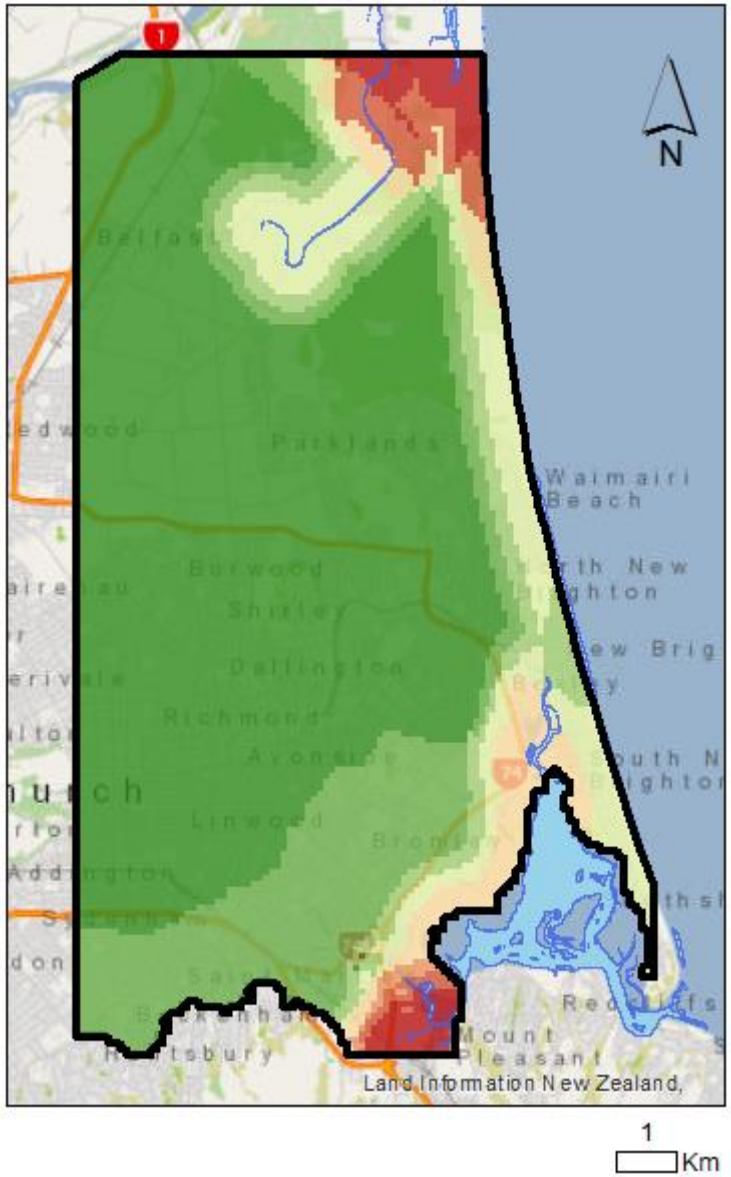

Figure 35. GALDIT index based on a 2 m sea level rise (fixed head) scenario.

In all scenarios, the majority of the study area (at least 85%) was categorized as having moderate vulnerability to SWI according to the GALDIT method. There was no area classified as having low vulnerability to SWI across all sea level scenarios. There was a shift towards the higher vulnerability GALDIT index bins in the SLR scenarios (Figure 36). The GALDIT index bins of the current and the 1 m SLR scenarios had similar percentages of study area occupation in the moderate vulnerability index bins. However, the 1 m SLR scenario had more raster cells belonging in the high vulnerability GALDIT index bins. The 2 m SLR scenarios had about 10% less area in the 5.0 – 5.6 GALDIT index bin compared to the current and the 1 m SLR scenarios. The scenarios that had the lowest to highest area classified as high vulnerability to SWI (GALDIT index of ≥ 7.5) were current sea level (6%), SLR 1 m fixed head (7%), SLR 2 m fixed flux (13%), and SLR 2 m fixed head (15%).

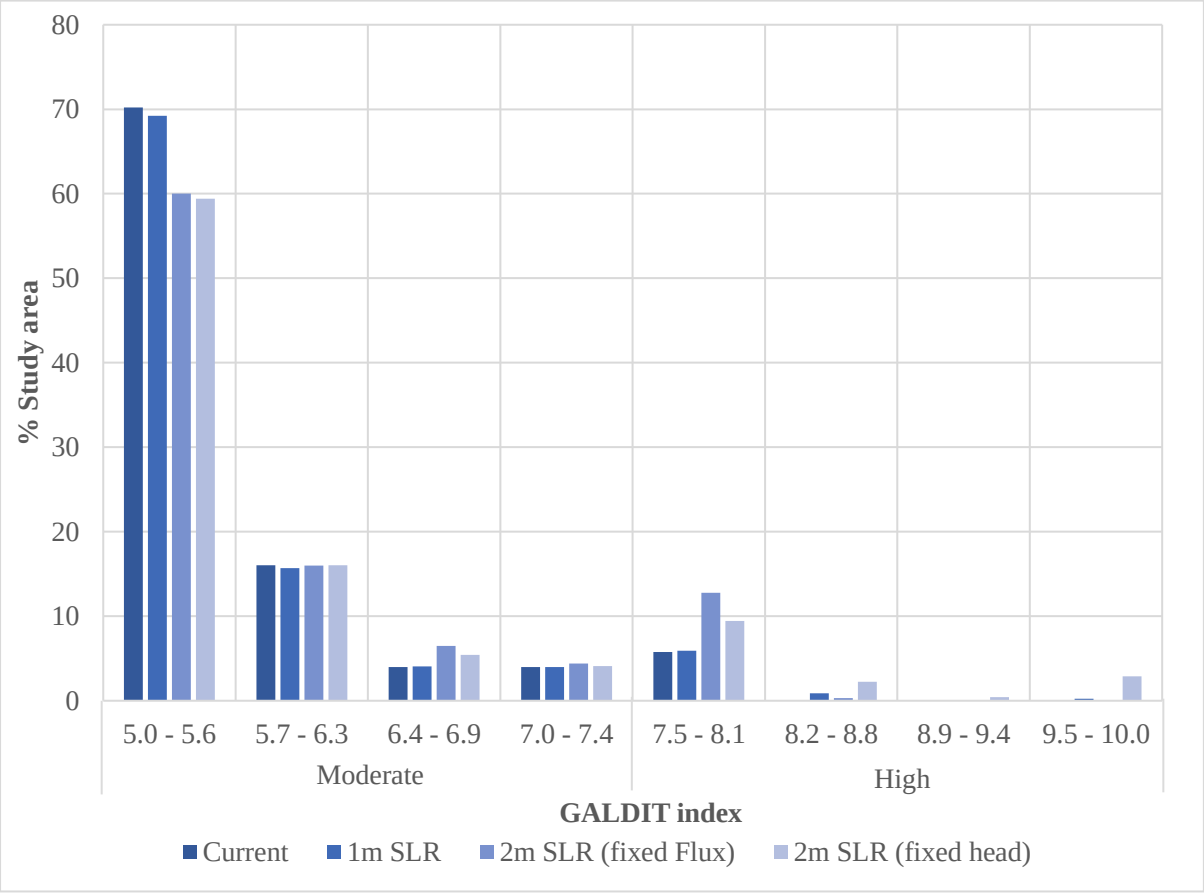

Figure 36. GALDIT index bins and their percentages of study area occupation based on the current, 1 m and 2 m (fixed flux and fixed head) sea level rise scenarios.

4.2. Analytic solutions in a GIS framework

Increased sea level with fixed head boundary condition significantly increased SWI vulnerability by decreasing fresh groundwater discharge to the coast and extending the seawater wedge toe position landwards.

Increased sea level with fixed flux boundary condition did not significantly impact fresh groundwater discharge to the coast, the seawater wedge toe position, and thus SWI vulnerability, when taking into account only the overlapping kilometres between all scenarios. In general, the fresh groundwater discharge was lowest and the toe extended furthest inland in the northern shore of the study area (Brooklands), around the estuary and particularly in the southwest side of the estuary (Woolston and Ferrymead).

The increase in SWI vulnerability under the different SLR scenarios was represented as the increase in x_T and decrease in q_0, rather than the increase in $\partial x_T / \partial z_0$. Locations of large inland extension of the toe indicate high propensity of the toe to move inland under SLR or other SWI stressors (Morgan & Werner, 2015). For example, x_T and $\partial x_T / \partial z_0$ had a strong correlation ($R^2 = 0.97$) in the current scenario (Figure 54 in Appendix B).

h_b was measured inland of the toe (i.e. $h_b \geq \delta z_0$) within the whole study area in the current and 2 m SLR (fixed flux) scenarios. While h_b was measured in the coastal side of the toe (i.e. $h_b < \delta z_0$) within some parts of the study area in the 1 m SLR and 2 m SLR (both fixed head) scenarios.

As mentioned previously, raster cells that intersected the raised sea, located less than 500 m from the coast, or located in areas of active SWI were not included in the results because they gave misleading values and were not comparable against values along the coast at a distance of 500 m perpendicular from the coast. Evidently there were no cells removed in the current sea level scenario. The cells removed were located in: (i) 0 – 0.6 km in the 1 m SLR fixed head scenario, (ii) 0 – 1.0, 10.1 – 13.0, and 17.4 km onwards in the 2 m SLR fixed flux scenario, and (iii) 0 – 1.3, 10.1 – 13.0, and 17.4 km onwards in the 2 m SLR fixed head scenario. There was no occurrence of active SWI (i.e., $h_b < h_{coast}$) in the current, 1 m SLR fixed head, and 2 m SLR fixed flux scenarios. Active SWI only occurred in the 2 m SLR fixed head scenario.

In the current scenario, q_0 was lowest in the southwest of the estuary (minimum of 1 m^2/day) (Figure 41), while x_T extended furthest inland in the northern shore of the study area (reaching 98 m from the coast) and the southwest of the estuary (reaching 49 m from the coast) (Figure 37).

In the 1 m SLR (fixed head) scenario, q_0 was also lowest in the southwest of the estuary (minimum of 0.4 m^2/day) (Figure 42), while x_T extended furthest inland in the northern shore of the study area (reaching 292 m from the coast) and the southwest of the estuary (reaching 154 m from the coast) (Figure 38).

In the 2 m SLR (fixed head) scenario, the active SWI sites were located in the northern shore of the study area (first 2 km of the coast) and the southwest of the estuary (last 0.6 km of the coast). The q_0 was expected to be lowest and x_T to extend furthest inland in the active SWI

sites. The average x_T in the 2 m SLR fixed head scenario was approximately 45% further inland than the x_T in the current and 2 m SLR fixed flux scenarios, where the cell locations overlapped between the three scenarios (i.e. x_T calculated at the same location between the scenarios). The two cells located directly below the active SWI site (at 1.4 – 1.5 km) along the coast were included in the active SWI site, although they did not meet the requirement of $h_b < h_{coast}$. The difference between h_b and h_{coast} was 0.01 for the first cell, which was considered very small. These two cells had x_T values of 7,400 m and 4,245 m, hence were represented as sites of active SWI. At 2 – 6 km, the q_0 increased and the x_T moved coastward as the location of calculation moved away from the active SWI site (Figure 43 and Figure 39). At 6 – 10 km along the coast, both q_0 and x_T had decreasing trends. The cells at 10 – 13 km were removed because they intersected the raised sea or were located less than 500 m from the new coast in the SLR scenario. At 13 – 16 km around the estuary, both q_0 and x_T had increasing trends. At 16 km and onwards, q_0 had a sharp decline while the x_T levelled off.

The 2 m SLR (fixed flux) scenario showed statistically similar q_0 and x_T to the current scenario. However, the 2 m SLR (fixed flux) scenario had an average toe position that was located slightly further inland (24.5 m) compared to the current scenario (24.0 m), where the cells overlapped between the two scenarios (i.e. toe position calculated at the same location between the two scenarios). The 2 m SLR (fixed flux) scenario also had less q_0 on average compared to the current scenario (9.9 vs. 10.2 m^2/day), where the cell locations overlapped between the two scenarios.

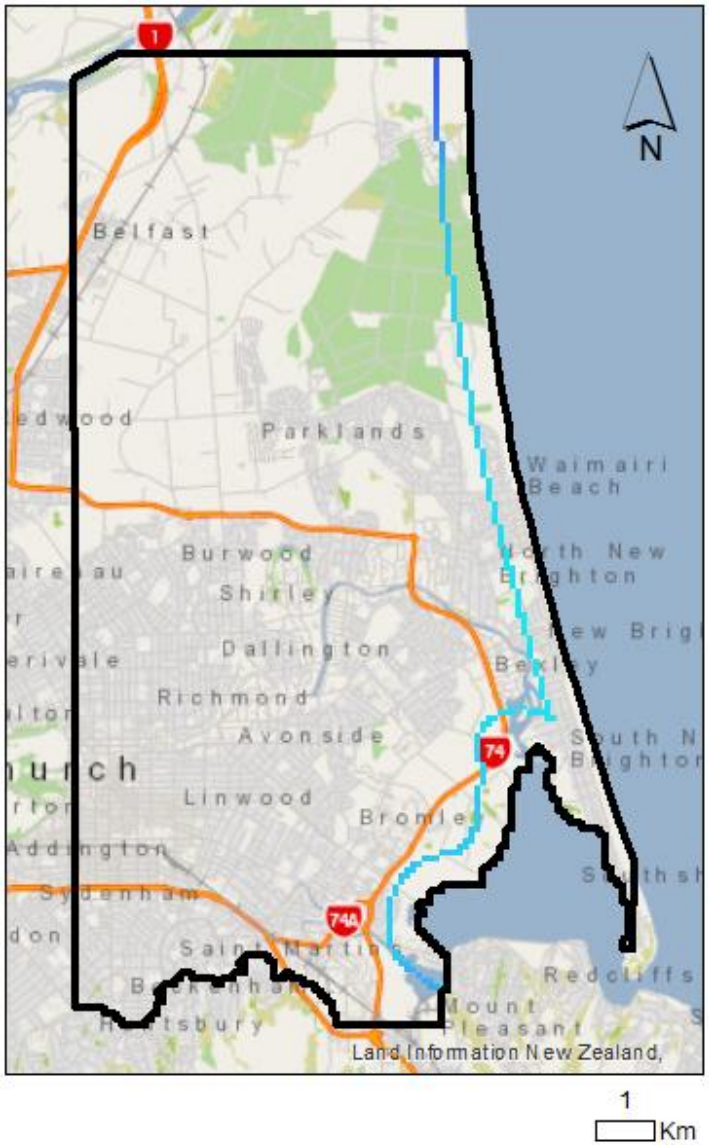

Figure 37. x_T (m) along the coast calculated at 500 m from the coast, in the current sea level scenario.

Figure 38. x_T (m) along the coast calculated at 500 m from the coast, in the 1 m SLR (fixed head) scenario.

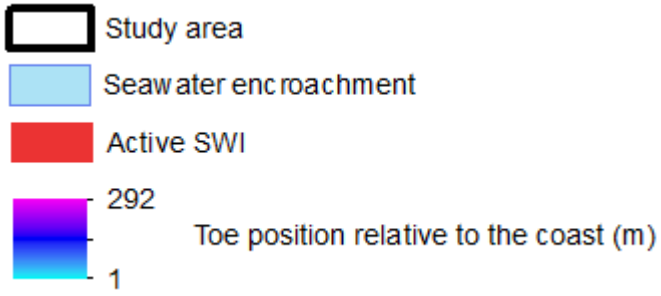

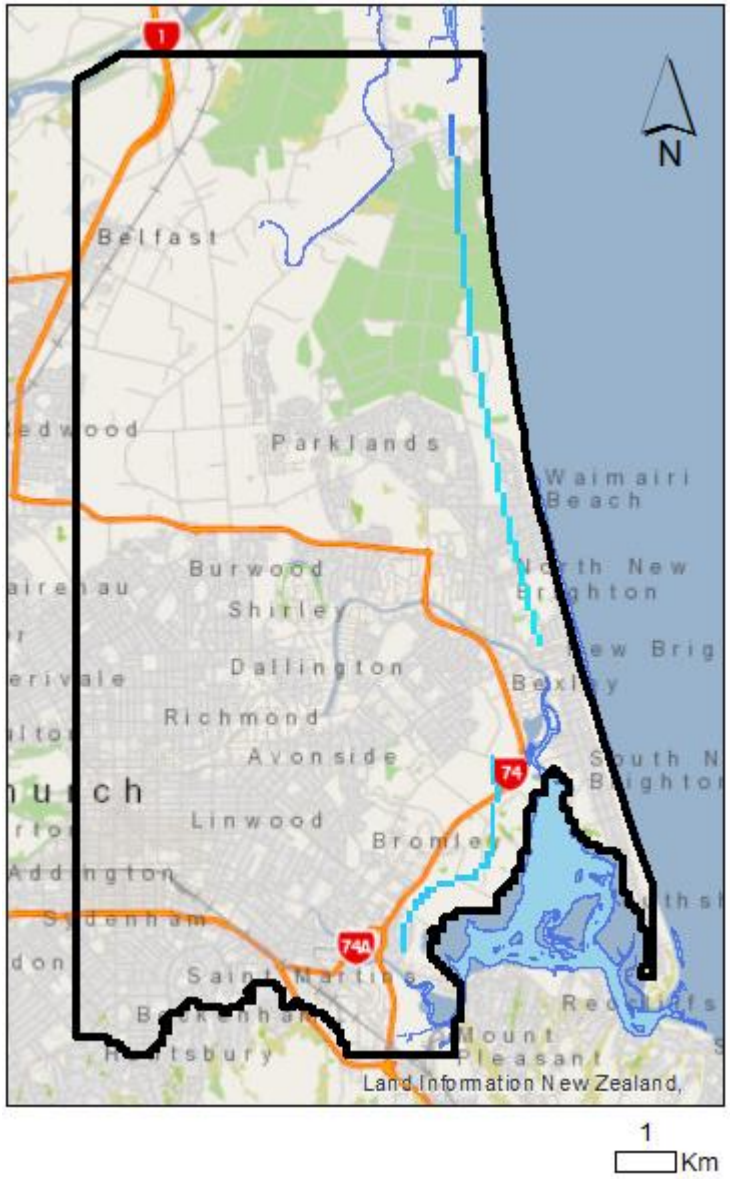

Figure 39. x_T (m) along the coast calculated at 500 m from the coast, in the 2 m SLR (fixed flux) scenario.

Figure 40. x_T (m) along the coast calculated at 500 m from the coast, in the 2 m SLR (fixed head) scenario.

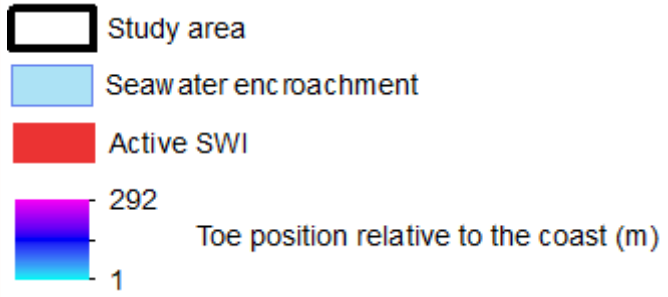

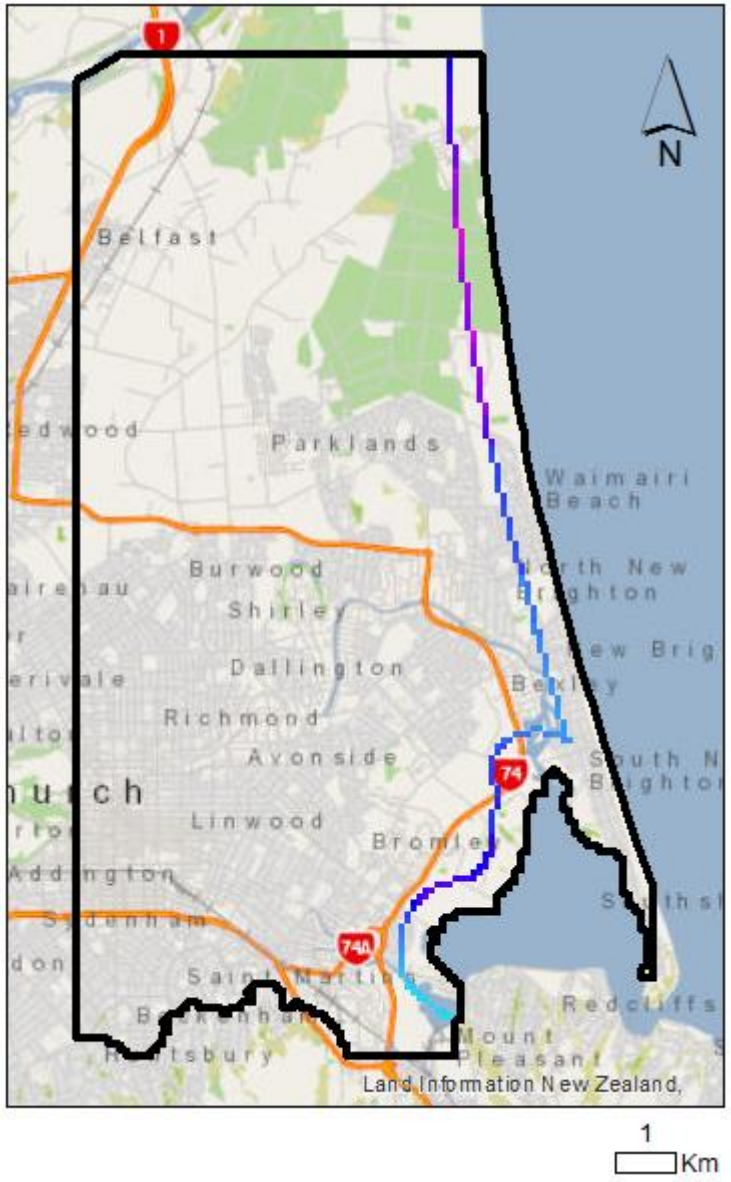

Figure 41. q_0 (m^2/day) along the coast calculated at 500 m from the coast, in the current sea level scenario.

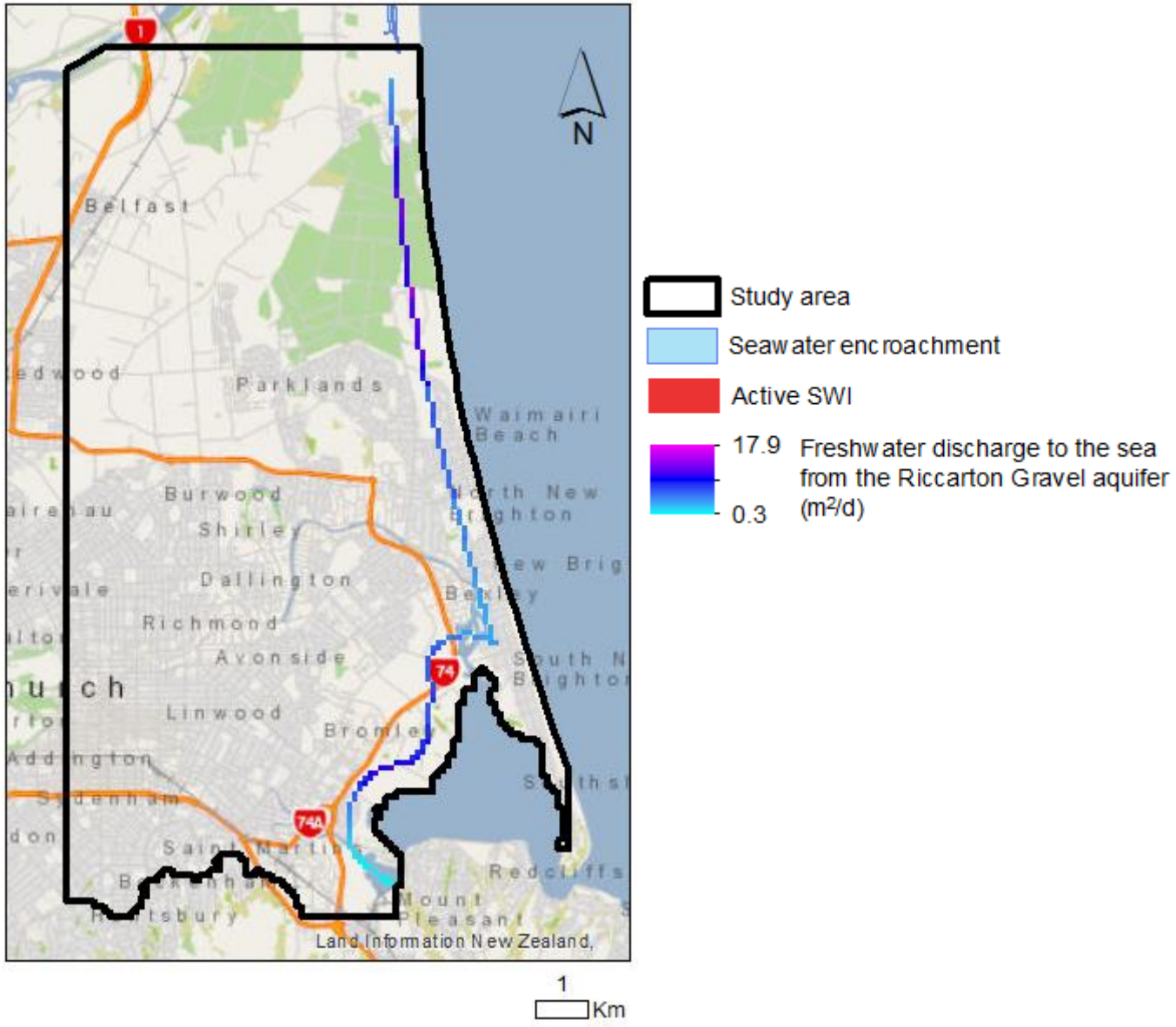

Figure 42. q_0 (m^2/day) along the coast calculated at 500 m from the coast, in the 1 m SLR (fixed head) scenario.

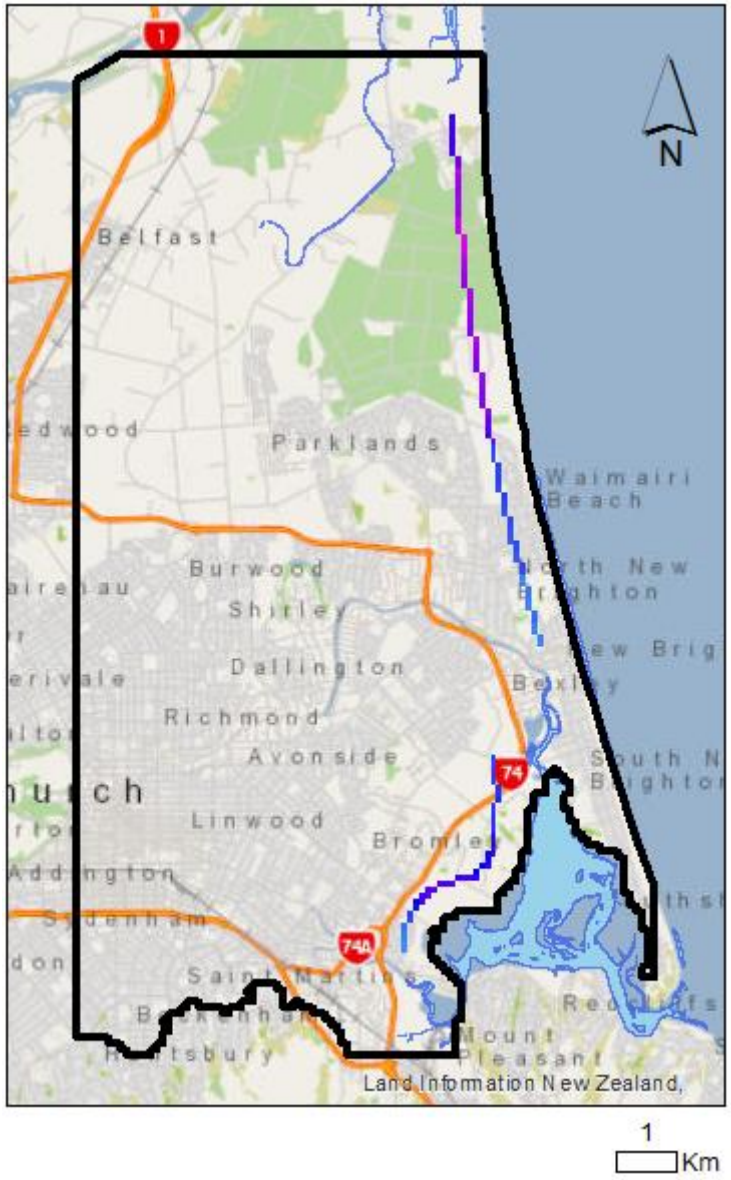

Figure 43. q_0 (m^2/day) along the coast calculated at 500 m from the coast, in the 2 m SLR (fixed flux) scenario.

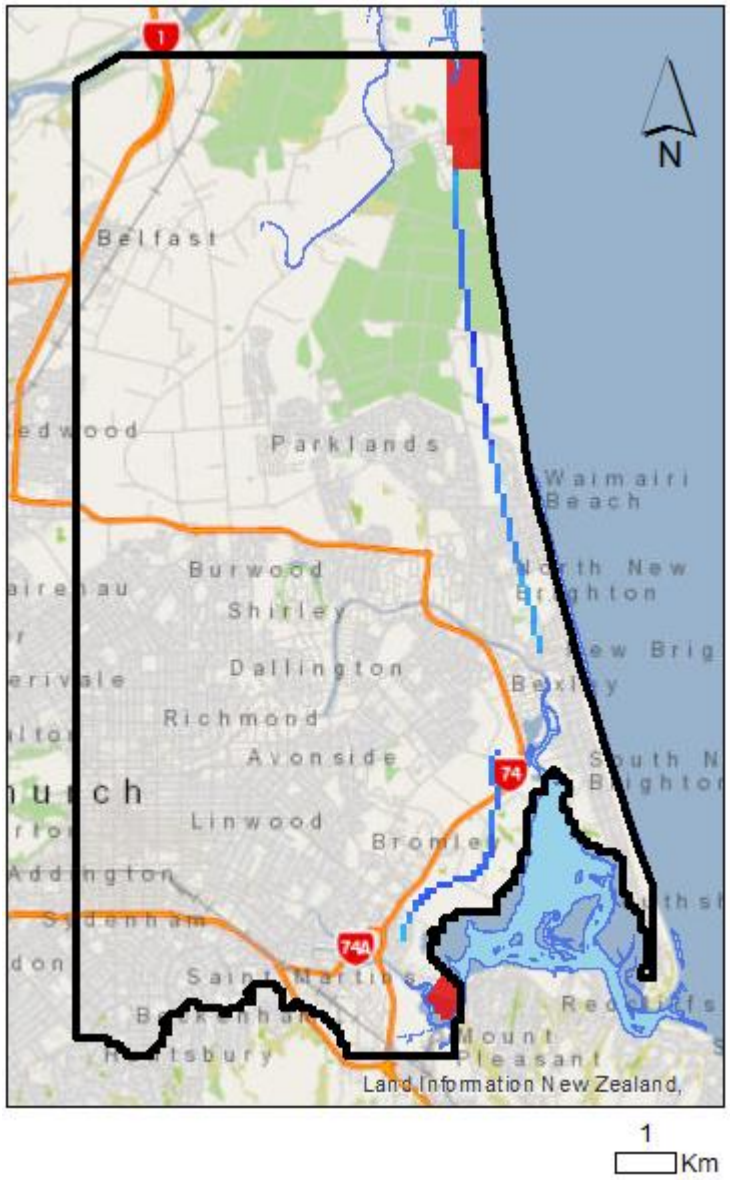

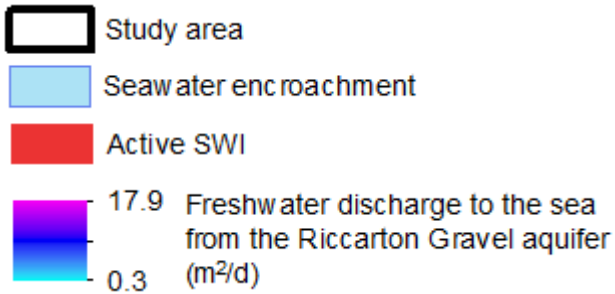

Figure 44. q_0 (m^2/day) along the coast calculated at 500 m from the coast, in the 2 m SLR (fixed head) scenario.

The q_0 and x_T followed a similar fluctuating pattern between the scenarios, however with differences in magnitude (Figure 45 and Figure 46). The sea level scenarios which had the highest to lowest q_0 and lowest to highest x_T on average were: current, 2 m SLR fixed flux, 1 m SLR fixed head, and 2 m SLR fixed head. In general, both q_0 and x_T followed the same trend, except for the front end of the coast where x_T declined while the q_0 increased, and the back end of the coast where x_T increased while the q_0 declined.

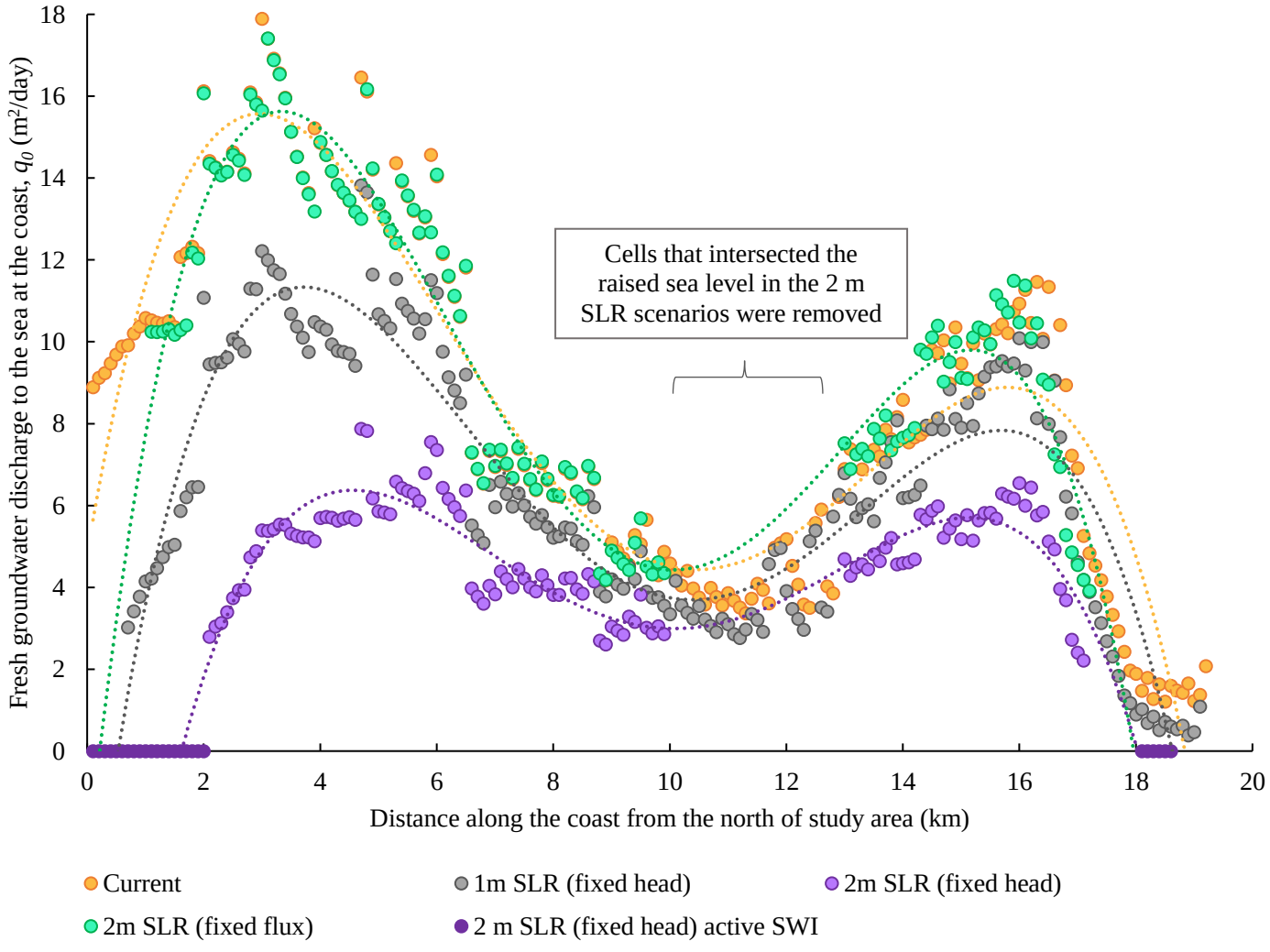

Figure 45. Fresh groundwater discharge to the sea at the coast, q_0 (m^2/s) along the coast calculated at 500 m perpendicular from the coast, based on the current sea level, 1 m SLR (fixed head), 2 m SLR (fixed head and fixed flux) scenarios.

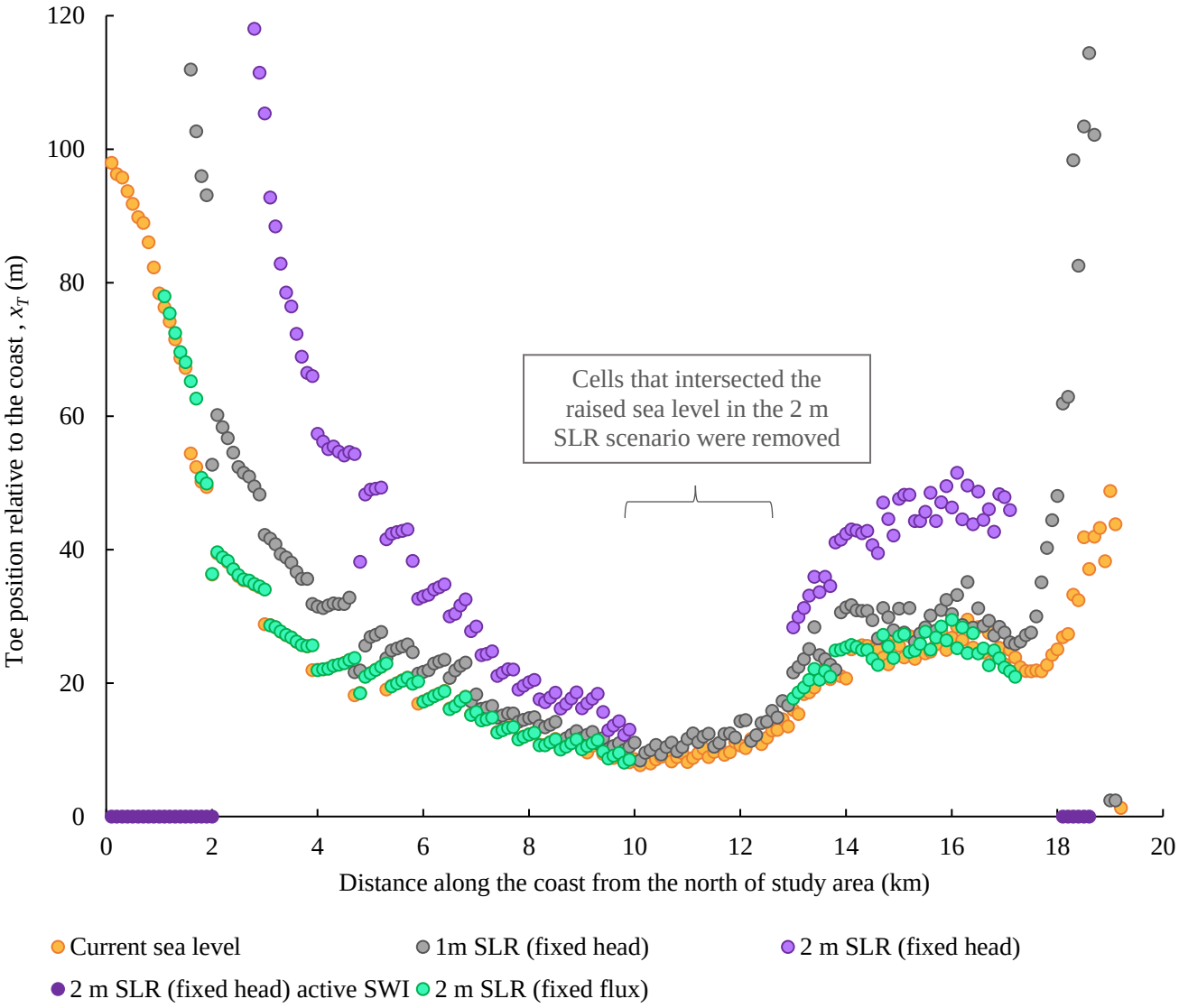

Figure 46. Seawater wedge toe position relative to the coast, x_T (m) along the coast calculated at 500 m perpendicular from the coast, based on the current sea level, 1 m SLR (fixed head), and 2 m SLR (fixed head and fixed flux) scenarios. Data points with x_T above 120 m was not displayed to improve the visual quality of the figure.

The q_0 fluctuated along the study area, with two obvious peaks across the different scenarios. The q_0 firstly peaked at 2 – 4 km (Bottle Lake Forest Park area) in the current, 1 m SLR fixed head, and 2 m SLR fixed flux scenarios. This first peak reached up to 17.9, 13.8, and 17.4

m^2/day in the current, 1 m SLR fixed head, and 2 m SLR fixed flux scenarios, respectively. Whereas the q_0 peak shifted at 4 – 6 km (Waimairi Beach area) in the 2 m SLR fixed head scenario, reaching up to 7.9 m^2/day. At 8 – 12 km, q_0 decreased and x_T moved coastward in all scenarios; the difference in q_0 and x_T between the scenarios decreased and the data points from the different scenarios nearly overlapped (Figure 45 and Figure 46). Around the estuary, the x_T increased gradually at 13 - 17 km, then increased steeply from about 18 km onwards if no active SWI occurred. While the q_0 increased from 13 km, reached a peak at 16 km (west of the estuary), then decreased steeply from here onwards. This peak reached up to 11.5 m^2/day in both current and 2 m SLR fixed flux scenarios, and 10.1 and 6.5 m^2/day in the 1 m and 2 m SLR fixed head scenarios, respectively.

The q_0 and x_T of the current and 2 m SLR fixed flux scenarios showed nearly constant overlaps, which reinforces that both scenarios were not statistically different to each other. The sudden drop in x_T at 19 km in the current and 1 m SLR scenarios is addressed in Section 5.2. The kilometre reference along the coast on the raster strip is displayed in Figure 47. In the SLR scenarios, the toe position shifted landwards, fresh groundwater discharge to the sea decreased, and therefore increased vulnerability to SWI occurred.

Figure 47. Kilometre reference along the coast displayed on the strip of raster cells.

The propensity for the toe to move under SLR, which is a measure of SWI vulnerability expressed as metre of toe movement per metre of SLR, was highest in the northern shore of the study area, reaching 97 m/m at 0.1 km. The propensity steeply declined, and began to increase around the estuary, then sharply increased at the southwest side of the estuary reaching 33 m/m at 19 km (Figure 48).

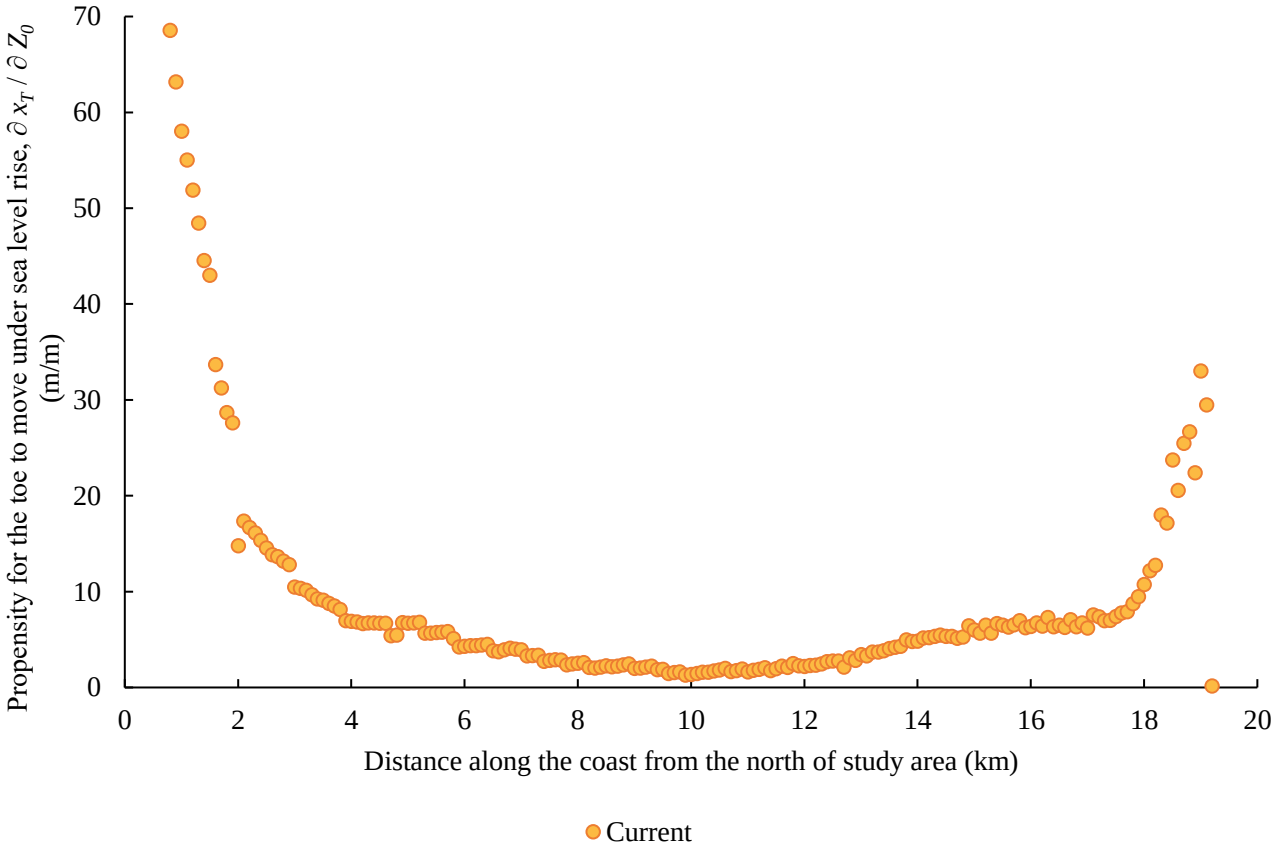

Figure 48. Propensity for the toe to move under SLR, $\partial x_T / \partial z_0$ along the coast calculated at 500 m perpendicular from the coast, based on the current sea level. Data points with $\partial x_T / \partial z_0$ above 120 m was not displayed to improve the visual quality of the figure.

5. Discussion

5.1. Comparison of GALDIT and analytic solutions in a GIS framework

The same set of raw data were used for GALDIT and analytic solutions, such as hydraulic conductivity, aquifer thickness, groundwater level above MSL, and distance from the coast to assess the SWI vulnerability of confined coastal aquifers. Hence, one can argue that both methods require similar effort to conduct. The potential advantages and disadvantages of each method are outlined in Table 4.

Table 4. The advantages and disadvantages of GALDIT vs. analytic solutions.

GALDIT	Analytic solutions
Advantages: • Takes into account a groundwater quality parameter, which was the impact of existing status of SWI, represented as Cl^- : [HCO_3^- + CO_3^{2-}]. • Relatively simpler to process the raster layers into GALDIT index maps due to the lack of equations involved. • Technically possible to assess a larger area instead of a strip of land along the coast. Disadvantages: • Assigns arbitrary numbers which lack theoretical underpinnings to each risk value category, which do not necessarily apply to all cases. * E.g., hydraulic conductivity of > 40 m/day was categorized as high risk, which may be suitable to some but not all cases. • Does not directly assess the coastal aquifer water balance. * • The GALDIT output is considerably less sensitive to changes in the parameter inputs than the analytic solutions output.	Advantages: • Is a physically-based and quantitative method based on conventional SWI mathematics. * • Takes into account the individual value of each cell and computes the theoretical seawater wedge toe position along the coast. • The output (toe position along the coast) is highly sensitive to changes in the parameter inputs. Disadvantages: • Does not take into account the existing groundwater quality status. • Requires more caution when combining the parameters together via the equations. Issues relating to cell alignment and sizes may be more important. • More steps were involved in processing the raster layers into the output. • SWI vulnerability rankings (e.g. low or high vulnerability) have not been interpreted according to the x_T, q_0, or $\delta x_T / \delta z_0$. * • May require additional data such as qualitative indicators to fully assess SWI vulnerability.⁺

* Werner et al. (2012), ⁺ Morgan et al. (2013a)

There were different parameters that each method take into account. GALDIT takes into account a groundwater quality parameter, which is the impact of existing status of SWI, represented as Cl^- : $[HCO_3^- + CO_3^{2-}]$. In contrast, the analytic solution does not take into account existing groundwater quality status, but takes into account the depth of the aquifer relative to MSL. Thus GALDIT requires additional groundwater quality data while analytic solution requires additional aquifer elevation data. Aside from this, the compilation of raw GIS data for GALDIT can be used for the analytic solution and vice versa. Although in the case of unconfined aquifers, the analytic solution requires an additional net recharge parameter to solve for toe position and fresh groundwater discharge to the sea (Morgan & Werner, 2015). Moreover, the propensity for the toe to move under different stresses can also be measured using the analytic solutions, for example $\delta x_T / \delta h_b$ (rate-of-change in toe position with change in inland head) (Werner et al., 2012).

The two methods agreed that thicker aquifers and lower inland heads exacerbate SWI vulnerability. In addition, GALDIT categorizes aquifers with higher hydraulic conductivity as having higher SWI vulnerability, regardless of aquifer type. The analytic solutions consider this to be true in the case of unconfined aquifers, however the SWI vulnerability of confined aquifers are insensitive to hydraulic conductivity based on the method (Morgan et al., 2013a). Furthermore, GALDIT did not take into account the depth of aquifer relative to MSL, while the analytic solutions account that deeper aquifers exacerbate SWI vulnerability.

Additionally, GALDIT ranked confined aquifers as being more vulnerable to SWI compared to unconfined aquifers. The reasoning of Lobo-Ferreira et al. (2007) for this was due to the larger cone of depression generated in confined aquifers following pumping compared to unconfined aquifers. As an example, SWI in confined aquifers had a much longer-lasting

impact than unconfined aquifers in Canterbury (ECan, 2012). The case of lateral SWI into an unconfined aquifer in Makikihi, South Canterbury (well J40/0042) showed fast recovery (several months) to background levels of conductivity when pumping was ceased, after periods of high conductivity linked to low groundwater levels, often reaching levels below MSL (ECan, 2012). In contrast, the case of localised SWI via downward seepage from the estuary into the confined Riccarton Gravel aquifer (well M36/1159) had been observed for 30-40 years, which shows the persistent impacts of SWI in confined aquifers (ECan, 2012).

The SWI vulnerability to SLR is higher in unconfined aquifers compared to confined aquifers based on the analytical solutions; SLR does not induce SWI in confined aquifers under fixed flux conditions, whereas SLR induces SWI in unconfined aquifers under fixed flux conditions (Morgan & Werner, 2015; Werner et al., 2012). In another regard, GALDIT was not especially designed to assess the risk of SWI due to SLR in coastal aquifers, instead assessing the risks based on current conditions. On a similar note, SLR was represented in both GALDIT and analytic solutions as the change in distance to coast and groundwater level above MSL, and additionally represented in the analytic solutions as the increase in the distance between the bottom of aquifer and MSL.

According to GALDIT, the 2 m SLR fixed flux scenario was more vulnerable to SWI compared to the 1 m SLR fixed head scenario. Whereas according to the analytic solutions, the opposite was true; confined aquifers with fixed flux are unaffected by SLR (Werner et al., 2012). In GALDIT and analytic solutions, SLR decreased the groundwater level relative to MSL and altered the distance from coast. Both of these parameters ("L" and "D"; Table 1) had the highest weights in determining SWI vulnerability according to the GALDIT method. Although the groundwater level relative to MSL was constant in the 2 m SLR fixed flux

scenario, the distance from coast decreased in various areas, such as around the Avon, Heathcote, and Styx Rivers. This was due to the projected seawater encroachment following SLR, which physically changed the coastline. The change in distance from the coast in the SLR scenarios may have had a greater effect on the GALDIT index compared to groundwater above MSL, which reflected the flux of groundwater discharge to the coast. This resulted in the 2 m SLR fixed flux scenario ranked as being more vulnerable to SWI compared to the 1 m SLR fixed head scenario, according to the GALDIT method. Additionally the movement of the coastline did not affect the distance from coast parameter in the analytic solutions, because only the toe position and fresh groundwater discharge cells located 500 m perpendicular from the coast were investigated (i.e., cells that were less than 500 m from the coast were removed).

Both methods agreed on the areas of highest vulnerability; the northern shore of the study area (Brooklands) and the southwest side of the estuary (Woolston and Ferrymead). For example, areas of active SWI based on the analytic solutions covered the area of highest SWI vulnerability based on the GALDIT method. However, the GALDIT index showed a weak correlation with the toe position across all scenarios ($R^2 = 0.34$; Figure 49).

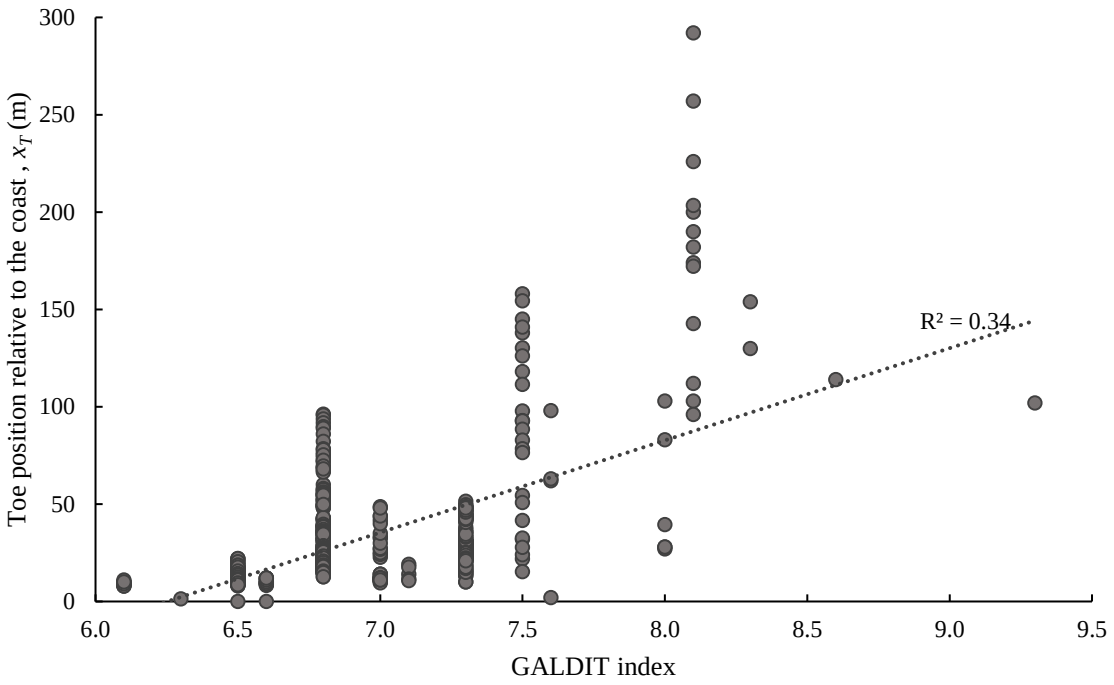

Figure 49. The correlation between toe position relative to the coast (m) and the GALDIT index across all scenarios (n=585). Cells that intersected the raised sea level, were in areas of active SWI, or located within 500 m of the coast based on SLR scenarios were not included.

The GALDIT index was not as sensitive in detecting variability in SWI vulnerability compared to the analytic solutions. The GALDIT index displayed little change along the coast as demonstrated by the flat trends, whereas the toe position varied more considerably along the coast (E.g., in the current scenario in Figure 50). The GALDIT method ranked at least 85% of the study area across all scenarios as having moderate vulnerability to SWI. Although, SWI vulnerability rankings (e.g., low, moderate, or high vulnerability) based on the analytic solutions have not been developed (Werner et al., 2012). Additionally, the GALDIT index maps may have shown clearer visualization compared to the to the x_T and q_0 maps, however it did not demonstrate the change in SWI vulnerability as quantitatively detailed as the analytic solutions.

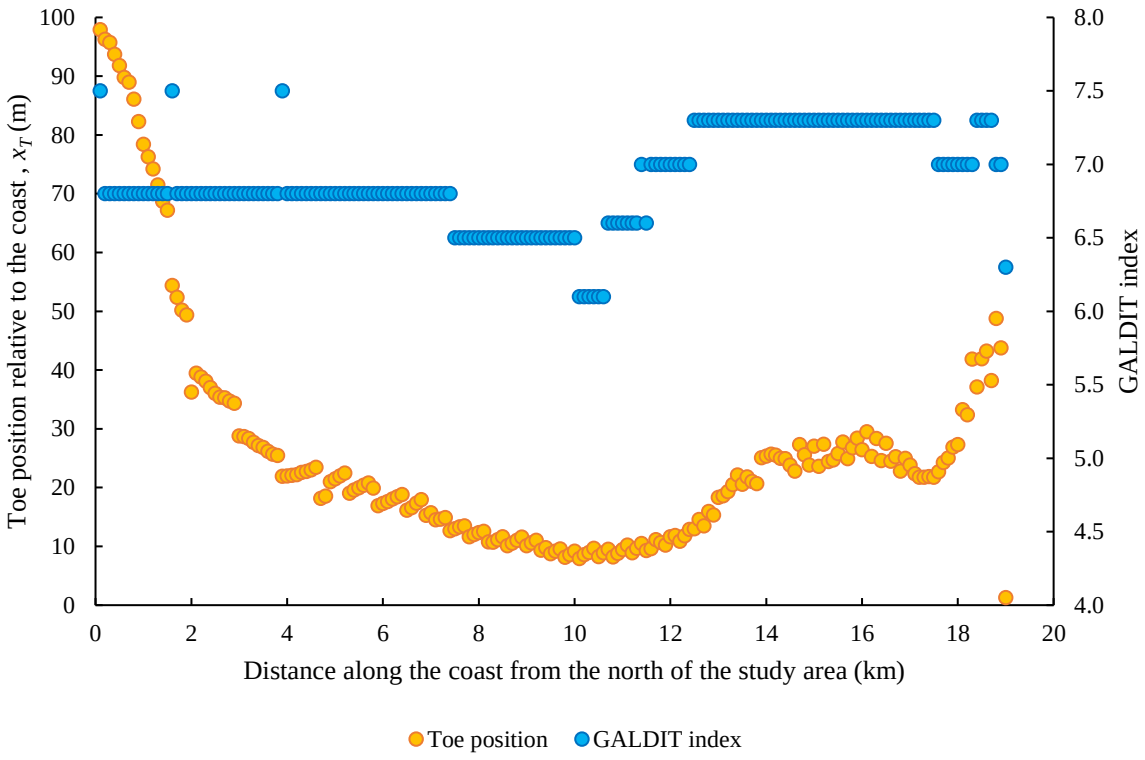

Figure 50. Toe position relative to the coast (m) in relation to the GALDIT index, at the current sea level scenario.

Conducting the SWI vulnerability assessments under SLR conditions using GIS with high resolution LiDAR data allowed the ability to take into account the physical change in coastline due to SLR. Based on the analysis, SLR caused seawater to encroach into surface water bodies. In the 1 m SLR scenario, seawater encroached into the Brooklands Lagoon, which forms part of the Waimakariri River mouth located around the northern shore of the study area. In the 2 m SLR scenario, seawater encroached further upstream into the Styx River that is connected to the Brooklands Lagoon, as well as into the Avon-Heathcote Estuary located in the southeast of the study area, and further upstream into the Avon and Heathcote Rivers that flow into the estuary. The encroachment of seawater into the lagoon, estuary, and lower reaches of rivers may oppose the popular belief that the largest impact of

SLR is the direct increase of sea level at the coast, rather than seawater encroachment into surface water bodies near the coast, which may lead to flooding in low-lying areas.

5.2. Analytic solutions

Sea level rise will impact Christchurch coastal aquifers by decreasing the fresh groundwater flux to the sea and moving the seawater-freshwater interface landwards. The scenarios ranked from lowest to highest SWI vulnerability based on their average toe position are: current sea level, 2 m SLR fixed flux, 1 m SLR fixed head, and 2 m SLR fixed head. In line with the results of Werner et al. (2012) for confined aquifers, the SLR scenarios with fixed head boundary conditions exacerbated the movement of toe position in the inland direction, as opposed to the fixed flux boundary condition. In the fixed flux scenario, the constant groundwater discharge to the sea and the increase of groundwater level (i.e., no change in inland heads relative to MSL) despite SLR in the confined aquifer buffered the SWI impacts, resulting in no significant change in the toe position or groundwater discharge to the sea. However in reality, the inland boundary conditions are likely to fall between the two extremes of fixed head and fixed flux (Lu et al., 2013).

The analytic solutions presented here does not calculate the actual toe position or fresh groundwater discharge to the sea, therefore the results would be different compared to field observations. The analytic solutions for confined aquifers inherently assume that the toe is anchored at the coast, whereas they are expected to discharge offshore in many locations worldwide (Morgan & Werner, 2015), including Christchurch. Therefore the application of offshore interface analytic solutions in GIS e.g., Werner and Robinson (2018) and Bakker et al. (2017), would be the next step forward. Nonetheless, the values of each cell were comparable to each other, hence the zones that were most vulnerable to SWI can be deduced.

In addition, it is important to note that the analytic solutions have several limitations inherent in the model. These include some key elements of SWI vulnerability that were not taken into account, such as temporal factors (e.g., seasonality, climatic events), spatial variations (e.g., in pumping, aquifer properties and geometry), physical processes (e.g., flooding, tidal effects), and other important elements (e.g., well salinity, previous SWI incidences, management practices, and level of knowledge regarding coastal aquifer processes) (Morgan & Werner, 2015). To overcome these limitations, additional information regarding these elements of SWI vulnerability can be separately compiled, such as in Cook et al. (2013).

Based on the current scenario, the toe position had a moderate negative correlation with groundwater level relative to MSL (R^2=0.66; Figure 58 in Appendix B). The toe position in the current scenario also showed a weak positive correlation with aquifer thickness (R^2=0.38; Figure 55 in Appendix B) and hydraulic conductivity (R^2=0.38; Figure 62 in Appendix B) based on the current scenario values. While the distance of bottom of aquifer and MSL, as well as location relative to the coast were not directly correlated with the toe position (Figure 60 and Figure 64, respectively, in Appendix B). This shows that the decrease of inland head, increase of aquifer thickness, and increase of hydraulic conductivity altogether exacerbated the toe movement landwards. Although further investigations showed that when hydraulic conductivity was increased exclusively, the toe position remained the same, implying that confined aquifers are unaffected by hydraulic conductivity based on the analytic solutions (Morgan et al., 2013a).

The sharp movement of toe position towards the coast at about 19 km along the coast across all scenarios can be associated with the thinning of Riccarton Gravel aquifer at the same

location, shown by the sharp decrease in aquifer thickness (Figure 57 in Appendix B) and distance between the bottom of aquifer and MSL (Figure 59 in Appendix B).

The dynamics of the equation parameters may explain the changes in the toe location. At about 8 – 12 km along the coast between the northern shore and the estuary, both q_0 and x_T were relatively low and displayed the smallest difference across the scenarios. This may be associated with the decrease in aquifer thickness (Figure 55) and the increase in groundwater level (Figure 57) at the location, which may acted as a buffer against SLR effects. In contrast, Brooklands which is located on the northern shore of the study area, had low groundwater levels and relatively large aquifer thickness, resulting in greater susceptibility to SWI.

5.2.1. Limitations of the analytic solutions applied in a GIS framework

The raster layers used in both GALDIT and analytic solutions had different resolutions or cell sizes. The lowest resolution raster layer used was 100 m. This resulted in output layers of 100 m resolution across the study area in both methods. In the analytic solutions, the area assessed for SWI vulnerability was the strip of land located 500 m from the coast (Figure 41 - Figure 40). When aiming to extract raster cells that were precisely located 500 m from the coast, several issues appeared. Cells that overlapped the 500 m from the coast line were not necessarily located 500 m from the coast. An example is illustrated in Figure 51; the centre of the cells that overlapped the line were predominantly not exactly 500 m from the coast. The low resolution of the output layers (100 m) was part of the issue. Consequently, the distance from the coast of the investigated x_T and q_0 cells (Figure 41 - Figure 46) ranged from 500 - 600 m. The accuracy of distance from the coast or x_b can be improved by using higher resolution layers. This can be achieved by using the resample tool, thereby increasing the resolutions of the input layers. The jagged nature of raster cells may also be one of the

disadvantages in working with raster cells, in contrast to the smoother coastline. However, the errors were not large enough to restrict the comparability between the obtained values, which were still considered representative of SWI vulnerability.

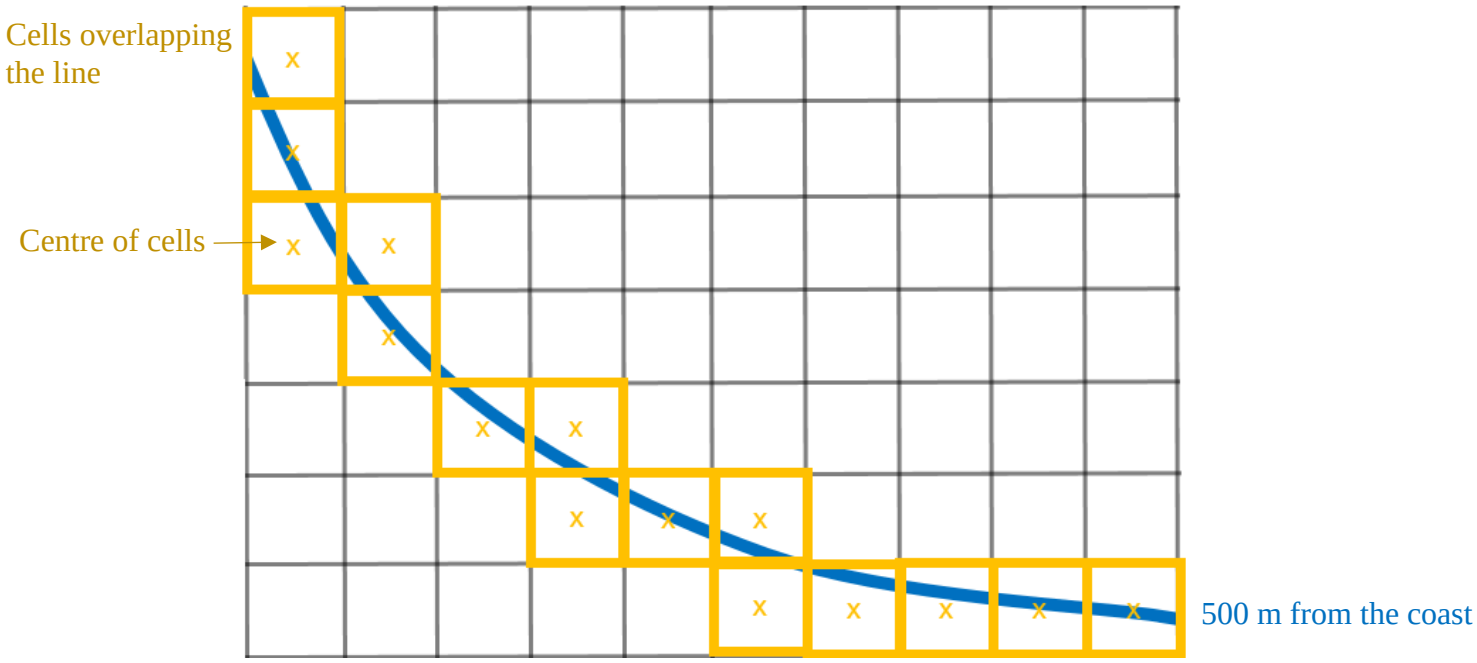

Figure 51. Illustration of the technical issue when aiming to extract or clip cells located 500 m from the coast. The blue line represents the location of 500 m from the coast, the yellow squares represent the raster cells that overlap the location of 500 m from the coast, while the centre of each cell is represented by the cross.

Another issue related to the GIS analysis was the alignment of raster cells. The cells of the input parameter raster layers were not perfectly aligned with each other, despite that they covered the same study area. This created implications when executing calculations using the raster calculator. The calculations were successful however when manually checking the calculation using the identify tool in several checkpoints, the results were often different by

several decimal points. The variation varied in different locations. It was observed that the error increased with results of higher value. Despite this, the calculations may not be wrong per se; ArcGIS internally processes raster calculations with different cell sizes and alignments, and produces a logical output that considers these. Using snap raster in the environment setting of the raster calculator may be an option to solve the issue. Due to time constraints, this study was unable to test this. This issue may have been more important in the analytic solutions compared to GALDIT.

Another issue due to the misalignment of raster cells is depicted in Figure 52. Two slightly misaligned raster layers were clipped using a polygon (outlined in dark green) located 500 m from the coast. The resulting clipped raster layers (blue and yellow) had slightly different cell formation (labelled A and B in Figure 52). The centre of the two cells (A and B) were not located on the same location relative to the coast, therefore they may be less comparable to each other compared to the other cells that overlapped. However, they were still treated as located on the same kilometre along the coast in the analysis.

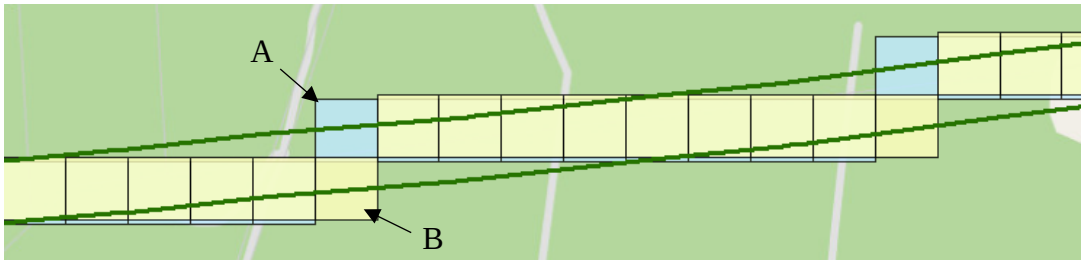

Figure 52. Misalignment of raster cells resulted in raster strips with different shapes (in blue and yellow), following clipping using the polygon outlined in dark green.

The strips of x_T and q_0 raster cells along the coast were produced by clipping a larger raster layer using a polygon along the coast that spanned from 500 m to 600 m from the coast (Section 3.4.5 and Figure 63 in Appendix B). Therefore, the average location of the raster cells investigated was 550 m from the coast. However, for simplicity reasons, the location of the raster cells investigated was referred to as 500 m from the coast.

5.3. Implications for Christchurch

Areas that are low-lying and close to the coast are most vulnerable to SLR. Based on the analysis, Brooklands was one of the first areas that would be affected by SWI due to SLR. Brooklands is the northernmost suburb in Christchurch, which was built on low-lying swamp land. In the fixed flux scenario, the groundwater level inland increases with SLR. The increase in groundwater level inland may cause freshwater inundation prior to seawater inundation following SLR, for example via the creation of new wetlands and the expansion of existing wetlands (Rotzoll & Fletcher, 2012). Additionally, liquefaction risks following earthquakes may also increase due to SLR (PCE, 2013). Brooklands experienced extensive damage from the 2010/2011 Christchurch earthquakes due to land subsidence and liquefaction, of which risks are heightened with groundwater levels or potentiometric head increasing towards the surface (PCE, 2013). Following earthquakes and aftershocks, artesian aquifers leak and become hydrologically connected, however the extent of this effect is currently investigated by Aqualinc (2018).

In the 2 m SLR scenarios, seawater was projected to encroach up the Styx, Avon, and Heathcote rivers. As droughts increase with climate change in the eastern side of New Zealand, river flows will reduce, which exacerbates the seawater encroachment up the rivers (MfE, 2009). In addition, SLR increases hydraulic heads at the coast, within estuaries and

lower reaches of rivers, which exacerbates the downward hydraulic gradient in the inland direction and results in increased pressure on the aquifers below (MfE, 2009).

There has been incidences of saline water leakage from the Avon-Heathcote Estuary through the confining aquitard, with the possibility of preferential inflow through unused boreholes, into the Riccarton Gravel aquifer in the Woolston area (Hertel, 1998; PDP, 2011). This occurred due to high levels of groundwater extraction for industrial and public supply and the lack of early SWI detection, which caused groundwater levels to decrease below high tide levels for prolonged periods (PDP, 2011; ECan, 2003). Additional factors that may exacerbate the effects of pumping and contribute to the incidence of SWI in Woolston include: (i) A buried volcanic ridge/sea stack complex was identified extending from Port Hills into Woolston which limits groundwater recharge, (ii) The Riccarton Gravel aquifer thinned in the area, and (iii) Deeper gravel aquifers are absent in the area (Hertel, 1998). As a result of SWI, the conductivity values from well M35/1159 located in the Woolston area were at a constant high, reaching up to 700 mS/m in the summer of 2001, and other groundwater quality parameters were also similar to seawater (ECan, 2003). However, management measures have since been put in place, such as controlling the rate of abstraction to keep groundwater level in the Riccarton Gravel aquifer above 1.5 m above MSL and to prevent pressure gradient changes that allow movement of contaminants into the aquifer (PDP, 2011). Under SLR conditions, the risk of saline water leakage into the aquifer may increase.

6. Conclusions

The main conclusions from the present study are:

- Sea level rise will impact Christchurch coastal aquifers by decreasing the fresh groundwater flux to the sea and moving the seawater-freshwater interface landwards.
- Analytic solutions, such as those developed by Morgan and Werner (2015), can be incorporated into a GIS framework for quantitatively assessing SWI vulnerability under SLR. This quantitative approach is superior to other qualitative methods such as GALDIT.
- The areas of Riccarton Gravel aquifer identified as most vulnerable to SWI under 1 m and 2 m SLR in Christchurch are Brooklands, Woolston, and Ferrymead.

Two SWI vulnerability assessment methods, GALDIT (Lobo-Ferreira et al., 2007) and analytic solutions of Morgan and Werner (2015) have been applied in the shallow confined Riccarton Gravel aquifer in Christchurch using GIS, under varying sea level scenarios and inland boundary conditions, which refer to the two different seawater-freshwater conditions under SLR; fixed flux and fixed head. The fixed flux boundary condition assumes that groundwater discharge to the sea remains constant despite SLR, and the groundwater level inland changes freely. The fixed head boundary condition assumes that the groundwater level inland remains the same despite sea level rise, it therefore assumes the worst SWI scenario.

The scenarios assessed were: current sea level, 1 m SLR with fixed head boundary, and 2 m SLR with both fixed flux and fixed head boundaries. The two methods indicated similar areas of vulnerability, however the analytic solution of Morgan and Werner (2015) was able to

more sensitively determine areas of greater SWI vulnerability quantitatively, making it a superior method compared to GALDIT in assessing SWI vulnerability.

In the Riccarton Gravel aquifer in Christchurch, areas of greatest SWI vulnerability were Brooklands, Woolston, and Ferrymead, linked primarily to the low inland heads. The maximum theoretical toe extension was 98 m in the current scenario and 292 m in the 1 m SLR (fixed head) scenario. The 2 m SLR fixed head scenario resulted in active SWI sites (i.e., maximum SWI vulnerability) around the Brooklands Lagoon and southwest of the Avon-Heathcote Estuary. This was because the hydraulic head onshore was less than the density-corrected head at the coast, implying that fresh groundwater discharge to the sea has ceased and the interface is moving inland under a landward-sloping hydraulic gradient. In the 1 m SLR scenario, seawater was projected to encroach into the Brooklands Lagoon, which forms part of the Waimakariri River mouth. In the 2 m SLR scenario, seawater was projected to encroach further upstream into the Styx River that is connected to the Brooklands Lagoon, as well as into the Avon-Heathcote Estuary, and further upstream into the Avon and Heathcote Rivers that flow into the estuary.

According to the analytical solutions, the 2 m SLR fixed flux scenario had almost no SWI impact due to the constant inland head despite SLR, except for the physical seawater encroachment. Whereas according to GALDIT, the 2 m SLR fixed flux scenario was more vulnerable to SWI compared to the 1 m SLR fixed head scenario. This was because the seawater encroachment that occurred in the 2 m SLR fixed flux scenario decreased the distance to coast (i.e., moved the coastline landwards), which, based on GALDIT, overrode the effect of decreased hydraulic head in the 1 m SLR fixed head scenario.

6.1. Recommendations

The development of the analytic solutions in a GIS framework in this study can be further improved by optimising the steps and working around the limitations of the method, such as aligning and resampling the cells of all input rasters to achieve a uniform and controlled output layer. A better understanding of how raster tools in GIS operate would also help in finding more effective ways to achieve the output. Both GIS analyses presented here depend on the quality of the data; the output is only as good as the inputs, hence their quality and careful manipulation are emphasized. Documentation of the process as well as data management are also important factors in this project.

The analytical solutions used in the present study assume that aquifers terminate at the coast and do not extend offshore, even though confined aquifers are known to extend beyond the coast and beneath the sea in many locations worldwide, including Christchurch. Therefore the application of offshore interface analytic solutions in GIS e.g., Werner and Robinson (2018) and Bakker et al. (2017), would be the next step forward.

References

Aqualinc. (2018). *Artesian groundwater contribute to Christchurch liquefaction and lateral spread damage?* Retrieved June 2018 from https://www.aqualinc.com/pages/82/christchurch-liquefaction-and-lateral-spread-damag.htm

Bakker, M. (2006). Analytic solutions for interface flow in combined confined and semi-confined, coastal aquifers. *Advances in Water Resources, 29*(3), 417-425.

Barlow, P. M. (2003). *Ground water in freshwater-saltwater environments of the Atlantic coast*. Reston, Virginia: U. S. Geological Survey. Retrieved July 18, 2017 from https://pubs.usgs.gov/circ/2003/circ1262/

Begg, J. G., Jones, K. E., & Barrell, D. J. A. (2015). *Geology and geomorphology of urban Christchurch and eastern Canterbury*. Lower Hutt, New Zealand: Institute of Geological and Nuclear Sciences Limited.

Bowden Environmental. (2017). *Step and constant discharge aquifer tests BX24/1578 Mundy Bros Ltd*. Retrieved from https://api.ecan.govt.nz/TrimPublicAPI/documents/download/3252143

Browne, G. H., & Naish, T. R. (2003). Facies development and sequence architecture of a Late Quaternary fluvial-marine transition, Canterbury Plains and shelf, New Zealand: implications for forced regressive deposits. *Sedimentary Geology, 158*, 57–86.

Brown, L. J., & Weeber, J. H. (1992). *Geology of the Christchurch urban area*. [Map 1 with scale 1:25,000]. 104 p. Lower Hutt, New Zealand: Institute of Geological and Nuclear Sciences Limited.

California Environmental Protection Agency (CalEPA). (2004). *Electrical conductivity/salinity fact sheet*. Retrieved 8 September 2017 from

https://www.waterboards.ca.gov/water_issues/programs/swamp/docs/cwt/guidance/3130en.pdf

Canterbury Maps. (2017a). *LWRP - Aquifer systems and sediments*. Retrieved from https://canterburymaps-ecan.opendata.arcgis.com/datasets/lwrp-aquifer-systems-and-sediments

Canterbury Maps. (2017b). *Piezometric contours.* Retrieved from https://canterburymaps-ecan.opendata.arcgis.com/datasets/piezometric-contours

Canterbury Maps. (2018a). *Aquifer test wells*. Retrieved on 22 March 2018 from https://canterburymaps-ecan.opendata.arcgis.com/datasets/aquifer-test-wells

Canterbury Maps. (2018b). *Groundwater take - consented activities*. Retrieved on 28 June 2018 from http://opendata.canterburymaps.govt.nz/datasets/groundwater-take-consented-activities

Canterbury Maps. (2018c). *Wells and bores.* Retrieved from https://canterburymaps-ecan.opendata.arcgis.com/datasets/wells-and-bores

Canterbury Regional Council (CRC) (1997). *Christchurch-West Melton groundwater hydrogeology*. Report prepared for Canterbury Regional Council by Richard Little, Woodward-Clyde. CRC report number U97 /28/l.

Chachadi, A. G., & Lobo-Ferreira, J. P. (2005, July 11-14). *Assessing aquifer vulnerability to sea-water intrusion using GALDIT method: Part 2 – GALDIT indicators description*. Paper presented at the The Fourth Inter-Celtic Colloquium on Hydrology and Management of Water Resources, Guimaraes, Portugal.

Chapman, D. (ed). (1996). *Water quality assessments - a guide to use of biota, sediments and water in environmental monitoring - second edition*. United Kingdom: E&FN Spon.

Retrieved from http://www.who.int/water_sanitation_health/resourcesquality/watqualassess.pdf

Charteris, S. (1999). *Geophysical investigations into the presence of saltwater in sediments and the definition of bedrock topography; Woolston, Heathcote Valley and Brighton Spit, Christchurch, New Zealand*. (Master's thesis, University of Canterbury, 1999).

Christchurch City Council (CCC). (2018, June). *The word on water: Latest on chlorination*. Retrieved 22 June 2018 from https://www.ccc.govt.nz/news-and-events/newsline/show/2692

Church, J. A., Clark, P. U., Cazenave, A., Gregory, J. M., Jevrejeva, S., Levermann, A., . . . Unnikrishnan, A. S. (2013). Sea Level Change. In T. F. Stocker, D. Qin, G.-K. Plattner, M. Tignor, S.K. Allen, J. Boschung, A. Nauels, Y. Xia, V. Bex, P.M. Midgley (Ed.), *Climate Change 2013: The Physical Science Basis. Contribution of Working Group I to the Fifth Assessment Report of the Intergovernmental Panel on Climate Change*. Cambridge, United Kingdom and New York, NY, USA: Cambridge University Press.

Cook, S.B., Dixon-Jain, P., Hocking, M., Sundaram, B., Morgan, L.K., Ivkovic, K.M., Werner, A.D., Norman, R., Caruana, L. & Garlapati, N. (2013). *A national-scale vulnerability assessment of SWI intrusion: Vulnerability Factor Analysis*. Record 2013/08. Geoscience Australia, Canberra and National Centre for Groundwater Research and Training, Adelaide. Retrieved from https://ecat.ga.gov.au/geonetwork/srv/eng/search#!c9a31b76-6723-721b-e044-00144fdd4fa6

Ebert, K., Ekstedt, K., & Jarsjo, J. (2016). GIS analysis of effects of future Baltic sea level rise on the island of Gotland, Sweden. *Natural Hazards and Earth System Sciences*, *16*(7), 1571-1582. doi:10.5194/nhess-16-1571-2016

Environment Canterbury (ECan). (2001). Our water in the balance: Christchurch West Melton rivers and groundwater: *Issues and options: A discussion document contributing to the preparation of the Natural Resources Regional Plan* (pp. 137).

ECan. (2003, November). *Coastal aquifer saltwater intrusion assessment guidelines*: *Report no. R04/18*. Canterbury, New Zealand: Aitchison-Earl, P., Ettema, M., Hanson, C., Hayward, S., Larking, R., Sanders, R., Scott, D., & Veltman, A. Retrieved from https://api.ecan.govt.nz/TrimPublicAPI/documents/download/585421

ECan. (2004, September). *Groundwater allocation limits: land-based recharge estimates: Report no. U04/97*. Canterbury, New Zealand: Scott, D. Retrieved from https://api.ecan.govt.nz/TrimPublicAPI/documents/download/611102

ECan. (2012, September). *Seawater intrusion network review: Report No. R12/35*. Canterbury, New Zealand: Scott, M., & Wilson, N. Retrieved from https://api.ecan.govt.nz/TrimPublicAPI/documents/download/1635169

ECan. (2015). *Christchurch groundwater quality monitoring 2015: Report no. R16/39.* Prepared for Christchurch City Council. Retrieved from https://api.ecan.govt.nz/TrimPublicAPI/documents/download/2963954

ECan. (2016). *Groundwater quality data: wells within 60 km of Christchurch* (Unpublished dataset). Christchurch, New Zealand. Retrieved July 2017.

ECan (2017). *Well search: M36/1159*. Retrieved from https://www.ecan.govt.nz/data/well-search/welldetails/TTM2LzExNTk%3D/TTM2LzExNTk%3D

Ettema, M. (1999). *Aquifer test at Woolston / Heathcote M36/0979 in the Riccarton aquifer*: *Report no. U99/20*. Retrieved from https://api.ecan.govt.nz/TrimPublicAPI/documents/download/301670

Ferguson, G., & Gleeson, T. (2012). Vulnerability of coastal aquifers to groundwater use and climate change. *Nature Clim. Change, 2*(5), 342-345. doi:http://www.nature.com/nclimate/journal/v2/n5/abs/nclimate1413.html#supplementary-information

Ferguson, G., & Gleeson, T. (2013). Reply to 'Threats to coastal aquifers'. *Nature Clim. Change, 3*(7), 605-606. doi:10.1038/nclimate1930

Fetter, C. W. (2001). *Applied Hydrogeology* (4th ed.). New Jersey, USA: Prentice Hall.

Forsyth, P. J., Barrell, D. J. A., & Jongens, R. (compilers) (2008). *Geology of the Christchurch area*. Institute of Geological and Nuclear Sciences 1:250 000 Geological Map 16. 1 sheet + 67 p. Lower Hutt, New Zealand: GNS Science.

Gornitz, V. M., Daniels, R. C., White, T. W., & Birdwell, K. R. (1994). The development of a coastal risk assessment database: Vulnerability to sea-level rise in the U.S. Southeast. *Journal of Coastal Research, 12*(12), 327-338.

Hansen, J., Sato, M., Hearty, P., Ruedy, R., Kelley, M., Masson-Delmotte, V., . . . Lo, K. W. (2016). Ice melt, sea level rise and superstorms: evidence from paleoclimate data, climate modeling, and modern observations that 2 °C global warming could be dangerous. *Atmos. Chem. Phys., 16*(6), 3761-3812. doi:10.5194/acp-16-3761-2016

Hertel, I. (1998). *Groundwater contamination in the Heathcote/Woolston area, Christchurch, New Zealand*. (Doctoral thesis, University of Canterbury, 1998). Retrieved from https://ir.canterbury.ac.nz/handle/10092/13050

Intergovernmental Panel on Climate Change (IPCC). (n.d.). *Organization*. Retrieved 31 October 2017 from https://www.ipcc.ch/organization/organization.shtml

Kooi, H., & Groen, J. (2001). Offshore continuation of coastal groundwater systems; predictions using sharp-interface approximations and variable-density flow modelling. *Journal of Hydrology, 246*(1-4), 19-35.

Lenntech. (n.d.). *Water Conductivity.* Retrieved from https://www.lenntech.com/applications/ultrapure/conductivity/water-conductivity.htm

Land Information New Zealand (LINZ). (2014). Canterbury - Rangiora LiDAR 1m DEM (2014). Last updated 10 Jan 2017. Retrieved from https://data.linz.govt.nz/layer/53552-canterbury-rangiora-lidar-1m-dem-2014/

LINZ. (2015). *Canterbury - Christchurch and Selwyn LiDAR 1m DEM (2015)*. Last updated 20 March 2017. Retrieved 12 October from https://data.linz.govt.nz/layer/53587-canterbury-christchurch-and-selwyn-lidar-1m-dem-2015/

LINZ. (2017a). *Lyttelton 1937 to NZVD2016 Conversion*. Last updated 3 August 2016. Retrieved 13 October 2017 from https://data.linz.govt.nz/layer/53432-lyttelton-1937-to-nzvd2016-conversion/

LINZ. (2017b). *Standard port tidal levels*. Last updated 30 June 2017. Retrieved 9 October 2017 from https://www.linz.govt.nz/sea/tides/tide-predictions/standard-port-tidal-levels

LINZ. (2018). *Definitions tidal terms*. Retrieved 19 March 2018 from https://www.linz.govt.nz/sea/tides/introduction-tides/definitions-tidal-terms

Lobo-Ferreira, J. P., Chachadi, A. G., Diamantino, C., & Henriques, M. J. (2007). Assessing aquifer vulnerability to seawater intrusion using the GALDIT method: part 1 - application to the Portuguese Monte Gordo aquifer. In J. P. Lobo-Ferreira & J. M. P. Viera (Eds.), *Water in Celtic Countries: Quantity, Quality and Climate Variability* (Vol. 310, pp. 161).

Lovell, M. & Weeber, J. (2000). *Plover Street exploration /monitoring wells (M36/5893, M36/5894, M36/5895) and an aquifer test in the Riccarton Gravel, Southshore, Christchurch*: *Report no. U00/17*. Retrieved from https://api.ecan.govt.nz/TrimPublicAPI/documents/download/301766

Lu, C., Werner, A. D., & Simmons, C. T. (2013). Threats to coastal aquifers. *Nature Clim. Change, 3*(7), 605-605. doi:10.1038/nclimate1901

McLean, L. (2018). *Hydrogeological investigation of the Christchurch City aquifer* (Master's thesis, University of Canterbury, 2018).

Michael, H. A., Post, V. E. A., Wilson, A. M., & Werner, A. D. (2017). Science, society, and the coastal groundwater squeeze. *Water Resources Research, 53*(4), 2610-2617. doi:10.1002/2017WR020851

Ministry for the Environment (MfE). (2009, March). *Preparing for coastal change: A guide for local government in New Zealand.* Retrieved from http://www.pce.parliament.nz/publications/preparing-new-zealand-for-rising-seas-certainty-and-uncertainty

Ministry for the Environment (MfE). (2017, December). *Tides around New Zealand (fact sheet 4: preparing for coastal change).* Retrieved 2 May 2018 from http://www.mfe.govt.nz/sites/default/files/media/MFE_Coastal_Fact%20Sheet%204.pdf

Moghaddam, H. K., Jafari, F., & Javadi, S. (2017). Vulnerability evaluation of a coastal aquifer via GALDIT model and comparison with DRASTIC index using quality parameters. *Hydrological Sciences Journal-Journal Des Sciences Hydrologiques*, *62*(1), 137-146. doi:10.1080/02626667.2015.1080827

Morgan, L. K., & Werner, A. D. (2014). Seawater intrusion vulnerability indicators for freshwater lenses in strip islands. *Journal of Hydrology, 508*(Supplement C), 322-327. doi:https://doi.org/10.1016/j.jhydrol.2013.11.002

Morgan, L. K., & Werner, A. D. (2015). A national inventory of seawater intrusion vulnerability for Australia. *Journal of Hydrology: Regional Studies, 4, Part B*, 686-698. doi:https://doi.org/10.1016/j.ejrh.2015.10.005

Morgan, L. K., Werner, A. D., Ivkovic, K. M., Carey, H., & Sundaram, B. (2013a). *A national-scale vulnerability assessment of seawater intrusion: First-order assessment of seawater intrusion for Australian case study sites (Record 2013/19)*. Geoscience Australia, Canberra, and NCGRT, Adelaide. Retrieved from https://www.ga.gov.au/products/servlet/controller?event=FILE_SELECTION&catno=74959

Morgan, L. K., Werner, A. D., Morris, M. J., & Teubner, M. D. (2013b). Application of a Rapid-Assessment Method for Seawater Intrusion Vulnerability: Willunga Basin, South Australia. In C. Wetzelhuetter (Ed.), *Groundwater in the Coastal Zones of Asia-Pacific* (pp. 205-225). Dordrecht: Springer Netherlands.

Motevalli, A., Moradi, H. R., & Javadi, S. (2018). A Comprehensive evaluation of groundwater vulnerability to saltwater up-coning and sea water intrusion in a coastal aquifer (case study: Ghaemshahr-juybar aquifer). *Journal of Hydrology, 557*, 753-773. doi:https://doi.org/10.1016/j.jhydrol.2017.12.047

Özyurt, G. (2007). *Vulnerability of coastal areas to sea level rise: a case study on Goksu Delta*. (Doctoral thesis, Middle East Techincal University, 2007). Retrieved from https://etd.lib.metu.edu.tr/upload/12608146/index.pdf

Parliamentary Commissioner for the Environment (PCE). (2015, November). *Preparing New Zealand for rising seas: certainty and uncertainty.* Retrieved from http://www.pce.parliament.nz/publications/preparing-new-zealand-for-rising-seas-certainty-and-uncertainty

Pattle Delamore Partners Limited (PDP). (2011, June). *New Zealand guidelines for the monitoring and management of sea water intrusion risk on groundwater: Report prepared for Envirolink (Project 420-NRLC50).* Christchurch, New Zealand: Callander, P., Lough, H., & Steffens, C. Retrieved from http://envirolink.govt.nz/assets/

Envirolink/420-NLRC50-Guidelines-for-the-monitoring-and-management-of-sea-water-intrusion-risks-on-groundwater.pdf

Ramsay, D., Bell, R., & Britton, R. (2009). *Preparing for coastal change: A guide for local government in New Zealand*. Wellington, New Zealand: Ministry for the Environment. Retrieved from http://www.mfe.govt.nz/sites/default/files/preparing-for-coastal-change.pdf

Reisinger, A., Kitching, R. L., Chiew, F., Hughes, L., Newton, P.C.D., Schuster, S.S., Tait, A., & Whetton, P. (2014). Australasia. In Barros, V.R., C.B. Field, D.J. Dokken, M.D. Mastrandrea, K.J. Mach, T.E. Bilir, M. Chatterjee, K.L. Ebi, Y.O. Estrada, R.C. Genova, B. Girma, E.S. Kissel, A.N. Levy, S. MacCracken, P.R. Mastrandrea, and L.L. White (Eds.), *Climate Change 2014: Impacts, Adaptation, and Vulnerability. Part B: Regional Aspects. Contribution of Working Group II to the Fifth Assessment Report of the Intergovernmental Panel on Climate Change* (p. 1381). Cambridge University Press, Cambridge, United Kingdom and New York, NY, USA.

Riahi, K., Rao, S., Krey, V., Cho, C., Chirkov, V., Fischer, G., . . . Rafaj, P. (2011). RCP 8.5—A scenario of comparatively high greenhouse gas emissions. *Climatic Change, 109*(1), 33. doi:10.1007/s10584-011-0149-y

Rotzoll, K., & Fletcher, C. H. (2013). Assessment of groundwater inundation as a consequence of sea-level rise. *Nature Clim. Change*, *3*(5), 477-481. doi:10.1038/nclimate1725. Retrieved from http://www.nature.com/nclimate/journal/v3/n5/abs/nclimate1725.html#supplementary-information

Strack, O. D. L. (1976). A single-potential solution for regional interface problems in coastal aquifers. *Water Resources Research, 12*(6), 1165-1174. doi:10.1029/WR012i006p01165

Talbot, J. D., Weeber, J. H., Freeman, M. C., Mason, C. R., & Wilson, D. D. (1986). *The Christchurch Artesian Aquifers*. A report prepared by the Resources Division of the Northern Canterbury Catchment Board and Regional Water Board, Christchurch. 159p.

Vernier Software & Technology. (n.d.). *Chloride and Salinity*. Retrieved 24 October 2017 from http://www2.vernier.com/sample_labs/WQV-15-COMP-chloride_salinity.pdf

Weeber, J. (2008, May). *Christchurch groundwater protection: A hydrogeological basis for zone boundaries, Variation 6 to the Proposed Natural Resources Regional Plan*. Report No. U08/21. ISBN 978-1-86937-802-8. Retrieved from https://api.ecan.govt.nz/TrimPublicAPI/documents/download/1059106

Werner, A. D., Ward, J. D., Morgan, L. K., Simmons, C. T., Robinson, N. I., & Teubner, M. D. (2012). Vulnerability Indicators of Sea Water Intrusion. *Ground Water, 50*(1), 48-58. doi:10.1111/j.1745-6584.2011.00817.x

Werner, A. D., & Robinson, N. I. (2018). Revisiting analytical solutions for steady interface flow in subsea aquifers: Aquitard salinity effects. *Advances in Water Resources, 116*, 117-126. doi:https://doi.org/10.1016/j.advwatres.2018.01.002

White, P. A., Kovacova, E., Zemansky, G., Jebbour, N., & Moreau-Fournier, M. (2012). Groundwater-surface water interaction in the Waimakariri River, New Zealand, and groundwater outflow from the river bed. *Journal of Hydrology (New Zealand), 51*, 1+.

Appendix A – Groundwater extraction

Groundwater extraction is one of the causes of SWI, in addition to sea level rise and lack of recharge (Werner et al., 2012; Ferguson & Gleeson, 2012). Groundwater extraction can lower hydraulic head onshore and therefore increase the risk of SWI. Population density can be an indicator of groundwater extraction, except where agriculture and industry uses a high amount of water, resulting in a pronounced increase in water use per capita (Ferguson & Gleeson, 2012). The consented maximum volume of groundwater extraction in m^3/day from the Riccarton Gravel aquifer within the study area (from the coast to about 8 km inland) is shown in Figure 53, as a representation of groundwater extraction in Christchurch. Only active and existing consents as per 28 June 2018 were included in the map. The wells that tap into the Riccarton Gravel aquifer were identified using the methods in Section 3.3.2.

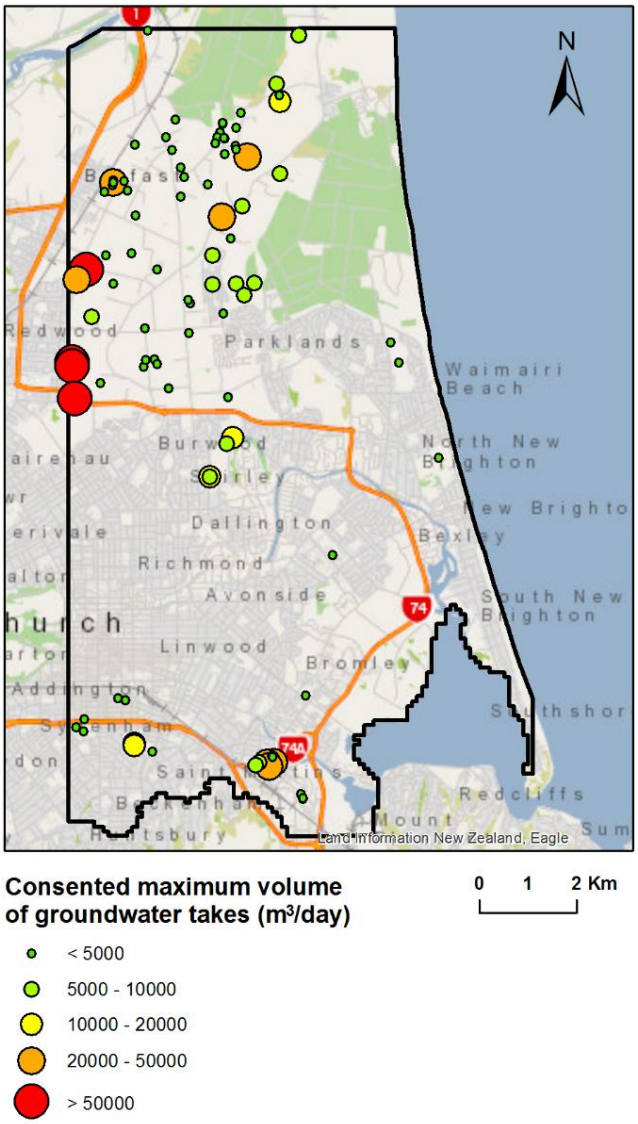

Figure 53. Consented maximum volume of groundwater takes (m^3/day) from the wells identified as tapping into the Riccarton Gravel aquifer, within the study area (Canterbury Maps, 2018b).

Appendix B – Analytical solutions and GIS flowcharts

Table 5. Notation.

Symbol	Description
x_T	Seawater wedge toe position [L]
W_{net}	Distributed net recharge [L^2/T]
δ	Density ratio [-] derived from $(\rho_s - \rho_f) / \rho_f$, where ρ_s [M/L^3] is seawater density, and ρ_f [M/L^3] is freshwater density
K	Aquifer hydraulic conductivity [L/T]
z_0	The distance between MSL and the bottom of the aquifer [L]
q_0	Freshwater discharge to the sea from an aquifer [L^2/T]
h_b	Hydraulic head or groundwater level relative to a datum (MSL) [L]
x_b	The distance from the coast (coastal boundary) to the location where groundwater level is measured (inland boundary) [L]
h_0	Saturated confined aquifer thickness inland of x_T [L]

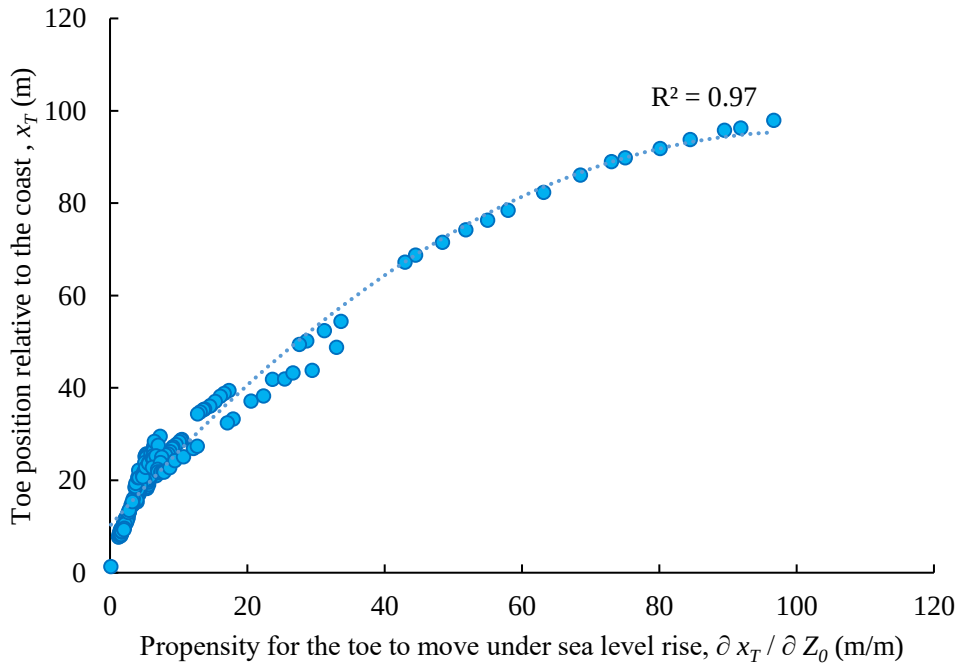

Figure 54. The correlation between x_T and $\partial x_T / \partial Z_0$ in the current sea level scenario.

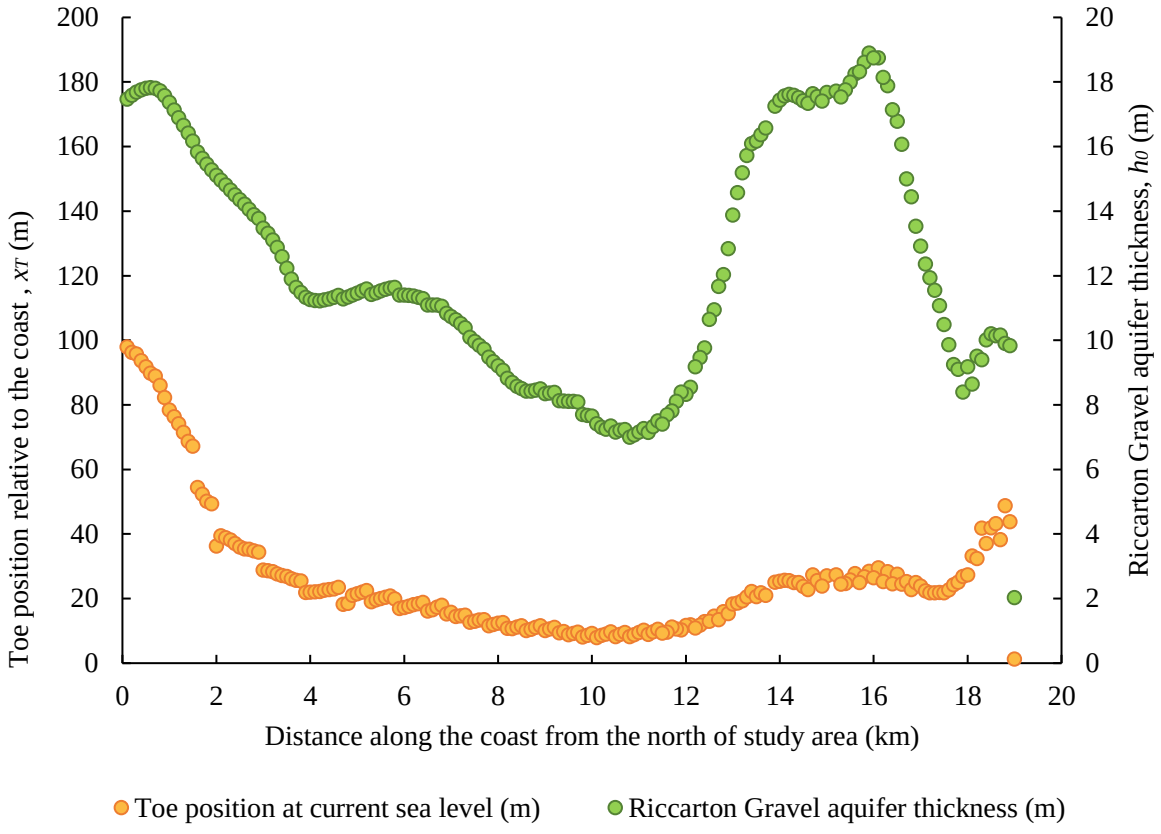

Figure 55. Toe position relative to the coast (m) and Riccarton Gravel aquifer thickness (m) along the coast of study area (km) in the current scenario.

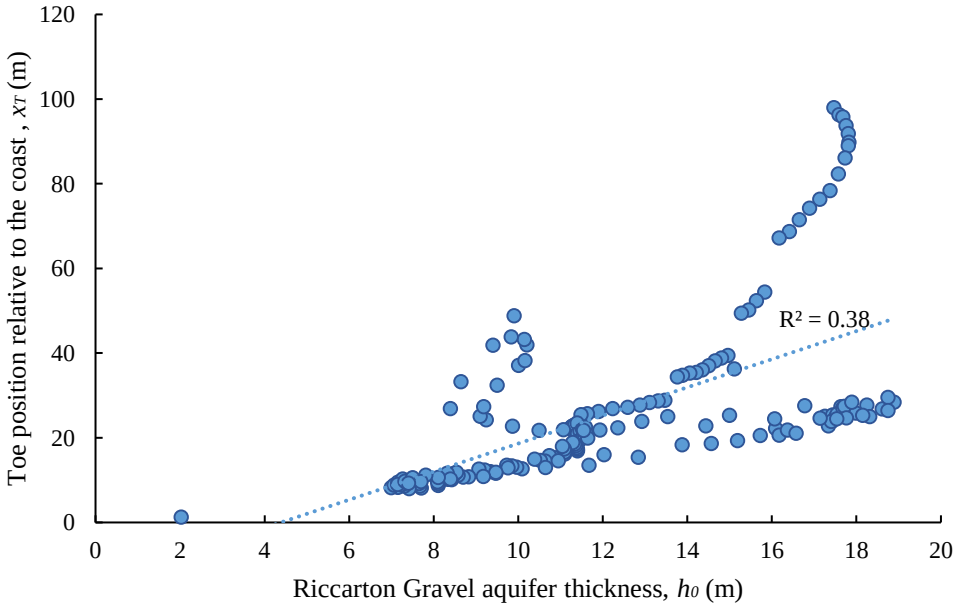

Figure 56. Correlation between toe position relative to the coast (m) and Riccarton Gravel aquifer thickness (m).

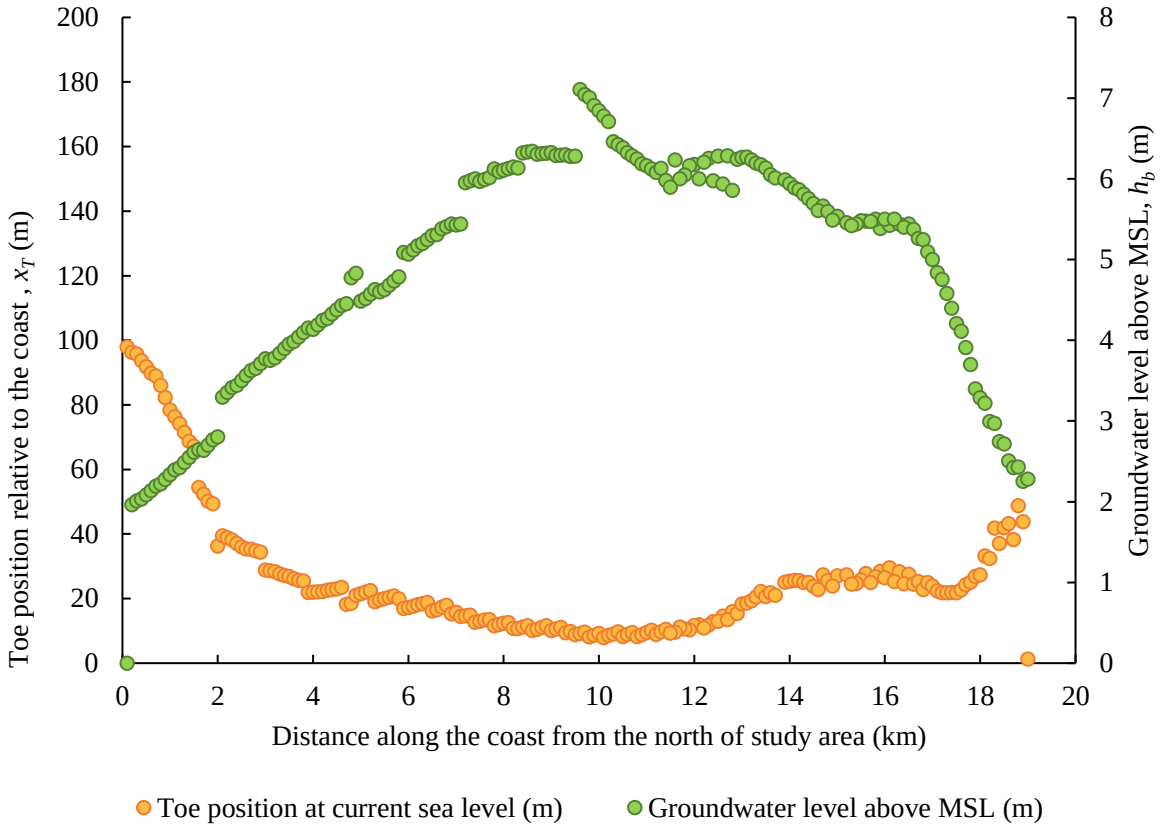

Figure 57. Toe position relative to the coast (m) and groundwater level above MSL (m) along the coast of the study are (km).

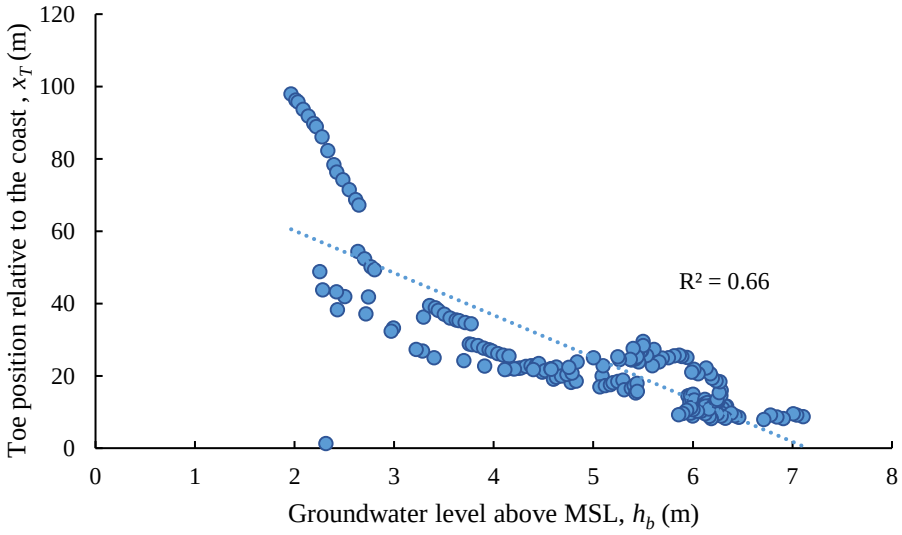

Figure 58. Correlation between toe position relative to the coast (m) and groundwater level above MSL (m).

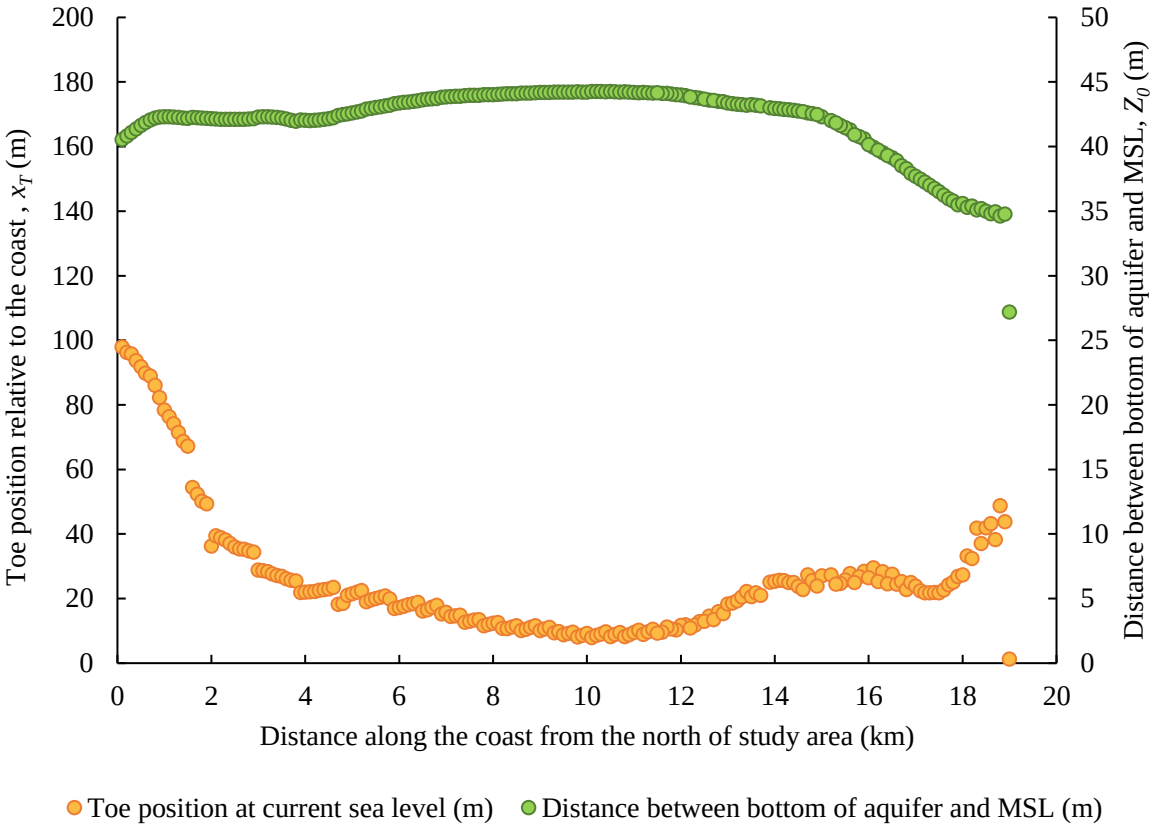

Figure 59. Toe position relative to the coast (m) and the distance between bottom of aquifer and MSL (m) along the coast of the study area (km).

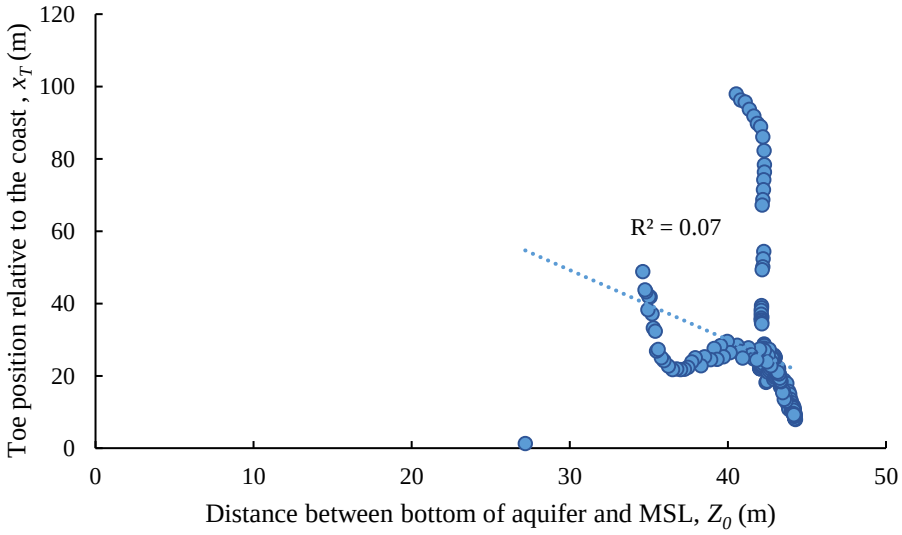

Figure 60. Correlation between the toe position relative to the coast (m) and the distance between bottom of aquifer and MSL (m).

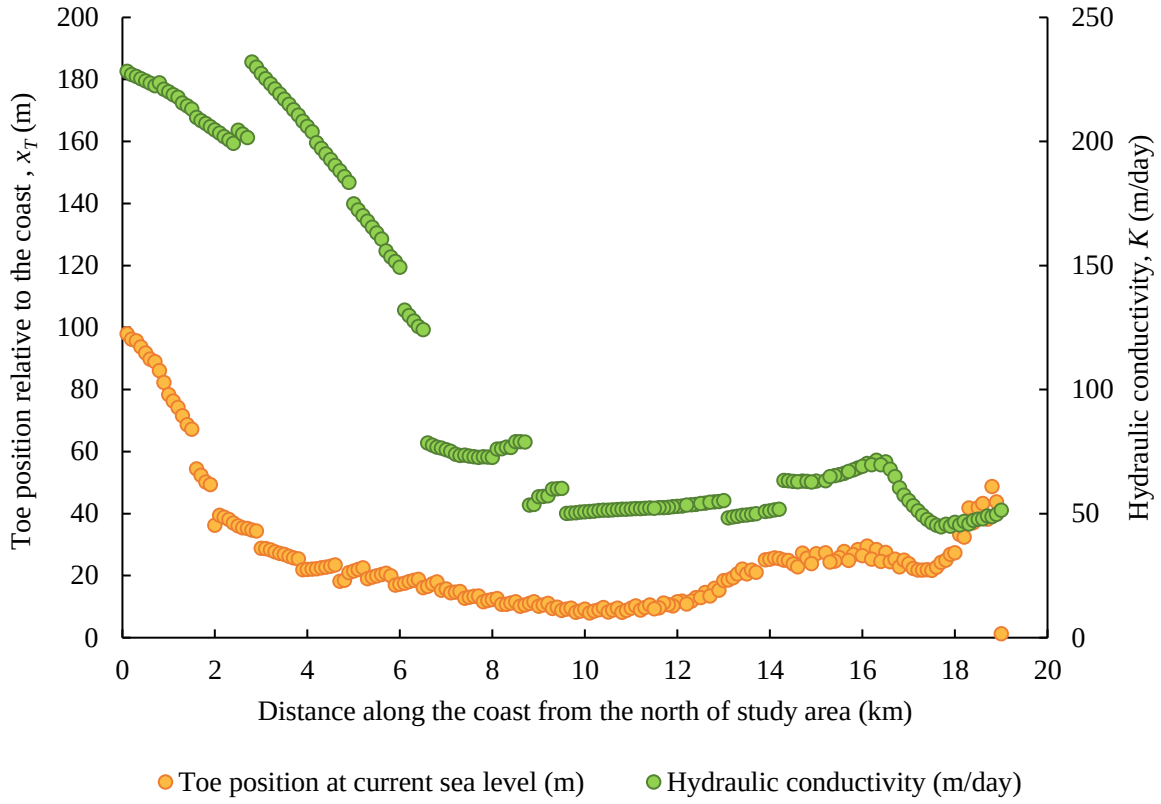

Figure 61. Toe position relative to the coast (m) and hydraulic conductivity (m/day) derived from empirical Bayesian kriging along the coast of the study area (km).

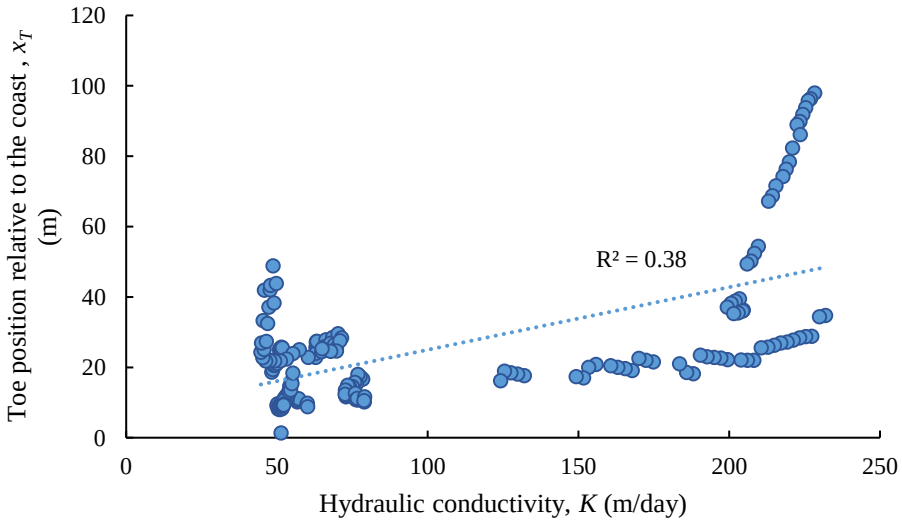

Figure 62. Correlation between toe position relative to the coast (m) and hydraulic conductivity (m/day).

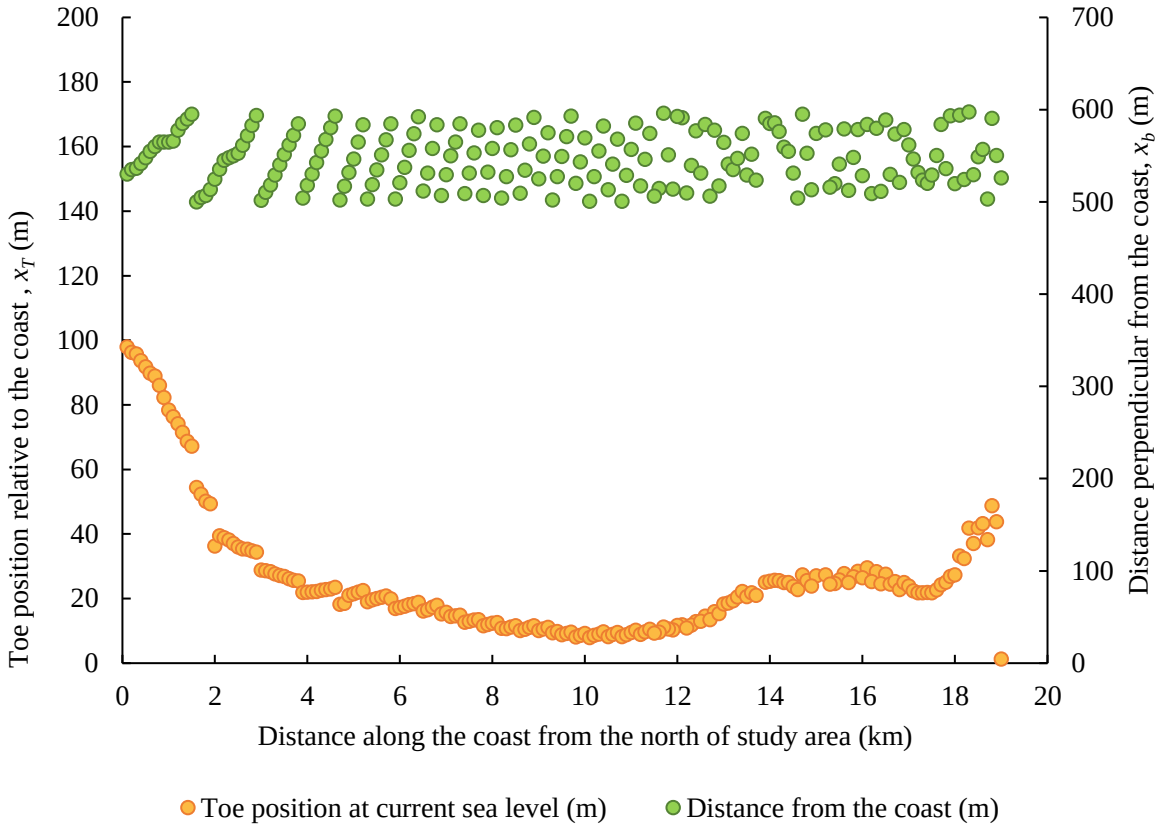

Figure 63. Toe position relative to the coast (m) and distance perpendicular from the coast (m) along the coast of the study area (km).

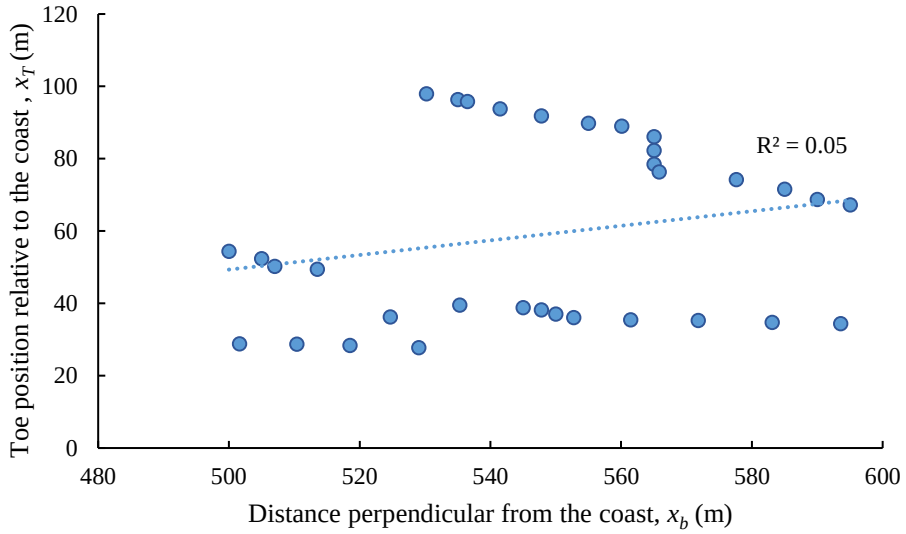

Figure 64. Correlation between toe position relative to the coast (m) and distance perpendicular to the coast (m).

Figure 65. GIS flowchart of the GALDIT method.

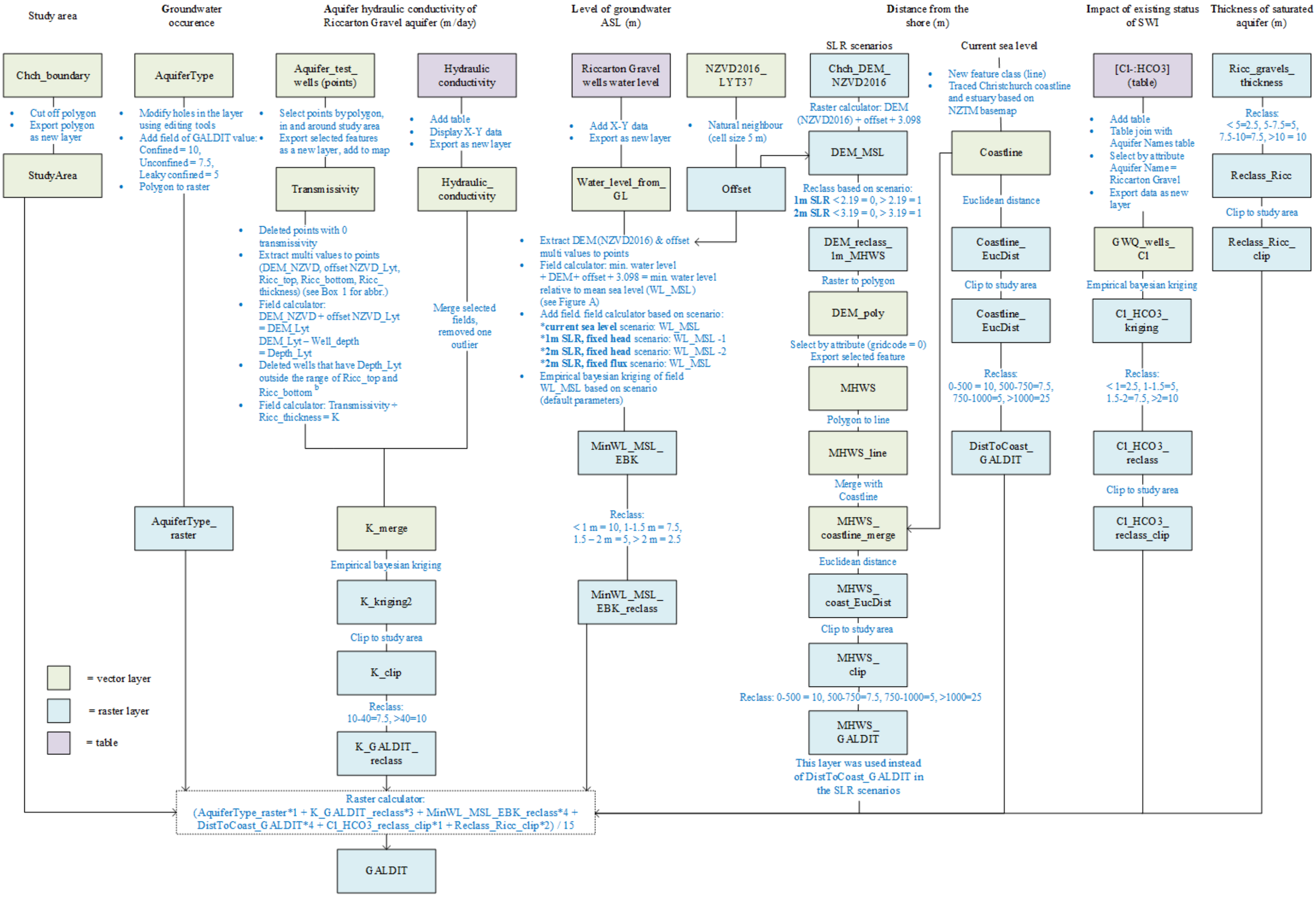

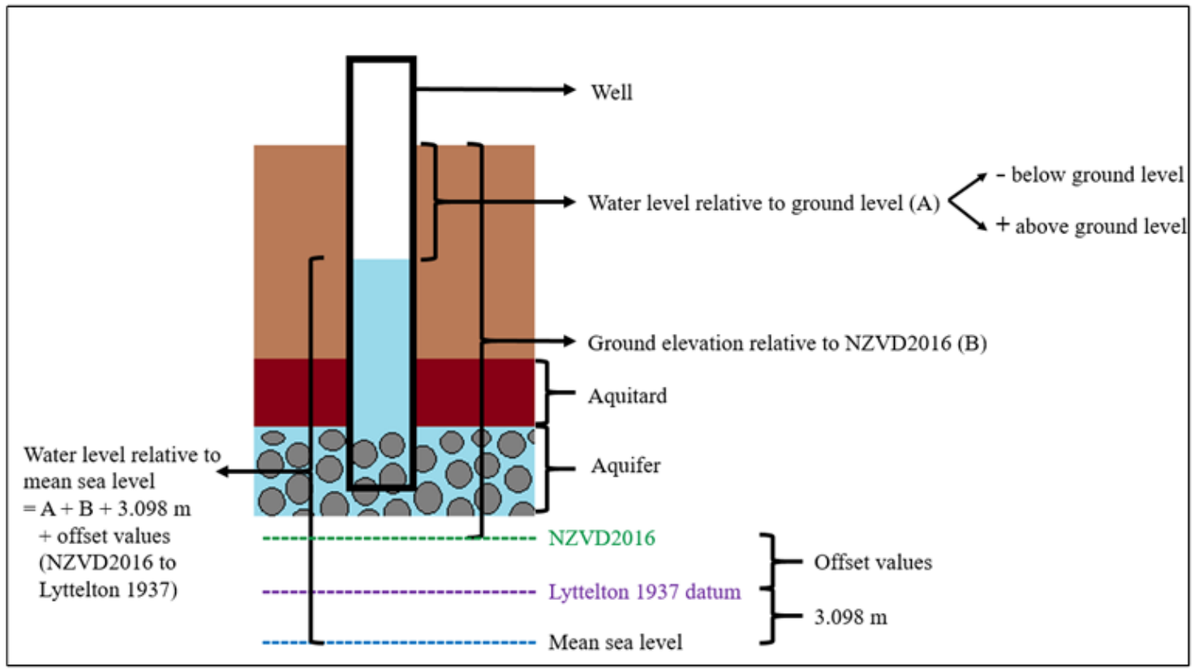

Figure A. The derivation of groundwater level relative to mean sea level.

Box 1: Abbreviations

DEM_NZVD = Digital elevation model or ground elevation relative to the NZVD2016 datum in metres.

DEM_Lyt = Digital elevation model or ground elevation relative to the Lyttelton 1937 datum in metres.

Depth_Lyt = Well depth in metres relative to the Lyttelton 1937 datum.

Offset NZVD_Lyt = Offset value between the NZVD2016 and the Lyttelton 1937 datum in metres. This was derived from the point layer offsets (LINZ, 2017b). Natural neighbor was used to generate a raster layer (5 m resolution).

Ricc_top = Top elevation of the Riccarton Gravel aquifer in metres, relative to the Lyttelton 1937 datum.

Ricc_bottom = Bottom elevation of the Riccarton Gravel aquifer in metres, relative to the Lyttelton 1937 datum.

Ricc_thickness = Thickness of the Riccarton Gravel aquifer in metres.

K = Hydraulic conductivity, can be derived from dividing transmissivity by saturated aquifer thickness.

SLR = Sea level rise

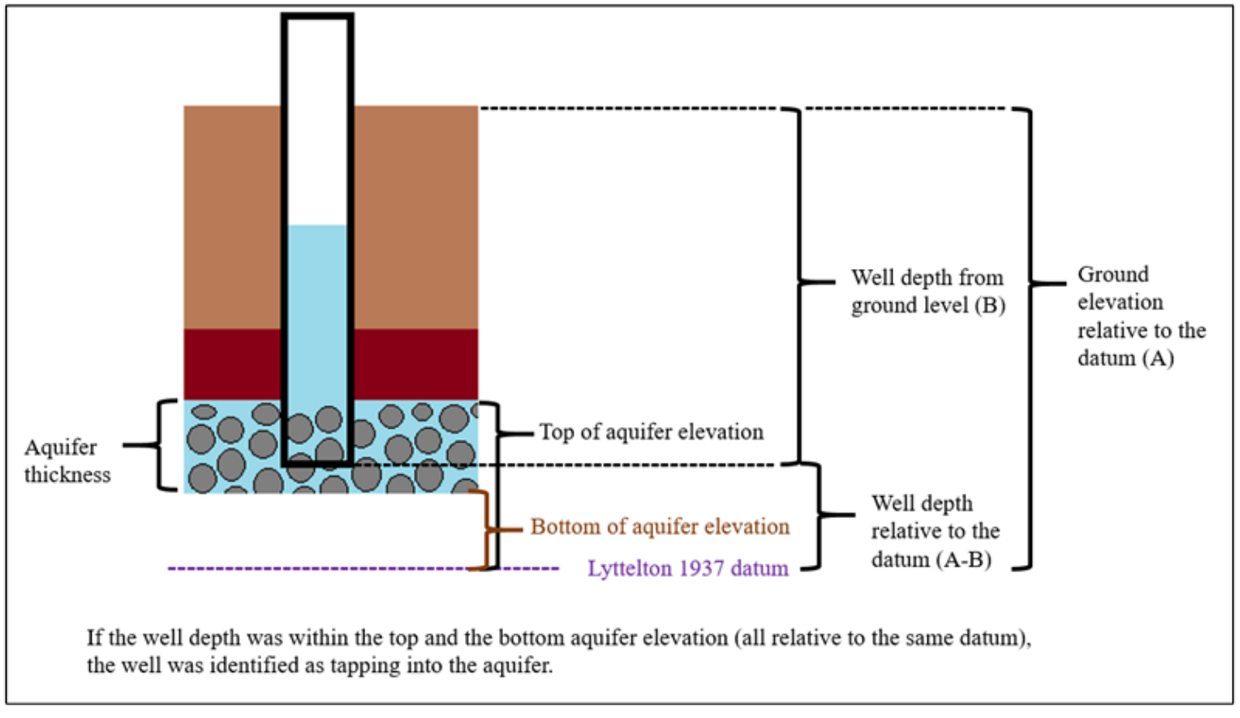

Figure B. Illustration of how each well was identified as tapping into the Riccarton Gravel aquifer.

Figure 66. Flowchart of the analytic solutions applied in a GIS framework.